VOLUME XLVI

GEMS & GEMOLOGY

SPRING 2010

Intense Pink CVD Synthetic Diamonds
Impact of Heat and UV on CVD Synthetics
"Sister" Stones to the Hope?
Confocal Raman to Identify Emeralds
Bastnäsite and Parisite from Malawi

THE QUARTERLY JOURNAL OF THE GEMOLOGICAL INSTITUTE OF AMERICA

OUR EDUCATION.
YOUR WORLD OF OPPORTUNITY.

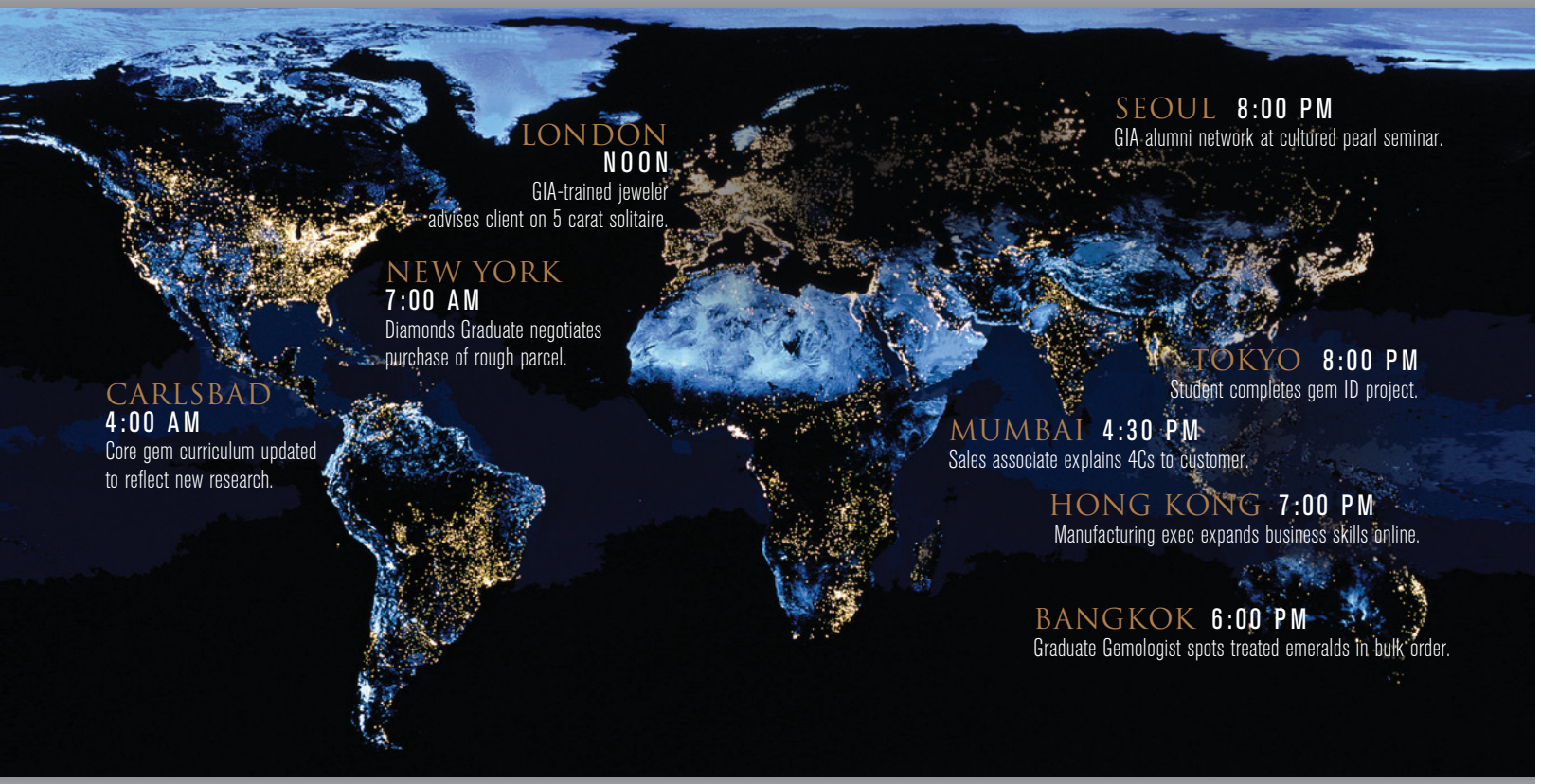

Almost anywhere you go, someone is using education acquired from GIA. Our international campuses, traveling classes, corporate seminars and online courses help individuals define and refine vital skills.

And GIA supports that learning with credentials valued throughout the gem and jewelry world.

WWW.GIA.EDU

GIA
GEMOLOGICAL INSTITUTE OF AMERICA®

CARLSBAD NEW YORK LONDON ANTWERP FLORENCE GABORONE JOHANNESBURG
MOSCOW MUMBAI BANGKOK HONG KONG BEIJING TAIPEI SEOUL OSAKA TOKYO

GMSGG

GEMS & GEMOLOGY®

Spring 2010 Volume 46, No. 1

pg. 5

pg. 22

EDITORIAL

FEATURE ARTICLES

NOTES & NEW TECHNIQUES

REGULAR FEATURES

pg. 67

GEMS & GEMOLOGY®

gia.edu/gandg

SUBSCRIPTIONS

Copies of the current issue may be purchased for **$29.95** plus shipping. Online subscriptions are $74.95 for one year (4 issues), $129.95 for two years (8 issues). Combination print + online subscriptions are $139.95 in the U.S. and $160 elsewhere for one year, and $269.95 in the U.S. and $305 elsewhere for two years. Canadian subscribers should add GST. Discounts are available for group subscriptions, renewals, GIA alumni, and current GIA students. For institutional rates, go to gia.edu/gandg. Subscriptions include *G&G's* monthly gemological e-newsletter, the *G&G eBrief*.

To purchase subscriptions and single issues (print or PDF), visit **store.gia.edu** or contact the Circulation Coordinator.

PDF versions of individual articles and sections from Spring 1981 forward can be purchased at **gia.metapress.com** for $12 each. Visit gia.edu/gandg for free online access to the 1934–2009 subject and author index and all 1934–1980 issues.

To obtain a Japanese translation of *Gems & Gemology,* contact GIA Japan at info@giajpn.gr.jp. Our Canadian goods and service registration number is 126142892RT.

DATABASE COVERAGE

Gems & Gemology's impact factor is 1.172 (ranking 12th out of the 26 journals in the Mineralogy category), according to the Thomson Reuters 2008 Journal Citation Reports (issued July 2009). *Gems & Gemology* is abstracted in Thomson Reuters products (*Current Contents: Physical, Chemical & Earth Sciences* and Science Citation Index—Expanded, including the Web of Knowledge) and other databases. For a complete list of sources abstracting *G&G*, go to gia.edu/gandg.

MANUSCRIPT SUBMISSIONS

Gems & Gemology welcomes the submission of articles on all aspects of the field. Please see the Guidelines for Authors on pp. 76–77 of this issue or contact the Managing Editor. Letters on articles published in *Gems & Gemology* are also welcome.

COPYRIGHT AND REPRINT PERMISSIONS

Gems & Gemology is published quarterly by the Gemological Institute of America, a nonprofit educational organization for the gem and jewelry industry.

Postmaster: Return undeliverable copies of *Gems & Gemology* to GIA, The Robert Mouawad Campus, 5345 Armada Drive, Carlsbad, CA 92008.

ABOUT THE COVER

Pink diamonds have long been one of the most sought-after of gems. The lead article in this issue, by Dr. Wuyi Wang and coauthors, describes a new production of strongly colored pink CVD lab-grown diamonds from Apollo Diamond Inc. The natural pink diamonds in these earrings weigh 1.09 and 1.03 ct; the radiant-cut yellow diamonds total 2.21 ct. Courtesy Alan Friedman Co., Beverly Hills, California. Composite photo by Robert Weldon.

Color separations for *Gems & Gemology* are by Pacific Plus, Carlsbad, California.
Printing is by Allen Press, Lawrence, Kansas.

 ISSN 0016-626X

'10

GEMS & GEMOLOGY
is pleased to announce the winners of the

Dr. Edward J. Gübelin Most Valuable Article Award

as voted by hundreds of G&G *readers. We extend our sincerest thanks to all the subscribers who participated.*

The votes are in, and we're pleased to announce the winners of the 2009 Dr. Edward J. Gübelin Most Valuable Article Award. For the second year, we opened the competition to online voting, and nearly 90% of this year's votes came from the online ballot.

The first-place article was "The 'Type' Classification System of Diamonds and Its Importance in Gemology" (Summer 2009), a guide to determining diamond type as well as its implications for identifying treated and synthetic diamonds. Placing second was "The French Blue and the Hope: New Data from the Discovery of a Historical Lead Cast" (Spring 2009), which used computer modeling and a recently found lead model of the French Blue to reveal important details about this fabled gem. Third place went to "Ruby and Sapphire Production and Distribution: A Quarter Century of Change" (Winter 2009), a review of the sources, treatments, and global developments that have transformed the corundum market.

• *First Place*

The "Type" Classification System of Diamonds and Its Importance in Gemology

Christopher M. Breeding and James E. Shigley

Christopher M. Breeding is a research scientist at the GIA Laboratory in Carlsbad, where he investigates origin of color in diamond and other gems. Dr. Breeding holds a PhD in geology from Yale University. **James E. Shigley** is distinguished research fellow at the GIA Laboratory in Carlsbad. The editor of the *Gems & Gemology in Review* series and contributing editor to the journal, he received his doctorate in geology from Stanford University.

Christopher M. Breeding

James E. Shigley

Dr. Edward J. Gübelin
MVA


François Farges


Scott Sucher


Herbert Horovitz


Jean-Marc Fourcault

•• *Second Place*

The French Blue and the Hope: New Data from the Discovery of a Historical Lead Cast

François Farges, Scott Sucher, Herbert Horovitz, and Jean-Marc Fourcault

François Farges is professor of environmental mineralogy at the Muséum National d'Histoire Naturelle (MNHN) in Paris, where he is also curator of France's national gem and mineral collection, established in 1633. Dr. Farges received his PhD in geochemistry from the University of Paris. **Scott Sucher** is principal of The Stonecutter in Tijeras, New Mexico. A former U.S. Air Force instructor pilot, he has created replicas of famous diamonds for more than 30 years. **Herbert Horovitz** is a jeweler in Geneva, Switzerland, who specializes in jewelry history. He studied jewelry at the Decorative Arts School of Geneva and is an avid collector of books on jewelry and gemstones. **Jean-Marc Fourcault** is the technician in charge of the mineral collection at MNHN. He specializes in microminerals and is vice director of Micromonteurs, a French microminerals society.


Russell Shor


Robert Weldon

••• *Third Place*

Ruby and Sapphire Production and Distribution: A Quarter Century of Change

Russell Shor and Robert Weldon

Russell Shor is senior industry analyst at GIA in Carlsbad. Well known in the industry for his reporting as diamond editor of *Jewelers' Circular Keystone* from 1980 to 1995, he also served as editor of *New York Diamonds* and *GemKey*. Mr. Shor has a degree in journalism from Temple University. **Robert Weldon,** a Graduate Gemologist, is manager of photography and laboratory publications at GIA in Carlsbad. Formerly senior writer and director of photography with *Professional Jeweler* and senior editor of colored gemstones at *Jewelers' Circular Keystone*, Mr. Weldon has contributed to scores of international publications and several gem-related books.

Congratulations to Ruediger Hein of Henderson, Nevada,
whose ballot was drawn from the many entries to win a three-year subscription to Gems & Gemology, *along with all three* Gems & Gemology in Review *volumes:* Treated Diamonds, Colored Diamonds, *and* Synthetic Diamonds.

What's *missing* from your collection?

Spring–Winter 2009

Spring 2006
"Paraíba"-type Tourmaline from Brazil, Nigeria, and Mozambique: Chemical Fingerprinting by LA-ICP-MS
Identification and Durability of Lead Glass–Filled Rubies
Characterization of Tortoise Shell and Its Imitations

Summer 2006
Applications of LA-ICP-MS to Gemology
The Cullinan Diamond Centennial
The Effects of Heat Treatment on Zircon Inclusions in Madagascar Sapphires
Faceting Transparent Rhodonite from New South Wales, Australia

Fall 2006—Special Issue
Proceedings of the 4th International Gemological Symposium and GIA Gemological Research Conference

Winter 2006
The Impact of Internal Whitish and Reflective Graining on the Clarity Grading of D-to-Z Diamonds at the GIA Laboratory
Identification of "Chocolate Pearls" Treated by Ballerina Pearl Co.
Leopard Opal from Mexico
The Cause of Iridescence in Rainbow Andradite from Japan

Spring 2007
Pink-to-Red Coral: Determining Origin of Color
Serenity Coated Colored Diamonds
Trapiche Tourmaline from Zambia

Summer 2007
Global Rough Diamond Production since 1870
Durability Testing of Filled Diamonds
Chinese Freshwater Pearl Culture
Yellowish Green Diopside and Tremolite from Tanzania
Polymer-Impregnated Turquoise

Fall 2007
The Transformation of the Cultured Pearl Industry
Nail-head Spicule Inclusions in Natural Gemstones
Copper-Bearing Tourmalines from New Deposits in Paraíba State, Brazil
Type Ia Diamond with Green-Yellow Color Due to Ni

Winter 2007
Latest CVD Synthetic Diamonds from Apollo Diamond Inc.
Yellow Mn-Rich Tourmaline from Zambia
Fluorescence Spectra of Colored Diamonds
An Examination of the Napoleon Diamond Necklace

Spring 2008
Copper-Bearing (Paraíba-type) Tourmaline from Mozambique
A History of Diamond Treatments
Natural-Color Purple Diamonds from Siberia

Summer 2008
Emeralds from Byrud (Eidsvoll), Norway
Creating a Model of the Koh-i-Noor Diamond
Coated Tanzanite
Coloring of Topaz by Coating and Diffusion Processes

Fall 2008
Identification of Melee-Size Synthetic Yellow Diamonds
Aquamarine, Maxixe-Type Beryl, and Hydrothermal Synthetic Blue Beryl
A New Type of Synthetic Fire Opal: Mexifire
The Color Durability of "Chocolate Pearls"

Winter 2008
Color Grading "D-to-Z" Diamonds at the GIA Laboratory
Rubies and Sapphires from Winza, Tanzania
The Wittelsbach Blue

Spring 2009
The French Blue and the Hope: New Data from the Discovery of a Historical Lead Cast
Gray-Blue-Violet Hydrogen-Rich Diamonds from the Argyle Mine
Hackmanite/Sodalite from Myanmar and Afghanistan
Pink Color Surrounding Growth Tubes and Cracks in Cu Tourmalines from Mozambique
Identification of the Endangered Pink-to-Red Stylaster Corals by Raman Spectroscopy

Summer 2009
Celebrating 75 Years of *Gems & Gemology*
The "Type" Classification System of Diamonds
Spectral Differentiation Between Copper and Iron Colorants in Gem Tourmalines
Andalusite from Brazil
Peridot from Sardinia, Italy

Fall 2009
Characterization of "Green Amber"
Crystallographic Analysis of the Tavernier Blue
"Fluorescence Cage": Visual Identification of HPHT-Treated Type I Diamonds
Ammolite Update
Polymer-Filled Aquamarine
Yellow-Green Haüyne from Tanzania
Aquamarine from Masino-Bregaglia Massif, Italy

Winter 2009
Ruby and Sapphire Production and Distribution: A Quarter Century of Change
Cutting Diffraction Gratings to Improve Dispersion ("Fire") in Diamonds
Chrysoprase and Prase Opal from Haneti, Central Tanzania
Demantoid from Val Malenco, Italy

For a complete list of articles from 1981 forward, visit www.gia.edu/gandg.

GEMS & GEMOLOGY®

The Quarterly Journal That Lasts A Lifetime

Now Available Online:

All Articles and Issues 1981–2009

Get PDF Articles at gia.metapress.com

Electronic (PDF) versions of all articles from Spring 1981 forward are available as part of *Gems & Gemology* Online.

Order Print and PDF Back Issues at store.gia.edu
or Call Toll Free 800-421-7250 ext. 7142
or 760-603-4000 ext. 7142
Fax 760-603-4070

E-Mail gandg@gia.edu
or write to
Gems & Gemology
PO Box 9022, Carlsbad, CA
92018-9022, USA

Complete volumes of 1992–2009 print back issues are available, as are limited issues from 1985–1991.

10% discount for GIA Alumni and active GIA students.

Order Your BACK ISSUES CHARTS & BOOKS Today!

STRONGLY COLORED PINK CVD LAB-GROWN DIAMONDS

Wuyi Wang, Patrick Doering, Joshua Tower, Ren Lu, Sally Eaton-Magaña, Paul Johnson, Erica Emerson, and Thomas M. Moses

This study characterizes CVD laboratory-grown diamonds from Apollo Diamond Inc. that have strong pink colors produced by high concentrations of NV centers. The samples examined weighed ~0.3–0.7 ct, and their color and clarity grades were comparable to top natural pink diamonds. A combination of optical centers were detected using photoluminescence and absorption spectroscopy. These centers are similar to those seen in previously studied pink-to-red diamonds that have been exposed to HPHT annealing, followed by irradiation and annealing at relatively low temperatures. These pink CVD products can be separated from natural and treated-color natural pink diamonds by a combination of gemological and spectroscopic properties, such as fluorescence color, growth zoning, and absorption features in the infrared and UV-Vis regions.

In the past decade, significant progress has been made with synthetic diamonds produced by the chemical vapor deposition (CVD) method. Not only are larger sizes and better qualities being reported in the as-grown material, but multiple treatments have been applied to some CVD synthetic diamonds to improve their color after initial growth (e.g., Linares and Doering, 1999, 2010; Martineau et al., 2004; Yan et al., 2004; Meng et al., 2008; Wang and Johnson, 2010). Faceted CVD-grown diamonds are being traded in the jewelry market, with a few having been identified in gem laboratories during routine testing (e.g., Chadwick, 2008a,b; Wang, 2009; Kitawaki et al., 2010).

As grown, gem-quality CVD synthetic diamonds are typically colorless, near-colorless, or various tones of brown. Other colors can be introduced by modifying the occurrence or arrangements of particular lattice defects, either during growth or with post-growth treatments. In this study, we describe a group of strongly colored pink CVD lab-grown diamonds (e.g., figure 1) provided for examination by Apollo Diamond Inc. Standard gemological properties and spectroscopic data are presented, as well as key identification features that help separate these new products from natural, treated-natural, and HPHT-grown synthetic pink diamonds.

MATERIALS AND METHODS

Apollo Diamond provided 19 faceted CVD lab-grown diamonds to the GIA Laboratory for examination (table 1). They ranged from 0.27 to 0.72 ct, and showed remarkably saturated pink coloration. These CVD lab-grown diamonds are representative of the current pink-colored production process used at Apollo Diamond.

Experienced diamond grading staff determined

See end of article for About the Authors and Acknowledgments.
GEMS & GEMOLOGY, Vol. 46, No. 1, pp. 4–17.

color and clarity grades using GIA's grading systems (see, e.g., King et al., 1994). Internal features were examined with both a standard gemological binocular microscope and a research-grade microscope, using a variety of lighting techniques. Reactions to ultraviolet (UV) radiation were checked in a darkened room with a conventional four-watt combination long-wave (365 nm) and short-wave (254 nm) UV lamp. We also examined all samples for fluorescence, phosphorescence, and growth characteristics using the Diamond Trading Company (DTC) DiamondView instrument (e.g., Welbourn et al., 1996). Phosphorescence images were collected with a 0.1 second delay and 5 seconds of exposure duration.

All spectroscopic analyses were conducted on all samples. We performed infrared absorption spectroscopy for the mid-IR (6000–400 cm^{-1}, at 1 cm^{-1} resolution) and near-IR (up to 11000 cm^{-1}, at 4 cm^{-1} resolution) ranges at room temperature with a Thermo-Nicolet Nexus 670 Fourier-transform infrared (FTIR) spectrometer equipped with KBr and quartz beam splitters. A beam condenser (6×) was employed to focus the incident beam on the sample, and we collected as many as 256 scans per spectrum to improve the signal-to-noise ratio. Dry N_2 gas was used to purge the sample chamber to reduce interference from CO_2 and water vapor in air. The spectra in the mid-IR region were normalized based on the two-phonon absorptions of diamond, and in the near-IR region based on its three-phonon absorptions. This allowed us to calculate absorption coefficients, as well as peak intensities and impurity concentrations.

Absorption spectra in the ultraviolet through visible to near-infrared range (UV-Vis-NIR, 250–1000 nm) were recorded with a custom-built instrument using multiple Avantes spectrometers, broad-band light sources, and CCD detectors. This high-resolution instrumentation enabled the detection of very weak and sharp absorptions in the UV-Vis-NIR region at liquid nitrogen temperature. The sampling interval in this four-channel device was 0.04–0.07 nm depending on specific wavelength ranges, with an entrance slit width in each spectrometer of 10 µm. A better than 0.2 nm spectral resolution was achieved. A very good signal-to-noise ratio was produced with 200 scans per spectrum. Samples were immersed in a specially designed liquid nitrogen bath which contains multiple layers of liquid nitrogen (patent pending), ensuring consistent temperature as well as a stable environment free of nitrogen gas bubbles.

Figure 1. These CVD lab-grown diamonds (0.27–0.62 ct; sample nos. top–APD-8097, APD-9747, and bottom–APD-17, APD-21), produced recently by Apollo Diamond Inc., show strong pink colors that are comparable to top natural pink diamonds. They were color graded Fancy Intense to Fancy Vivid pink to purplish pink. Composite photo by Jian Xin (Jae) Liao.

The same cooling device was also used for photoluminescence (PL) spectral analysis with a Renishaw InVia Raman confocal microspectrometer. Four lasers with five excitation wavelengths were employed to activate various types of defects. An argon-ion laser was operated at two excitation wavelengths: 488.0 nm (for the range 490–850 nm) and 514.5 nm (for the range 517–850 nm). PL spectra were collected in the 640–850 nm range using a He-Ne laser (632.8 nm), and in the 835–1000 nm range using a diode laser (830.0 nm). In addition, a He-Cd metal-vapor laser (325.0 nm) was used for the 370–800 nm range. Up to three scans were accumulated for all PL analyses to achieve a better signal-to-noise ratio.

RESULTS

Color. All the samples had a strongly saturated pink hue, with color grades ranging from Fancy Intense

TABLE 1. Pink CVD lab-grown diamonds from Apollo Diamond Inc. examined for this study.

Sample no.	Weight (ct)	Cut	Color	Clarity	Fluorescence to long-wave UV	Fluorescence to short-wave UV
APD-11	0.63	Round brilliant	Fancy Vivid purple pink	VS_1	Strong orange	Moderate orange
APD-12	0.63	Rectangular brilliant	Fancy Vivid purplish pink	VS_1	Strong orange	Strong orange
APD-13	0.61	Round brilliant	Fancy Vivid purple pink	VS_1	Strong orange	Moderate orange
APD-14	0.65	Round brilliant	Fancy Vivid purplish pink	VS_2	Strong orange	Moderate orange
APD-15	0.72	Rectangular brilliant	Fancy Deep purplish pink	VS_2	Strong orange	Strong orange
APD-16	0.64	Round brilliant	Fancy Intense purplish pink	VS_2	Strong orange	Strong orange
APD-17	0.62	Rectangular brilliant	Fancy Deep pink	VS_1	Strong orange	Moderate orange
APD-18	0.45	Round brilliant	Fancy Intense pink	VS_1	Strong orange	Moderate orange
APD-19	0.53	Square brilliant	Fancy Intense pink	VS_1	Moderate orange	Moderate orange
APD-20	0.61	Round brilliant	Fancy Intense pink	VS_1	Moderate orange	Moderate orange
APD-21	0.27	Square brilliant	Fancy Vivid pink	VS_2	Strong orange	Moderate orange
APD-22	0.38	Rectangular brilliant	Fancy Deep pink	SI_1	Moderate orange	Moderate orange
APD-8094	0.48	Round brilliant	Fancy Vivid purplish pink	VS_1	Strong orange	Strong orange
APD-8095	0.67	Round brilliant	Fancy Vivid purple pink	VS_1	Strong orange	Strong orange
APD-8096	0.28	Round brilliant	Fancy Intense purplish pink	VVS_2	Moderate orange	Strong orange
APD-8097	0.36	Round brilliant	Fancy Intense purplish pink	VS_1	Strong orange	Strong orange
APD-9747	0.60	Rectangular brilliant	Fancy Vivid purple pink	VS_1	Moderate orange	Moderate orange
APD-9748	0.64	Round brilliant	Fancy Intense pink	VS_2	Moderate orange	Moderate orange
APD-9749	0.47	Round brilliant	Fancy Deep purplish pink	SI_2	Moderate orange	Moderate orange

to Fancy Deep (again, see figure 1 and table 1). Seven samples were pure pink; the remaining 12 also had a purple component. In general, all the CVD-grown diamonds showed even color distribution with no visible color concentrations.

Clarity. The samples had relatively high clarity. As shown in table 1, most (16) were given VS clarity grades, one was VVS, and only two received SI grades. Clarity grades were usually impacted by pinpoints and small black inclusions with irregular shapes (probably non-diamond carbon; figure 2). Small radial fractures were observed surrounding some of the relatively large inclusions. Typically, the small inclusions and pinpoints were randomly distributed. In two samples, they occurred together in cloud-like groups.

Reaction to UV Radiation. All the samples consistently showed moderate-to-strong orange fluorescence to both long- and short-wave UV radiation. Obvious turbidity (i.e., "chalkiness") was also observed. No phosphorescence to conventional long- or short-wave UV radiation was seen.

When exposed to the high-intensity ultra-short UV wavelength of the DTC DiamondView (~225 nm), all samples showed strong orange or orangy red fluorescence (figure 3). The fluorescence was evenly distributed in only three of the samples; all others had bands of weaker orange color. In general, the fluorescence bands were uniform in thickness—though thickness varied in portions of some samples—with sharp, well-defined boundaries that were oriented nearly parallel to the table facet (figure 3, center and right). Narrow growth striations, a common feature in CVD-grown diamond, were

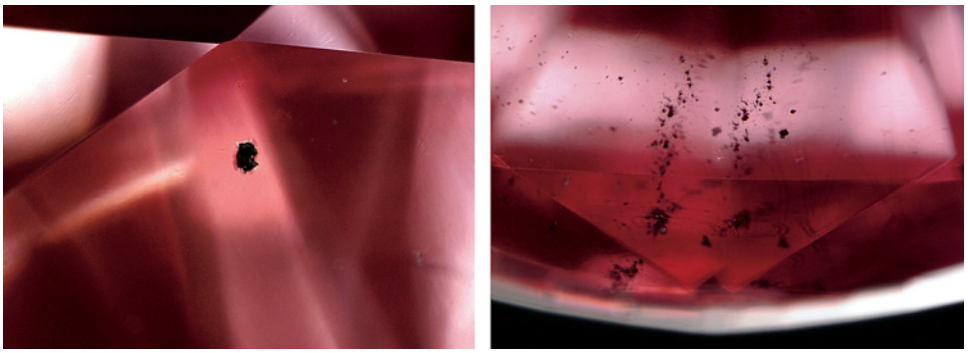

Figure 2. Most of the samples had VS clarity grades. The internal features that most affected clarity were small black inclusions (left, image width 1.4 mm) with irregular morphology and occasionally with small radial fractures, and pinpoints (right, image width 1.7 mm). Photomicrographs by W. Wang.

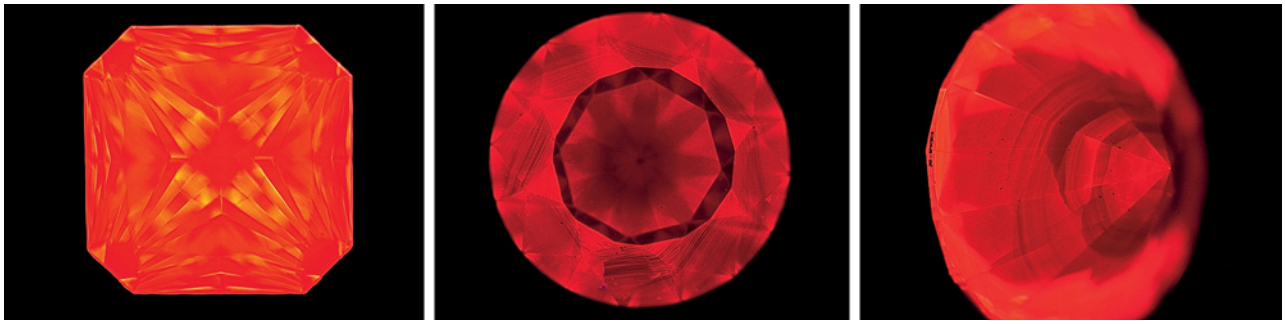

Figure 3. These pink CVD-grown diamonds display strong orange to orangy red fluorescence in the DiamondView. The fluorescence is typically chalky, as shown on the left (0.63 ct). Most samples showed bands of weaker orange fluorescence oriented nearly parallel to the table face (center and right; 0.28 and 0.47 ct, respectively). Characteristic striated growth features also are readily seen in the center sample. Photos by W. Wang.

NEED TO KNOW

- CVD laboratory-grown diamonds from Apollo Diamond Inc. have strongly saturated pink colors produced by high concentrations of NV centers.
- The samples show distinctive moderate-to-strong orange UV fluorescence (typically banded) to both long- and short-wave UV radiation.
- Internal graining, high strain, and zoned orange fluorescence, along with spectral features, distinguish these from similar-appearing natural, treated, and other synthetic diamonds.

observed in the DiamondView fluorescence of many of the samples. In addition, all samples had a weak-to-moderate orange-red phosphorescence reaction in the DiamondView (see images in the *G&G* Data Depository at www.gia.edu/gandg).

Graining and Birefringence. Graining was a common feature in all the Apollo CVD lab-grown diamonds studied. However, in contrast to that observed in natural diamonds, the internal graining in most of the CVD samples had indistinct boundaries. A few samples, however, had graining with relatively well-defined linear outlines (figure 4).

Varying intensity of anomalous double refraction was another important feature. When we viewed these synthetic diamonds with magnification and crossed polarizers, we saw low- to very high-order interference colors including red, blue, green, and even white (figure 5), with irregular, linear, or occasionally cross-hatched "tatami" type patterns. Extremely high-order interference colors with characteristic symmetrical patterns were commonly seen surrounding small black inclusions—a good indication of high localized internal strain.

Wang et al. (2007) reported the presence of distinct laser grooves on some of the cylindrical CVD samples they documented. The grooves remained on the girdles after the samples were faceted. In this study, similar laser grooves were observed on two of the samples that had unpolished girdles. In both samples, however, they were far less apparent than on the faceted samples examined for the earlier report, with the edges being more rounded (figure 6).

Infrared Absorption Spectroscopy. Defect-related absorptions were observed in three IR regions (1500–1100, 3300–2700, and 7000–5800 cm^{-1}). The main features in the 1500–1100 cm^{-1} region (figure 7) included a sharp peak at 1344 cm^{-1} and a broad band at ~1130 cm^{-1} attributed to isolated nitrogen, a

Figure 4. Internal graining was difficult to see in this group of CVD lab-grown diamonds. In a few samples, the graining formed straight lines. Photomicrograph by W. Wang; image width 2.1 mm.

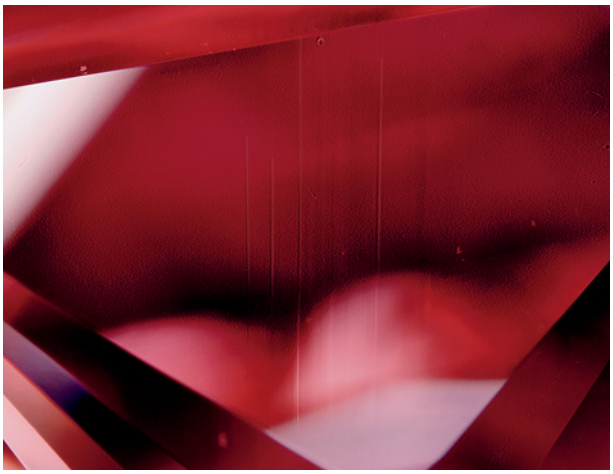

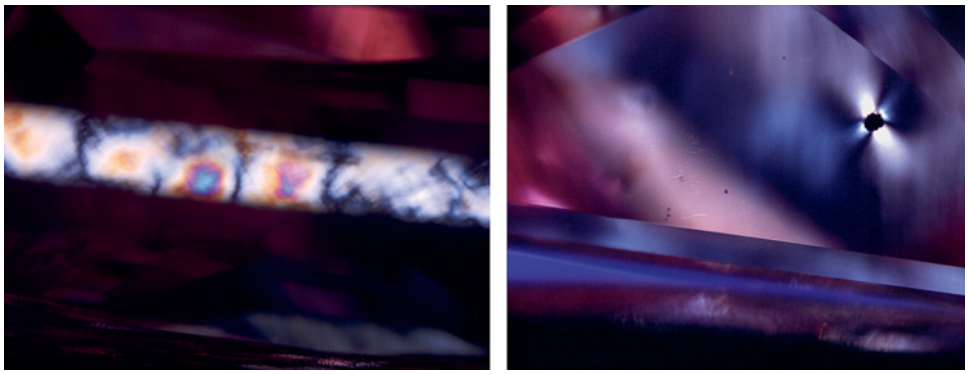

Figure 5. Anomalous double refraction commonly was seen as low- to high-order interference colors in the samples (left, image width 2.2 mm). Very high-order interference colors also surround this black inclusion (right, image width 1.8 mm). Photomicrographs by W. Wang.

sharp and relatively strong peak at 1332 cm^{-1} possibly from positively charged nitrogen (N^+; Lawson et al., 1998), a sharp H-related peak at 1405 cm^{-1}, and absorption from the H1a defect at 1450 cm^{-1}. The H1a center is commonly observed in nitrogen-containing diamonds that have been irradiated and subsequently annealed at relatively low temperatures (~300°C; Clark et al., 1956). A few other sharp peaks at 1502, 1379, 1375, 1363, and 1341 cm^{-1} were also observed, but their assignments are not clear—except for the 1502 cm^{-1} peak, which is ascribed to interstitial nitrogen and may arise from a different charge state of the H1a center (Collins et al., 1988). In addition, we saw a broad band at ~1295 cm^{-1}, which was positioned significantly higher than the A form of aggregated nitrogen (1280 cm^{-1}). These absorption features were detected in all samples, but with some obvious variations in intensity. For example, the peak at 1341 cm^{-1} ranged from being as strong as the 1344 cm^{-1} peak to as weak as a minor shoulder. In general, though, these absorptions were very weak in intensity.

Since nitrogen impurities were detectable in all samples with IR spectroscopy, they were considered type I diamonds, despite being very close to type IIa. The intensity of the N-related 1344 cm^{-1} peak varied from 0.07 to 0.17 cm^{-1}, corresponding to 1.2–2.9 ppma of isolated nitrogen. Pink CVD lab-grown diamonds from Apollo examined by Wang et al. (2007) contained comparable amounts of isolated nitrogen, but those stones showed no IR features at 1502, 1450 (H1a), 1405, or 1295 cm^{-1} (again, see figure 7).

In the 3300–2700 cm^{-1} region (figure 8), the dominant absorption feature is the H-related band at 3107 cm^{-1} (0.23–0.82 cm^{-1} in intensity). The CVD-specific H-related peak at 3123 cm^{-1} is comparatively much weaker (0.01–0.03 cm^{-1}). Other absorptions in this region include weak peaks at 3310, 3030, 2990, 2975, 2949, and 2786 cm^{-1}, and broad bands at 2917, 2879, and 2835 cm^{-1}. Assignments of these absorptions in general are unclear. Note that the H-related peak at 3107 cm^{-1} was not detected in the pink Apollo CVD lab-grown diamonds examined previously (figure 8, bottom spectrum; Wang et al., 2007) or in other CVD samples from the same source (Wang et al., 2003).

Two extremely weak absorption peaks were detected in the near-IR region, at 6902 and 5892 cm^{-1} (figure 9). These peaks have not been reported previously in CVD synthetic diamonds. Their intensities varied from 0.004 to 0.025 cm^{-1}, with a good positive correlation (see *G&G* Data Depository) that suggested they may originate from the same defect. The absorption at 7353 cm^{-1} and numerous other peaks

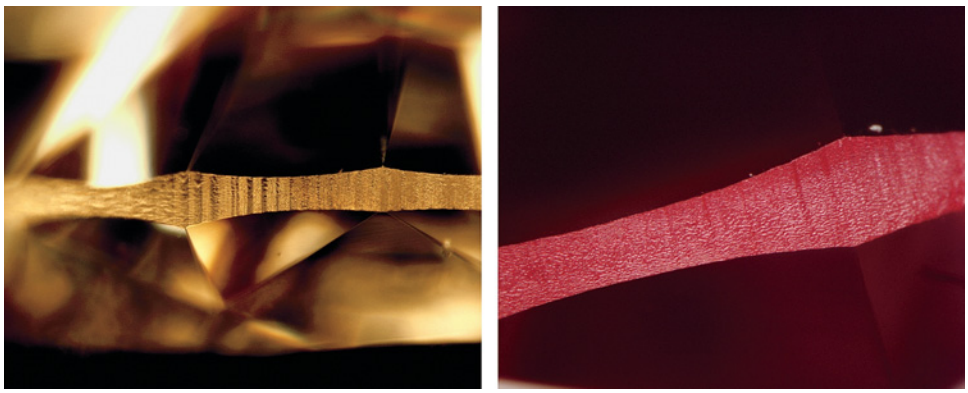

Figure 6. Two of the samples showed laser grooves on their girdles. Compared to the laser grooves seen on other CVD synthetic diamonds in a previous study (left; Wang et al., 2007), the grooves are not as sharp (right). Photomicrographs by W. Wang; image widths 1.1 mm (left) and 1.9 mm (right).

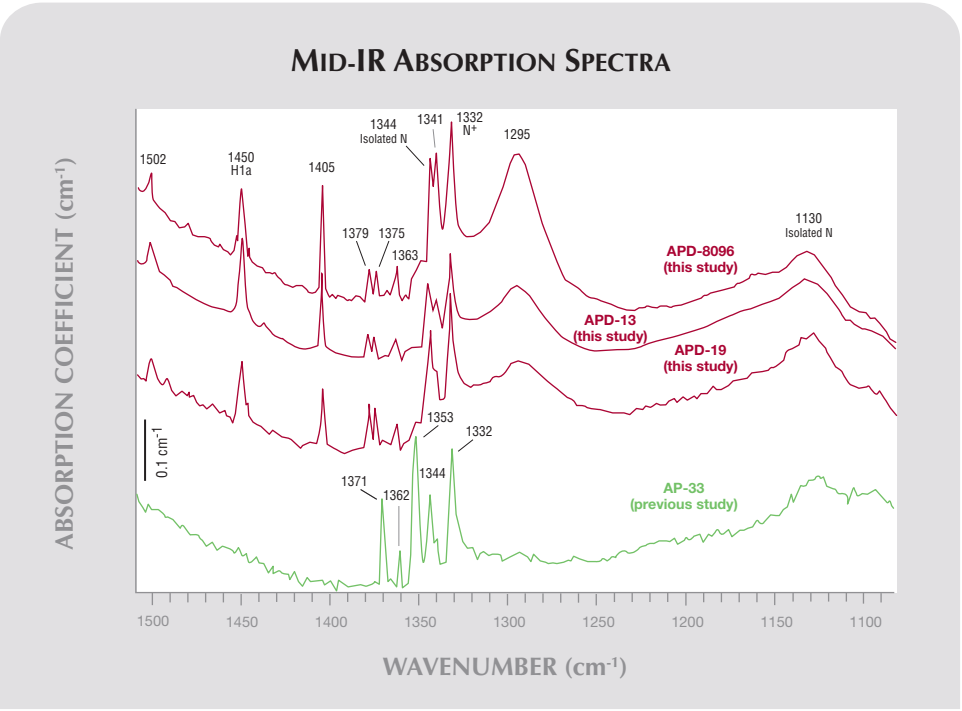

Figure 7. In the 1500–1100 cm^{-1} region of the IR spectrum, three representative pink CVD samples from the present study mainly show features due to isolated nitrogen, H-related defects, H1a, and possibly N^{+}, as well as several smaller unassigned absorptions. The band at ~1295 cm^{-1} is significantly higher in wavenumber than that due to the A-form of aggregated nitrogen in diamond (1280 cm^{-1}). A representative spectrum (AP-33) from pink CVD synthetic diamonds previously reported by Wang et al. (2007) is shown for comparison. Spectra are shifted vertically for clarity.

reported in the previously examined pink CVD synthetic diamonds (Wang et al., 2007; not shown here) were not detected in the current samples.

UV-Vis-NIR Absorption Spectroscopy. Consistent and strong absorption features in our high-resolution spectra included 574.9 (NV^{0}), 594.3, and 637.0 (NV^{-}) nm, and their sidebands (figure 10). The peak at 594.3 nm is usually referred to as the "595 nm" feature in gemological publications, and is typical of high-energy-beam irradiation and annealing (e.g., Collins, 1982). A weak absorption from the H3

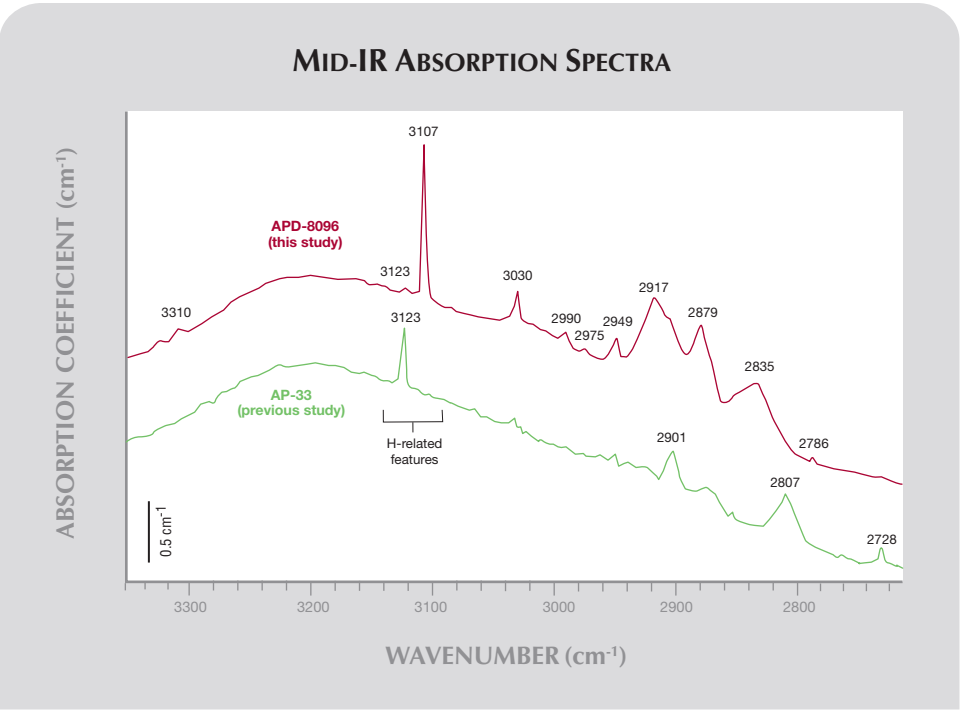

Figure 8. In contrast to typical CVD synthetic diamonds, the 3123 cm^{-1} optical center in these newer pink CVD products was very weak relative to the 3107 cm^{-1} H-related peak. The latter peak is usually absent from CVD synthetic diamonds, as shown by the representative spectrum of sample AP-33. Spectra are shifted vertically for clarity.

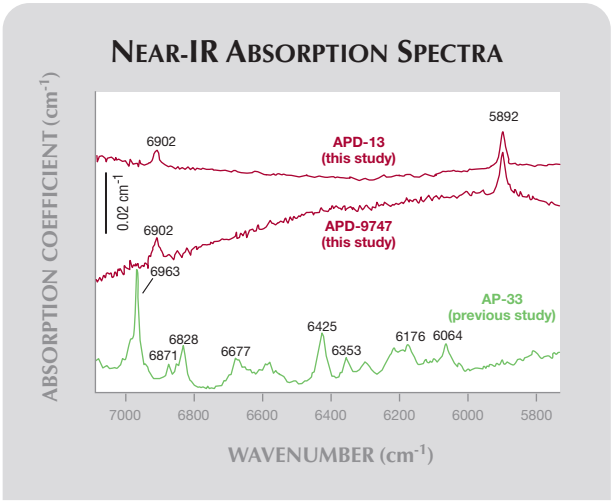

Figure 9. In the near-IR region, weak optical centers with correlative intensity were detected at 6902 and 5892 cm^{-1}. These peaks have not been reported in CVD-grown diamonds, while several other near-IR features typical of such products (e.g., spectrum of earlier sample AP-33) were not detected in this new group of samples. Spectra are shifted vertically for clarity.

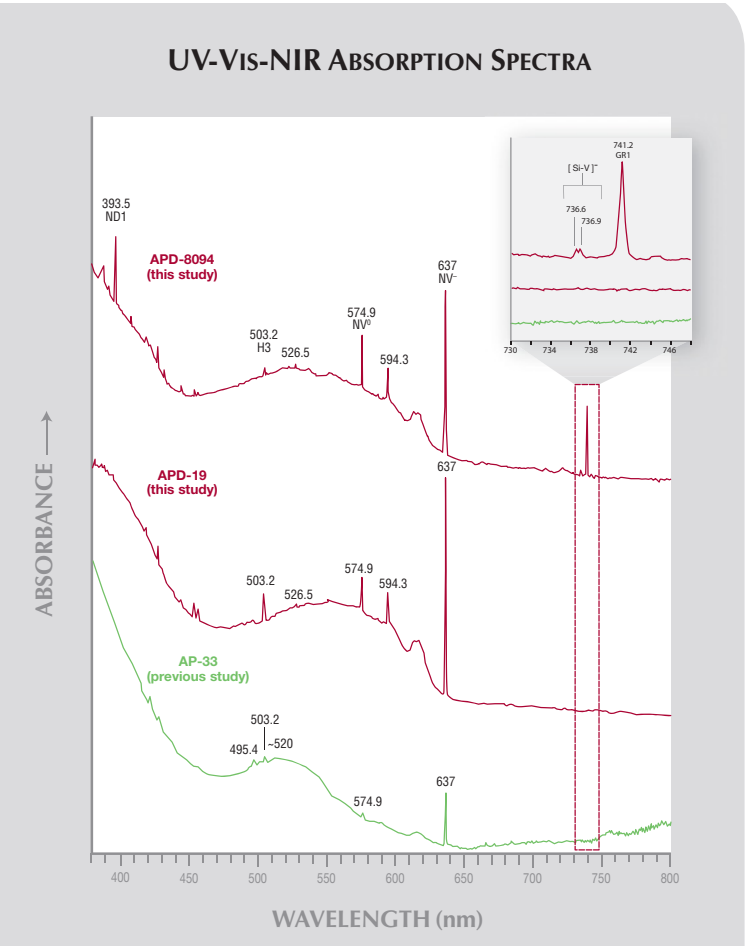

defect (503.2 nm) and a strong, broad band from isolated nitrogen centered at ~270 nm (not shown in the figures; Dyer et al., 1965) were also observed in all samples. It is important to note that the isolated-nitrogen concentration was high enough to be detected with both IR and UV-Vis absorption spectroscopy.

A sharp GR1 line with a zero phonon line (ZPL) at 741.2 nm and its related sidebands were recorded at varying intensities in all but two of the pink CVD samples. In those with a relatively strong GR1 line, additional absorptions from the ND1 defect (negatively charged vacancy) with ZPL at 393.5 nm and the [Si-V]$^-$ defect (doublet at 736.6/736.9 nm) were also observed (figure 10, inset). Only four samples did not show these Si-related absorptions in the UV-Vis-NIR spectra. In addition, several weak, sharp absorptions—including at 404.8, 424.7, 429.5, 430.4, 441.9, 451.6, 454.3, and 454.7 nm—were consistently observed but not attributed (figure 11).

Photoluminescence and Raman Spectroscopy. Many PL emission lines were recorded using five laser excitations in the UV-to-IR region. Some emission systems were observed with multiple excitation wavelengths. The major PL features are summarized below on the basis of individual laser excitation in each defect's most sensitive region.

With UV laser excitation (325.0 nm; figure 12), the major and consistent emissions in all samples included two weak but clear lines at 388.9 and 415.2 (N3) nm, with clear side bands at ~430 and ~440 nm that were associated with the N3 ZPL. (Note that PL side bands are located on the opposite side of the ZPL than they are in absorption spectroscopy.) The sharp line at 388.9 nm and the related broad bands at ~400 and 410 nm are attributed to the 389 nm center, which previously has been associated with radiation damage in all types of diamonds and is particularly strong in those containing isolated nitrogen (Zaitsev, 2001).

Figure 10. Strong absorptions due to the NV centers with ZPLs at ~637 and 574.9 nm effectively absorb light in the yellow, green, and orange regions of the visible spectrum, and create transmission windows above 637 nm (red) and at ~450 nm (blue component). In addition, defects such as GR1, 594.3 nm, and ND1 with varying intensities were detected. A representative spectrum of an earlier pink CVD synthetic diamond (AP-33) is shown for comparison. The inset shows the GR1 and [Si-V]$^-$ centers. Spectra are shifted vertically for clarity.

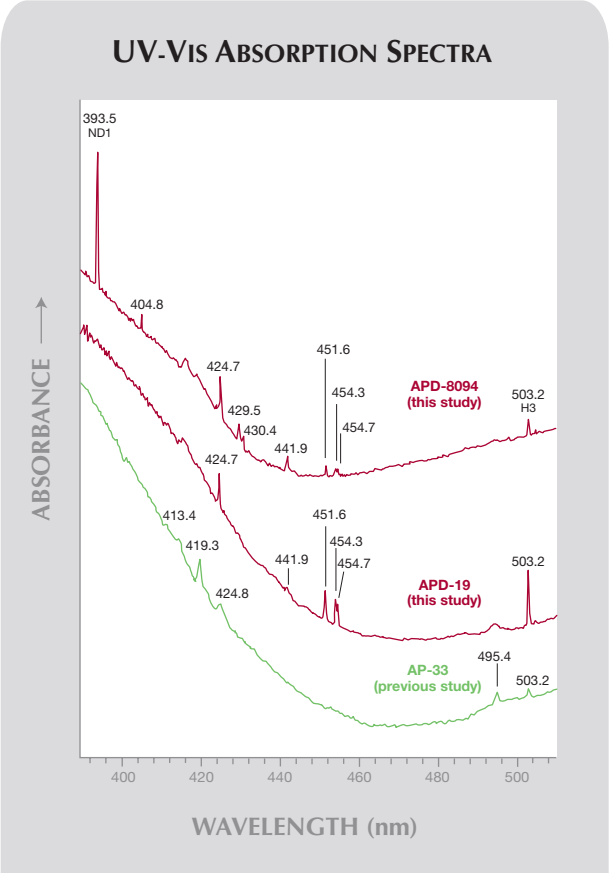

Figure 11. Several weak and sharp optical centers, such as those at 404.8, 424.7, 429.5, 430.4, 441.9, 451.6, 454.3, and 454.7 nm, were consistently observed in the absorption spectra of the present samples in the blue light region. These peaks have not been reported in previous CVD synthetic diamonds (e.g., AP-33). Spectra are shifted vertically for clarity.

PL spectra collected using blue laser (488.0 nm) excitation revealed relatively strong and consistent emissions in the 490–510 nm region (figure 13). Assignable emissions included the H4 (495.9 nm), H3 (503.2 nm), and 3H (503.5 nm) defects. Intensity of 3H emission varied significantly between samples, and did not show a clear correlation with other absorption or emission features. The 3H peak was clearly separated from H3 in four samples, occurred as a weak shoulder in six, and was not detected in the other nine. In addition, emissions at 498.2 and 505.0 nm were observed. All the emission centers described here were also present in the UV-Vis-NIR absorption spectra, but were weak due to a lower signal-to-noise ratio.

Green laser (514.5 nm) excitation revealed strong

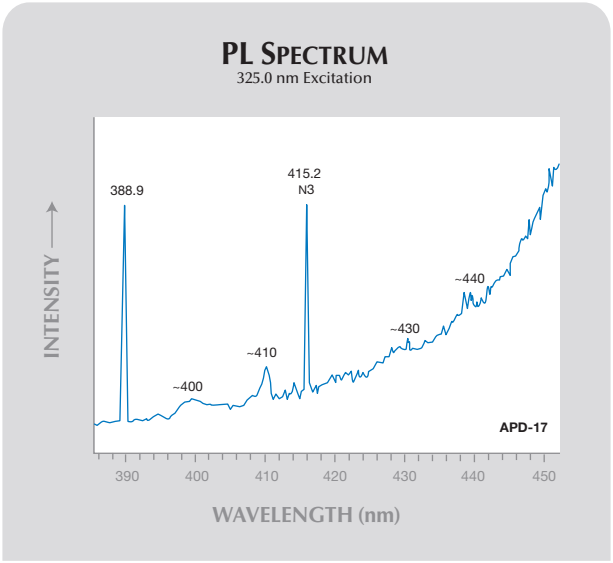

Figure 12. The PL spectra of all samples with 325.0 nm UV laser excitation revealed a line at 388.9 nm and a portion of the N3 system with ZPL at 415.2 nm.

NV center emission systems in all samples, with ZPLs at 574.9 and 637.0 nm (figure 14). The 574.9 nm line was generally stronger. The 637.0/574.9 intensity ratio ranged from 0.10 to 0.90, with an

Figure 13. Relatively strong and consistent PL emissions in the 490–510 nm region were observed with 488.0 nm laser excitation, including H4, H3, and 3H. The intensity of the 3H emission varied significantly from sample to sample. Spectra are shifted vertically for clarity.

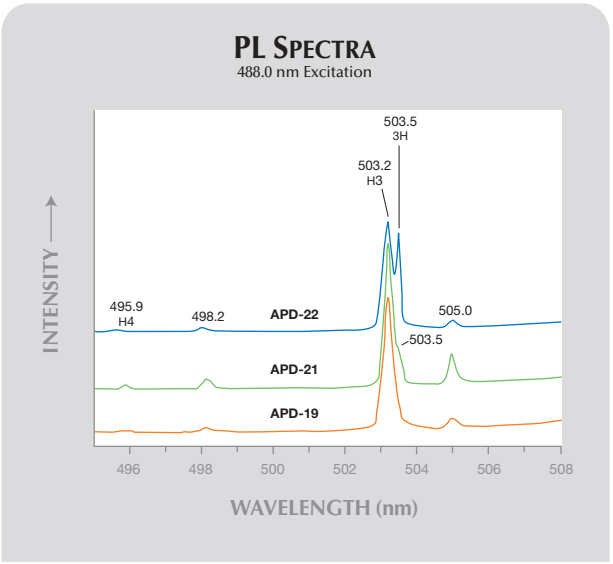

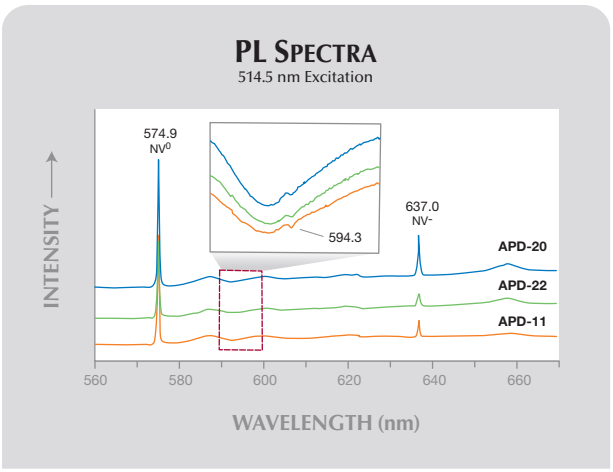

Figure 14. Green laser (514.5 nm) excitation revealed strong PL emission systems of NV centers in all the pink CVD-grown diamonds, with ZPLs at 574.9 and 637.0 nm. A doublet at 596.5 and 597.0 nm is common in CVD synthetic diamonds, but is absent here. Instead, a negative peak at 594.3 nm, also detected in the UV-Vis absorption spectra, is observed. Spectra are shifted vertically for clarity.

average of 0.34. The full width at half maximum (FWHM) of the 574.9 nm peak showed limited variation of 0.32–0.47 nm, with an average of 0.38 nm. In contrast, the FWHM of the 637.0 nm line varied from 0.35 to 0.74 nm, with an average of 0.50 nm. There was a positive correlation between the FWHMs of these two peaks, as seen in natural-color and HPHT-treated natural type IIa diamonds (see *G&G* Data Depository).

Doublet emission at 596.5 and 597.0 nm has been documented as a common feature of colorless, near-colorless, and brown CVD synthetic diamonds (Wang et al., 2003, 2007), but it was not detected in this group of pink CVD lab-grown stones. Instead, a negative peak at 594.3 nm, which was easily detected with UV-Vis absorption spectroscopy, was observed in the PL spectra. A similar negative GR1 peak (ZPL at 741.2 nm) was seen in all samples in which UV-Vis detected a GR1. (These negative peaks are actually caused by absorption features present when a luminescence spectrum is collected.) Due to the strong fluorescence from NV centers, Si-related defects could not be detected with 514.5 nm laser excitation.

When excited by a red laser (632.8 nm), the doublet emissions caused by the $[Si\text{-}V]^-$ defect at 736.6 and 736.9 nm (generally referred to as the 737 nm defect: Vavilov et al., 1980; Clark et al., 1995; Iakoubovskii et al., 2001) were confirmed in all but four samples (figure 15). In addition, emission from GR1 (741.2 nm) was observed in all but five samples. Of those that did not show GR1, three also had no detectable Si-related features, suggesting a possible correlation between these defects. Also, weak but consistent emissions at 796.9 and 806.4 nm (not shown) were observed in all samples. These features have not been reported in other CVD synthetic diamonds, and their assignments are unknown.

Analysis with the 830.0 nm laser revealed a weak but sharp emission at 945.5 nm in all samples from another Si-related defect, $[Si\text{-}V]^0$ (Evans et al., 2006). An emission at 949.0 nm, assignment of which is not available, also occurred. Many other weak lines were detected in the 840–910 nm region, including those at 866.7, 867.8, 876.7, and 878.3 nm, which are not attributable.

DISCUSSION

The pink Apollo CVD lab-grown diamonds examined here are notably different from previous gem-quality CVD products, which were colorless, near-colorless, or some shade of brown. Although pink CVD synthetic diamonds were reported by Wang et al. (2007), the strong pink hue and even color distri-

Figure 15. The 736.6 and 736.9 nm doublet due to $[Si\text{-}V]^-$ was recorded with varying intensity in the PL spectra of most of the present samples. The 632.8 nm laser was the most sensitive excitation for detecting this center, which was not resolved with the 514.5 nm laser. A weak correlation between this center and the GR1 was observed. Spectra are shifted vertically for clarity.

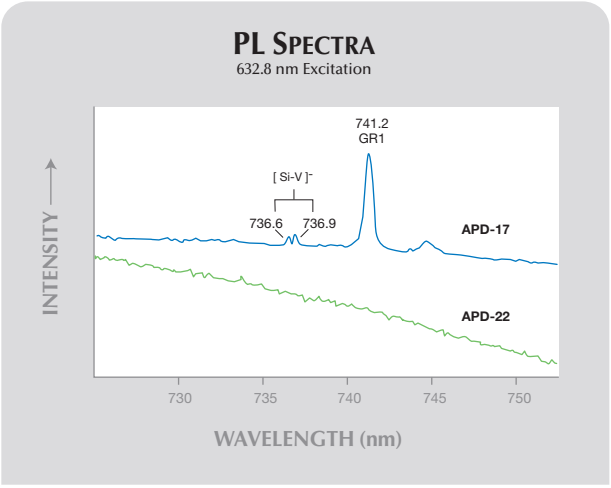

bution of the present samples are distinctive, and unlike those normally seen in natural or treated pink diamonds (e.g., Wang, 2009). In contrast to most previously examined CVD synthetics (Wang et al., 2003, 2007), these new samples did not contain surface-reaching fractures. The moderate-to-strong orange UV fluorescence to both long- and short-wave UV radiation was notably different from that previously reported for pink CVD lab-grown diamonds from Apollo (Wang et al., 2007), which displayed only very weak to weak orange to orangy yellow fluorescence to short-wave UV. The banded nature of the fluorescence in most of the new products is typical of CVD-grown diamonds. The high-order interference colors seen between crossed polarizers were in sharp contrast to the gray colors that are typical of natural type IIa diamonds, but comparable to other single-crystal CVD-grown diamonds.

The strong pink coloration of these new CVD samples is caused by NV centers, which efficiently absorb most yellow, green, and orange wavelengths. As a result, two transmission "windows" are created in the visible-light spectrum: one at a slightly higher wavelength than 637 nm, introducing a pink-to-red hue component to the bodycolor; and the other centered at ~450 nm, passing blue light and thus producing a blue component. Depending on the intensity of the blue transparency, many of the samples exhibited a strong pink color with varying amounts of a purple modifier. For example, the wavelength of maximum transmission in the blue region for sample APD-8094 was ~430 nm, toward the violet end of the visible spectrum, so the stone had a purplish hue. Sample APD-18, which had no purplish overtone, had maximum transmission at ~475 nm, toward the greenish end of the blue region. Sample AP-33 (from the previous study) was brownish pinkish orange; although it transmitted in the blue region at about the same position as APD-19, it lacked the NV^0 absorption (ZPL at 574.9 nm) needed to absorb the orange wavelengths.

Specific spectral features—such as a 3123 cm^{-1} absorption in the mid-IR region (Fuchs et al., 1995a,b); the 7353, 6855, 6425, and 5562 cm^{-1} absorptions in the near-IR region; and the doublet emissions at 596.5 and 597.0 nm—were common in previously studied CVD synthetic diamonds and were also important for their identification. However, the pink CVD lab-grown diamonds in this study had a distinctly different combination of lattice defects. In particular, H-related absorptions occurred dominantly at 3107 and 1405 cm^{-1}, while the 3123 cm^{-1} peak was extremely weak or nearly absent (again, see figures 7 and/or 8). The 3107 and 1405 cm^{-1} bands have not been previously reported in CVD synthetic diamonds, but they are common features of natural type Ia diamonds; they show correlated intensities and are attributed to the same H-related defect. A similar relationship in intensity between these two peaks was observed in this group of CVD lab-grown diamonds, indicating that they originate from the same defect as found in natural diamonds.

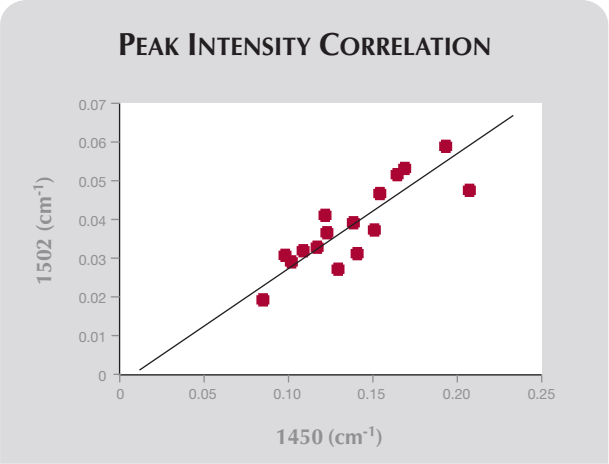

Figure 16. The intensities of the 1450 and 1502 cm^{-1} absorption peaks show good correlation, with a trend that can be extrapolated through the graph's origin.

The presence of some optical centers seen in previous studies of irradiated diamonds is another notable feature of these pink CVD synthetic diamonds. Absorption caused by H1a at 1450 cm^{-1} (again, see figure 7), which has been attributed to an interstitial defect seen in irradiated diamonds in a previous study (Collins et al., 1988), was observed in all samples. The positive correlation in intensity between the 1450 and 1502 cm^{-1} bands (figure 16) suggests that the 1502 cm^{-1} center is also related to this defect center. Other well-known defects—including GR1, ND1, 594.3 nm, and 388.9 nm—were observed in the UV-Vis and/or PL spectra (again, see figures 10 and 12). Furthermore, there were no doublet emissions at 596.5 and 597.0 nm in the PL spectra, and the previously documented (Wang et al., 2007) absorptions at 7353, 6855, 6425, and 5562 cm^{-1} in the near-IR region were also absent from this group of pink CVD lab-grown diamonds (figure 9).

Lattice Defect Configurations. Intense brown coloration is common in CVD synthetic diamonds produced at a high growth rate. As in natural type IIa diamonds, brown in CVD synthetics can be reduced by high-temperature annealing (Wang et al., 2003; Charles et al., 2004; Yan et al., 2004; Meng et al., 2008), although the causes of the brown hue in this material are not fully understood (Jones, 2009). Occasionally, HPHT-annealed CVD synthetic diamonds have been submitted to gem laboratories for identification (e.g., Chadwick, 2008a,b; Wang and Johnson, 2010; Kitawaki et al., 2010).

The characteristics of the H-related features in the present samples are particularly noteworthy: the near-absence of the 3123 cm^{-1} line and the presence of the 3107 cm^{-1} absorption. Cruddace et al. (2007) proposed that the 3123 cm^{-1} absorption in CVD synthetic diamond corresponded to the NVH^- center, and Cruddace (2007) found that in most cases this line annealed out above 1500°C. Meng et al. (2008) also found that the 3123 cm^{-1} line (reported as 3124 cm^{-1}) disappeared after annealing at 1600°C for 10 minutes. (However, Khan et al. [2009] observed that heating below 600°C caused NVH^0 to be converted to NVH^-, resulting in the disappearance of the 3123 cm^{-1} line. It was therefore proposed that this line is in fact related to NVH^0 rather than NVH^-.) The 3107 cm^{-1} absorption was not reported in any of these annealing experiments, but Charles et al. (2004) found that it was not generated until the temperature reached 2200°C.

Adding low concentrations of nitrogen to the CVD growth environment can have an important impact on the growth rate, as well as on the nature and concentrations of the defects that are incorporated as the material grows (Teraji and Ito, 2004; Tallaire et al., 2006). In most studies of CVD-grown diamond, most incorporated nitrogen is detected in the single substitutional (i.e., isolated) form, with smaller amounts detected in the NV^0 and NV^- states.

The H3 defect [$(NVN)^0$, 503.2 nm] forms in nitrogen-bearing diamonds through combination of the nitrogen A aggregate and a vacancy. This defect is often found in diamonds that have been irradiated and annealed at relatively high temperatures (e.g., Collins, 1982, 2001) or is associated with distinct plastic deformation features. While common in irradiated/annealed type Ia diamonds, varying concentrations of the H3 defect also occur in some natural-color type Ia diamonds. The presence of H3 centers was confirmed in both PL and absorption spectroscopy (again, see figures 10, 11, and 13).

With low-temperature PL spectroscopy, NV centers are almost always detected in as-grown CVD synthetic diamonds, except for rare high-purity samples (Martineau et al., 2004; Wang et al., 2005b). While NV emissions may be dominant in PL spectra, typically they are virtually undetectable or very weak in UV-Vis absorption spectra and have little, if any, effect on bodycolor. In the CVD samples in this study, however, high concentrations of NV centers were evident in our spectroscopic studies and also were the main cause of the pink color and distinctive orange fluorescence.

Si-related Optical Centers in Diamond. The pink CVD lab-grown diamonds in this study displayed relatively high concentrations of Si-related defects compared to those in other reports (Wang et al., 2003; 2005b; 2007; Martineau et al., 2004). Among the 19 samples analyzed, 15 showed detectable 737 nm lines (attributed to the negatively charged silicon split-vacancy $[Si\text{-}V]^-$) with the use of UV-Vis absorption spectroscopy, which was not sensitive enough to detect Si-related optical centers in previous CVD synthetic diamonds. A weak, but clear, 945.5 nm line (attributed to the neutral silicon split-vacancy $[Si\text{-}V]^0$) occurred in the PL spectra of all samples. This is the first report of a 945.5 nm center in CVD lab-grown diamonds from Apollo Diamond Inc. The 737 nm line was not observed in the PL spectra of four samples, probably due to the high spectral background from the luminescence of NV centers. The presence of Si-related defects is an important, but not unique, feature of CVD synthetic diamonds. Si-related defects also have been observed in a few natural diamonds (Breeding and Wang, 2008; GIA unpublished data).

Pink Diamond: Natural, Treated, and Synthetic. Two features are associated with pink color in natural untreated diamonds: NV centers and the 550 nm band (e.g., Collins, 1982). Natural pink diamonds colored by NV centers are type IIa and usually have very low color saturation, based on GIA's experience testing many samples of this type in the laboratory. In contrast, those that are colored by the 550 nm band, which include type IIa diamonds as well as type Ia diamonds from the Argyle mine, typically are more highly saturated. Purple modifiers are also common in those stones.

Several treatment techniques have been devel-

Figure 17. Some of Apollo Diamond's gems have been set into attractive jewelry. The 14K white gold pendant contains a 0.45 ct pink CVD lab-grown diamond surrounded by colorless CVD gems with a total weight of 1.03 ct. The CVD-grown diamonds in the platinum ring have a total weight of 1.08 ct. Courtesy of Bostonian Jewelers, Boston; photo by Robert Weldon.

oped to introduce a pink-to-red hue into both natural and synthetic diamonds. HPHT annealing has been used to enhance the pre-existing 550 nm band and thus intensify the pink color of a diamond, but the method depends on the properties of the starting material and is suitable primarily for type IIa diamonds (Hall and Moses, 2000; Fisher et al., 2009). (In addition, no laboratory process to create the 550 nm absorption band has been reported; Collins, 1982, 2001.) Consequently, enhancement of the 550 nm band can produce only very limited quantities of pink diamonds.

The other widely used technique involves conversion of trace amounts of isolated nitrogen into NV centers through a combination of irradiation and annealing processes. The trace amounts of isolated nitrogen needed for such a treatment (1) can occur naturally in the starting materials (i.e., as in type Ib diamonds), (2) can be generated at high temperatures by disaggregation of other nitrogen-bearing defects in natural diamonds through HPHT treatment, or (3) can be incorporated during synthetic growth. Treated orange, pink, or red diamonds from natural starting materials (Wang et al., 2005c; Wang, 2009) and from HPHT-grown synthetic starting materials (Shigley et al., 2004) have been well documented. The samples described in this study, however, are the first group of CVD synthetic diamonds GIA has examined with pink color caused by NV centers, and this also was documented in treated-color red natural diamonds in which the NV centers were produced by HPHT annealing and subsequent irradiation and annealing at relatively low temperatures (Wang et al., 2005a).

Compared to the intense pink or purplish pink coloration of the CVD-grown diamonds in this study (again see, e.g., figure 1; also figure 17), the previous generation of pink CVD products from Apollo Diamond (Wang et al., 2007) displayed obvious brown and orange modifiers, as well as much weaker saturation. Despite some absorption from NV centers, those earlier samples were mainly colored by a broad absorption band centered at ~520 nm, and they showed significant differences in their IR and UV-Vis absorption features. Twitchen et al. (2007) successfully developed orange-to-pink colorations when they annealed brown CVD synthetic diamonds, but their

samples showed no typical radiation-related optical centers.

In brief, the strongly colored pink CVD-grown diamonds examined for this study show many similarities in gemological and spectroscopic features with treated orange-pink-red diamonds that were exposed to HPHT annealing followed by irradiation and annealing at relatively low temperatures (Wang et al., 2005a,c).

Identification Features. Separation of these treated pink CVD lab-grown diamonds from other pink diamonds can be readily achieved using various gemological and spectroscopic features. Outstanding gemological features of this group of pink CVD synthetic diamonds include a strong and even color saturation, internal graining with indistinct boundaries or well-defined linear outlines, a high degree of internal strain, black inclusions with irregular morphologies and/or pinpoint inclusions, and moderate-to-strong orange fluorescence to both long- and short-wave UV radiation. The DiamondView fluorescence images displayed a banded structure and characteristic striated growth pattern. This is a key feature in separating these CVD-grown diamonds from other pink-to-red diamonds, either natural-color or treated-color from natural or HPHT-grown synthetic starting materials.

Useful spectroscopic properties include absorptions at 3123 (very weak), 1502, 1450 (H1a), 1405, 1344, and 1295 cm^{-1} in the mid-IR region, and 6902 and 5892 cm^{-1} in the near-IR region. Strong absorptions from GR1, NV centers, 594.3 nm, and ND1 in the UV-Vis-NIR region are also useful. The occurrence of Si-related features in PL and absorption spectra continues to be one of the most useful characteristics for identifying CVD synthetic diamonds, including the strong pink samples examined in this study.

CONCLUSIONS

Highly saturated natural pink diamonds are rare. Consequently, several techniques have been developed to introduce pink color into natural and HPHT-grown synthetic diamonds. The CVD-grown diamonds examined in this study have pink hues that are comparable to those of their natural counterparts and offer a potential new source of attractive gems in the marketplace (again, see figure 17). Proper identification of this gem material can be achieved through a combination of standard gemological properties (e.g., unusual internal graining, high strain, and distinctive zoned orange fluorescence) and several characteristic spectroscopic features. There is no doubt that the growth technique will continue to improve, and CVD synthetic diamonds of better and better quality will be produced.

ABOUT THE AUTHORS

Dr. Wang (wwang@gia.edu) is director of research and development, Dr. Lu is research scientist, Mr. Johnson is coordinator of advanced testing, Ms. Emerson is research technician, and Mr. Moses is senior vice president at the GIA Laboratory, New York. Dr. Eaton-Magaña is research scientist at the GIA Laboratory, Carlsbad. Mr. Doering is vice president, and Mr. Tower is senior scientist, at Apollo Diamond Inc., Boston.

ACKNOWLEDGMENTS

The authors thank Ivana Balov, Siau Fung Yeung, and Dr. Christopher M. Breeding in the GIA Laboratory for their many suggestions and assistance in this study. Dr. Robert Linares and his team at Apollo Diamond are specially thanked for their continued cooperation with GIA and for their efforts to work with the jewelry industry to develop a better understanding of CVD synthetic diamonds.

REFERENCES

Breeding C.M., Wang W. (2008) Occurrence of the Si-V defect in natural colorless gem diamonds. *Diamond and Related Materials*, Vol. 17, No. 7–10, pp. 1335–1344.

Chadwick K. (2008a) Lab Notes: First CVD synthetic diamond submitted for dossier grading. *G&G*, Vol. 44, No. 1, pp. 67–69.

Chadwick K. (2008b) Lab Notes: HPHT-treated CVD synthetic diamond submitted for dossier grading. *G&G*, Vol. 44, No. 4, pp. 365–367.

Charles S.J., Butler J.E., Feygelson B.N., Newton M.E., Carroll D.L., Steeds J.W., Darwish H., Yan C.-S., Mao H.K., Hemley R.J. (2004) Characterization of nitrogen doped chemical vapor deposited single crystal diamond before and after high pressure, high temperature annealing. *Physica Status Solidi (a)*, Vol. 201, No. 11, pp. 2473–2485.

Clark C.D., Ditchburn R.W., Dyer H.B. (1956) Absorption spectra of natural and irradiated diamonds. *Proceedings of the Royal Society of London A*, Vol. 234, pp. 363–381.

Clark C.D., Kanda H., Kiflawi I., Sittas G. (1995) Silicon defects in diamond. *Physical Review B*, Vol. 51, No. 23, pp. 16681–16688.

Collins A.T. (1982) Colour centers in diamond. *Journal of Gemmology*, Vol. 18, No. 1, pp. 35–75.

Collins A.T., Davies G., Kanda H., Woods G.S. (1988) Spectroscopic studies of carbon-13 synthetic diamond. *Journal of Physics C: Solid State Physics*, Vol. 21, pp. 1363–1376.
Collins A.T. (2001) Colour of diamond and how it may be changed. *Journal of Gemmology*, Vol. 27, No. 6, pp. 341–359.
Cruddace R.C. (2007) Magnetic resonance and optical studies of point defects in single crystal CVD diamond. Ph.D. Thesis, University of Warwick, United Kingdom.
Cruddace R.C., Newton M.E., Smith H.E., Davies G., Martineau P.M., Twitchen D.J. (2007) Identification of the 3123 cm^{-1} absorption line in SC-CVD diamond as the NVH^- defect. *Proceedings of the 58th De Beers Diamond Conference*, Warwick, UK, July 11–13, pp. 15.1–15.3.
Dyer H.B., Raal F.A., Du Preez L., Loubser J.H.N. (1965) Optical absorption features associated with paramagnetic nitrogen in diamond. *Philosophical Magazine*, Vol. 11, pp. 763–774.
Evans D.J.F., Kelly C.J., Leno P., Martineau P.M., Taylor A.J. (2006) Silicon doped single crystal CVD diamond grown using silane. *Proceedings of 57th De Beers Diamond Conference*, Cambridge, UK, July 10–12, pp. 38–40.
Fisher D., Sibley S.J., Kelly C.J. (2009) Brown colour in natural diamond and interaction between the brown related and other colour-inducing defects. *Journal of Physics: Condensed Matter*, Vol. 21, article no. 364213 [10 pp.].
Fuchs F., Wild C., Schwarz K., Koidl P. (1995a) Hydrogen-related IR absorption in chemical vapour deposited diamond. *Diamond and Related Materials*, Vol. 4, No. 5–6, pp. 652–656.
Fuchs F., Wild C., Schwarz K., Muller-Sebert W., Koidl P. (1995b) Hydrogen induced vibrational and electronic transitions in chemical vapor deposited diamond, identified by isotopic substitution. *Applied Physics Letters*, Vol. 66, No. 2, pp. 177–179.
Hall M.S., Moses T. (2000) Gem Trade Lab Notes: Diamond—Blue and pink, HPHT annealed. *G&G*, Vol. 36, No. 3, pp. 254–255.
Iakoubovskii K., Adriaenssens G.J., Dogadkin N.N., Shiryaev A.A. (2001) Optical characterization of some irradiation-induced centers in diamond. *Diamond and Related Materials*, Vol. 10, No. 1, pp. 18–26.
Jones R. (2009) Dislocations, vacancies and the brown colour of CVD and natural diamond. *Diamond and Related Materials*, Vol. 18, pp. 820–826.
Khan R.U.A., Martineau P.M., Cann B.L., Newton M.E., Twitchen D.J. (2009) Charge transfer effects, thermo and photochromism in single crystal CVD synthetic diamond. *Journal of Physics: Condensed Matter*, Vol. 21, No. 36, article no. 364214 [9 pp.].
King J.M., Moses T.M., Shigley J.E., Liu Y. (1994) Color grading of colored diamonds at the GIA Gem Trade Laboratory. *G&G*, Vol. 30, No. 4, pp. 220–242.
Kitawaki H., Abduriyim A., Kawano J., Okano M. (2010) Gem News International: Treated CVD-grown pink synthetic diamond melee. *G&G*, Vol. 46, No. 1, pp. 68–69.
Lawson S.C., Fisher D., Hunt D.C., Newton M.E. (1998) On the existence of positively charged single-substitutional nitrogen in diamond. *Journal of Physics: Condensed Matter*, Vol. 10, pp. 6171–6180.
Linares R.C., Doering P.J. (1999) Properties of large single crystal diamond. *Diamond and Related Materials*, Vol. 8, No. 2–5, pp. 909–915.
Linares R.C., Doering P.J. (2010) *Chemical Vapor Deposition Colored Diamond*. U.S. Patent Application 2010/0028556 A1, Feb. 4.
Martineau P.M., Lawson S.C., Taylor A.J., Quinn S.J., Evans D.J.F., Crowder M.J. (2004) Identification of synthetic diamond grown using chemical vapor deposition (CVD). *G&G*, Vol. 40, No. 1, pp. 2–25.
Meng Y.F., Yan C.S., Lai J., Krasnicki S., Shu H., Yu T., Ling Q., Mao H.K., Hemley R.J. (2008) Enhanced optical properties of chemical vapor deposited single crystal diamond by low-pressure/high-temperature annealing. *Proceedings of the National Academy of Sciences*, Vol. 105, No. 46, pp. 17620–17625.
Shigley J.E., McClure S.F., Breeding C.M., Shen A.H., Muhlmeister S.M. (2004) Lab-grown colored diamonds from Chatham Created Gems. *G&G*, Vol. 40, No. 2, pp. 128–145.
Tallaire A., Collins A.T., Charles D., Achard J., Sussmann R., Gicquel A., Newton M.E., Edmonds A.M., Cruddace R.J. (2006) Characterisation of high-quality thick single crystal diamond grown by CVD with a low nitrogen addition. *Diamond and Related Materials*, Vol. 15, pp. 1700–1707.
Teraji T., Ito T. (2004) Homoepitaxial diamond growth by high-power microwave-plasma chemical vapor deposition. *Journal of Crystal Growth*, Vol. 271, pp. 409–419.
Twitchen D.J., Martineau P.M., Scarsbrook G.A. (2007) *Colored Diamond*. U.S. Patent 7172655, Feb. 6.
Vavilov V.S., Gippius A.A., Zaitsev B.V., Deryagin B.V., Spitsyn B.V., Aleksenko A.E. (1980) Investigation of the cathodoluminescence of epitaxial diamond films. *Soviet Physics-Semiconductors*, Vol. 14, pp. 1078–1079.
Wang W. (2009) Lab Notes: Diamond—Fancy red, irradiated and annealed. *G&G*, Vol. 45, No. 3, p. 208.
Wang W., Johnson P. (2010) Lab Notes: Red CVD synthetic diamond with multiple treatments. *G&G*, Vol. 46, No. 1, pp. 52–54.
Wang W., Moses T., Linares R., Shigley J.E., Hall M., Butler J.E. (2003) Gem-quality synthetic diamonds grown by the chemical vapor deposition method. *G&G*, Vol. 39, No. 4, pp. 268–283.
Wang W., Smith C.P., Hall M.S., Breeding C.M., Moses T.M. (2005a) Treated-color pink-to-red diamonds from Lucent Diamonds Inc. *G&G*, Vol. 41, No. 1, pp. 6–19.
Wang W., Tallaire A., Hall M.S., Moses T.M., Achard J., Sussmann R.S., Gicquel A. (2005b) Experimental CVD synthetic diamonds from LIMHP-CNRS, France. *G&G*, Vol. 41, No. 3, pp. 234–244.
Wang W., Moses T.M., Pearce C. (2005c) Lab Notes: Orange diamonds treated by multiple processes. *G&G*, Vol. 41, No. 4, pp. 341–342.
Wang W., Hall M.S., Moe K.S., Tower J., Moses T.M. (2007) Latest-generation CVD-grown synthetic diamonds from Apollo Diamond Inc. *G&G*, Vol. 43, No. 4, pp. 294–312.
Welbourn C.M., Cooper M., Spear P.M. (1996) De Beers natural versus synthetic diamond verification instruments. *G&G*, Vol. 32, No. 3, pp. 156–169.
Yan C.-S., Mao H.-K., Li W., Qian J., Zhao Y.S., Hemley R.J. (2004) Ultrahard diamond single crystals from chemical vapor deposition. *Physica Status Solidi (a), Rapid Research Note*, Vol. 201, No. 4, pp. R25–R27.
Zaitsev A.M. (2001) *Optical Properties of Diamond: A Data Handbook*. Springer-Verlag, Berlin, 502 pp.

Color Alterations in CVD Synthetic Diamond with Heat and UV Exposure: Implications for Color Grading and Identification

Rizwan U. A. Khan, Philip M. Martineau, Bradley L. Cann, Mark E. Newton, Harpreet K. Dhillon, and Daniel J. Twitchen

In response to heat and UV exposure, some synthetic diamond gemstones grown by chemical vapor deposition exhibit large, reversible changes in color. A significant reduction in color was achieved by heating several CVD synthetic gemstones to >450°C. Conversely, a darker color was observed in samples following exposure to UV radiation (such as that used in gem testing). Both the heated and UV-exposed samples returned to their initial (stable) color when they were illuminated for >30 minutes with a standard daylight-equivalent lamp used for grading. However, these color states did not change with time when the samples were kept in the dark. Heating and UV exposure also influenced the strengths of various IR absorption features that might be used to identify such a sample as a CVD synthetic. These nonpermanent changes might affect the apparent color grade of a CVD synthetic diamond, and care must be employed in the interpretation of spectroscopic features used to determine a stone's natural or synthetic origin.

In recent years, chemical vapor deposition (CVD) techniques to grow synthetic diamond have evolved to the point that high-quality single crystals of moderate size can be produced (see, e.g., Achard et al., 2007). Gemological laboratory equipment (e.g., the infrared spectrometer and Diamond Trading Company's (DTC) DiamondView verification instrument) can be used to identify CVD-grown diamond gems as synthetic (Wang et al., 2003, 2007; Martineau et al., 2004), based on a number of properties detectable under special test conditions. These synthetic gemstones are now being marketed by, for example, Apollo Diamond Inc. of Boston, and the numbers being submitted to gemological laboratories are increasing (see, e.g., Chadwick and Breeding, 2008; Wang and Moses, 2008; Wang and Johnson, 2010).

Under some circumstances, adding a small concentration of nitrogen to the growth environment increases the growth rate (Teraji and Ito, 2004; Tallaire et al., 2006) while also resulting in the uptake of different types of point defects within the diamond lattice. Some of these defects are known: for example, single substitutional nitrogen (N_S) and nitrogen-vacancy (NV) centers. Other defects formed by the addition of nitrogen manifest themselves in a gradual rise in absorption toward shorter wavelengths (which results in brown coloration) and broad bands at ~360 and 515 nm (Martineau et al., 2004). However, those other defects have not been convincingly identified, and little has been reported about the properties of these absorption bands.

In certain rare natural diamonds, the color and absorption spectra can vary with either heating or extended storage in the dark; that is, such stones display thermochromic and/or photochromic effects. These are commonly called chameleon diamonds

See end of article for About the Authors and Acknowledgments.
GEMS & GEMOLOGY, Vol. 46, No. 1, pp. 18–26.

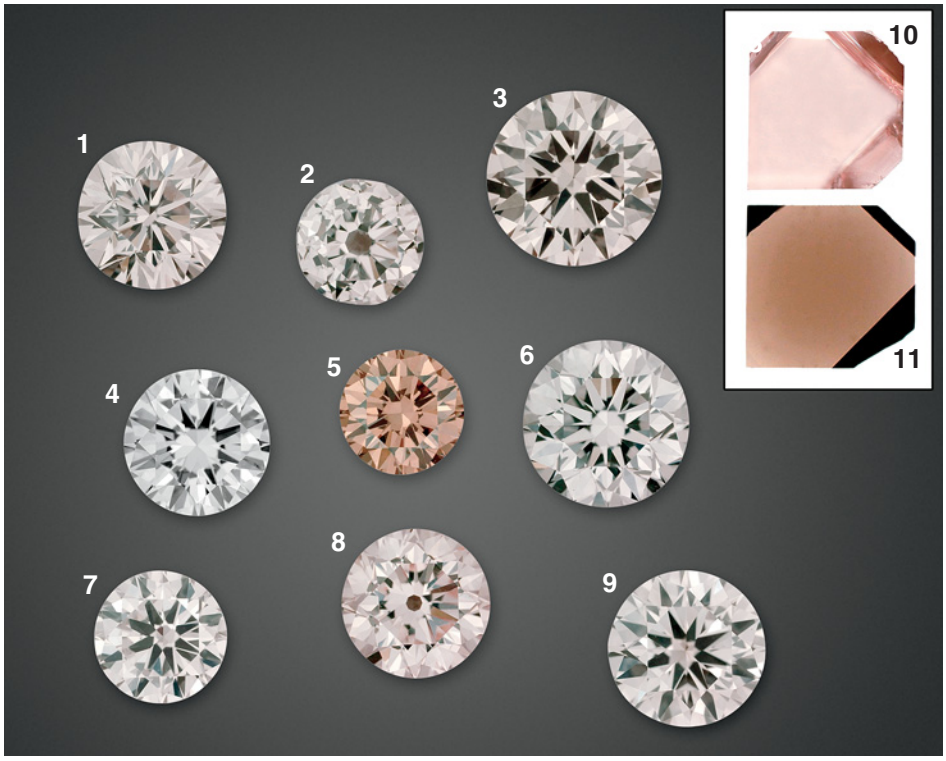

Figure 1. The 11 CVD synthetic diamond samples examined for this study are shown here in their initial "stable" state (i.e., before exposure to heat or a UV lamp). The numbers on the nine round brilliants (0.40–0.92 ct) and two tabular plates (0.22 and 0.35 ct) correspond to the sample numbers used in table 1 and throughout the article. Composite photo by R. Khan.

(see, e.g., Hainschwang et al., 2005; Fritsch et al., 2007). "Classic" chameleon diamonds generally change from a stable "olive" green color to an unstable yellow, and "Reverse" stones change from a stable light yellow to an unstable greenish yellow or yellowish green. The unstable colors are induced by heating to ~150°C or prolonged storage in the dark, whereas the stable colors are achieved by exposure to normal (incandescent or fluorescent) lighting conditions. The chameleon effect is due to variations in the strength of two broad optical absorption features centered at ~480 and ~800 nm.

Pink natural diamonds also often exhibit a color alteration from pink to brown on UV exposure (de Weerdt and Van Royen, 2001). The pink color is a result of a broad optical absorption feature at 550 nm, and it may be reversibly bleached by exposure to the radiation from a UV lamp.

Temporary changes in color are usually caused by the transfer of electrons between defects, which alters the charges of the defects and therefore their influence on the absorption spectrum. These effects sometimes also lead to phosphorescence, where some of the electronic charge becomes trapped and then de-traps over a matter of seconds. Chameleon diamonds often exhibit phosphorescence.

The purpose of this article is to investigate temporary changes in color (and spectra) that may occur in CVD synthetic diamond in response to standard jewelry-manufacturing procedures (e.g., exposure to heat) or gemological testing (e.g., exposure to UV radiation). This is important, as any temporary change in color might potentially affect the grades given on laboratory reports. A previous study (Khan et al., 2009) had already established that charge-transfer processes were occurring in CVD synthetic diamond with UV exposure and heating. This article explores how these two processes affect the color of a number of standard gem-quality CVD synthetic diamond samples (figure 1), and categorizes any changes they produce in spectroscopic features that gemologists might use to identify a diamond as a CVD synthetic.

MATERIALS AND METHODS

The CVD synthetic diamond samples used for this study were grown by Element Six Ltd. within the DTC's Consumer Confidence Technical Research program, a fundamental aim of which has been to develop knowledge and instruments that will aid the identification of synthetics and treated diamonds. The samples investigated, which were grown for research purposes only, were all standard CVD synthetics similar to those discussed in a previous publication (Martineau et al., 2004). For all the samples, CVD layers were deposited on substrates of type Ib synthetic diamond that had been grown by a high-pressure, high-temperature (HPHT) process; after

deposition, the substrate was removed. Generally, greater degrees of brown coloration correlated with increased amounts of nitrogen added during deposition. A total of 11 samples were studied, all of which were from different deposition runs. The nine faceted CVD synthetics (0.40–0.92 ct) and two tabular plates (0.22 and 0.35 ct) were prepared using laser cutting and standard polishing techniques. We used the tabular plates for spectroscopic characterization, because their parallel geometry made it easier to obtain quantitative measurements (e.g., the strength of IR features).

The CVD synthetic diamond samples studied are shown in figure 1 and described in table 1. They exhibited a wide range of color, with two (nos. 4 and 6) being colorless or near-colorless, one (no. 5) being Fancy brown, two being pale pink (nos. 8 and 10), and the remainder falling somewhere between near-colorless and brown (see table). All the samples except numbers 4 and 6 were grown with a small concentration of nitrogen in the growth environment. Samples 4 and 6 were nominally undoped. Samples 8 and 9 were HPHT treated: sample 8 at a moderate temperature (~1600°C), and sample 9 at a higher temperature (2200°C); both samples were brown before HPHT treatment.

Each sample was examined in its initial (i.e., stable) state. Then we exposed each of the samples to UV radiation and studied them, after which we heated each of the samples and re-examined them. For UV exposure, we employed either a mercury-xenon arc lamp (Thermo-Oriel 66902 with 6292 HgXe bulb, emitting a broad spectrum with several sharp peaks between 250 and 400 nm and extending into the near-infrared), or the ultra-short-wave xenon strobe lamp of a DiamondView luminescence imaging instrument (wavelength range between 120 and 227 nm; a low pass filter removed higher wavelengths). We obtained comparable results in either case; only short exposures (<5 minutes) were required for the full color alteration to be induced. For heating, we used a standard laboratory hot stage (Linkam TH1500) to heat the sample in the dark to 550°C over 15 minutes before cooling it back to room temperature. We attempted other heating conditions as well and generally found that exposure to >450°C for typically a few—that is, less than five—minutes had the same effect. Note that in both cases these are lower than the temperatures expected for, say, the retipping of gold prongs in a ring (i.e., ~700–800°C to melt gold solder; Knuth, 1994).

Color grading was performed at the Forevermark laboratory, which uses diamond color master sets that are based on standards universally accepted by

TABLE 1. The CVD synthetic diamond samples studied, with color grades as assigned in their initial state, after UV exposure, and after heating.

Sample no.	Weight and shape[a]	N_S^0 (ppm)[b]	HPHT treatment	Color (initial, stable)	Color after UV exposure (for 5 mins.)	Color after heating (to 550°C for 15 mins.)	Magnitude of color difference[c]
1	0.56 ct RB	0.13	None	L (brown)	M (brown)	H (brown)	Large
2	0.42 ct RB	0.11	None	K (brown)	K (brown)	H (brown)	Moderate
3	0.92 ct RB	0.20	None	P-T (brown)	W-X (brown)	M (brown)	Large
4	0.51 ct RB	0.02	None	E	E	D	Small
5	0.40 ct RB	1.7	None	Fancy brown	Fancy Deep brown	W-X (brown)	Large
6	0.80 ct RB	0.02	None	G (brown)	G (brown)	E	Moderate
7	0.45 ct RB	Unknown	None	J (brown)	J (brown)	E	Large
8	0.55 ct RB	Unknown	1600°C	L (pink)	N (pink)	J (pink)	Large
9	0.67 ct RB	Unknown	2200°C	H (brown)	H (brown)	G (brown)	Small
10	0.35 ct plate (2.1 mm thick)	0.5	None	Pale pink	Pink	Near-colorless	Moderate
11	0.22 ct plate (1.1 mm thick)	2.4	None	Brown	Deep reddish brown	Pale brown	Large

[a] *RB = round brilliant. The colors of the tabular plates (samples 10 and 11) are qualitative assessments only.*
[b] *The initial N_S^0 concentrations. These values are observed to vary considerably with exposure to UV radiation or heating; ppm = parts per million atomic.*
[c] *The magnitude of the color difference is defined as follows: large represents >4 grades between heating and UV exposure; moderate, >2 grades; and small, <2 grades.*

leading international diamond grading laboratories. All the samples were graded in a dark room, using a standard overhead desk-mounted light with two 15-watt General Electric F15T18-D Daylight tubes. Samples were graded with the tray holder ~8 in. (20 cm) from the light source and the grader ~12 in. (30 cm) from the synthetic gemstone (similar to conditions discussed in King et al., 2008). All samples were color graded three times: (1) in their initial state (i.e., the stable color), (2) after UV exposure, and (3) after heating. Grading was for research purposes only, as the Forevermark laboratory does not issue reports for synthetic diamond gemstones.

To record the bodycolor of the samples, optical micrographs were taken of each one with a computer-controlled Leica DC300F CCD camera attached to a Wild M420 optical microscope using a Volpi Intralux 150 H fiber-optic lamp for illumination. All samples were photographed in their initial state, after UV exposure, and after heating.

To quantify any spectroscopic changes and further investigate the defect centers involved, we recorded the optical absorption spectra of the two tabular plates (nos. 10 and 11) using an ultraviolet-visible–near infrared (UV-Vis-NIR) spectrometer (Perkin-Elmer Lambda 9), with the sample at room temperature. For sample 11, we also recorded the spectrum with the sample cooled to liquid-nitrogen temperature (–196°C/77°K) by means of an Oxford Instruments DN cryostat. We calculated absorption coefficients by dividing the measured absorbance by the sample thickness. To ascertain any changes in the strength of the IR features known to be present in the spectra of CVD synthetic diamond, we also recorded Fourier-transform infrared (FTIR) absorption spectra on these plates using a Nicolet Magna IR 750 FTIR spectrometer at a resolution of 0.5 cm^{-1}. All spectroscopic analyses were conducted on the samples in their initial state, after UV exposure, and after heating.

We investigated the temporal stability of the three states by placing two synthetic diamond gemstones (nos. 3 and 5) in the dark (i.e., in stone papers in a closed box) and re-grading them periodically over a total of three weeks. This was performed on the samples in their initial state, after UV exposure, and after heating.

We also illuminated three of the samples (nos. 1, 3, and 5) with daylight-equivalent grading lamps at a distance similar to that typically employed for grading (~8 in. from the light source; see, e.g., King et al., 2008) for >30 minutes and re-graded them in an attempt to simulate the effect of cumulative lighting. In addition, we investigated whether it was necessary to illuminate the samples after UV exposure but before heating. Returning the samples to their "stable" state in this manner was found to have no effect on the outcome of the measurements performed after heating; that is, the order of UV/heat exposure did not play a significant role.

NEED TO KNOW

- As-grown nitrogen-containing CVD synthetic diamond will commonly show less color with heating to >450°C and more color after exposure to UV radiation.
- Both types of color alteration are reversible—no permanent structural change is imparted via these heating and UV exposure procedures.
- The three color states (stable, UV-exposed, and heated) do not change with time when the synthetic gemstones are kept in the dark, but the stable color can be induced by prolonged exposure to a standard daylight-equivalent lamp.
- Heat and UV exposure can also modify the strength of certain IR absorption features that have been used to help identify CVD synthetic diamond.

RESULTS AND DISCUSSION

Appearance of the Samples. Very marked changes in color were observed in the majority of the CVD synthetics investigated (again, see table 1). Figure 2 illustrates two of the samples studied (nos. 3 and 5) in each of their three states. As compared to their initial state (figure 2, left), they darkened slightly after UV exposure (figure 2, center) and, conversely, lost most of their color saturation after heating (figure 2, right). In their altered states, even prolonged exposure to light from the fiber-optic illuminator during photography changed their color (so the authors were careful to acquire images promptly). This effect was most noticeable in the samples after heating.

Color Grading. Compared to the initial state, all the samples had less color after heating, whereas UV exposure produced a darker color in some cases (with no difference in five samples). By repeating the measurements several times with successive UV exposure and heating steps, we established that these color alterations were reversible.

As was the case with photography, we noted that illumination from grading lamps affected the

Figure 2. These images illustrate samples 3 (top; 0.92 ct) and 5 (bottom; 0.40 ct) in their initial (stable) states (left), after UV exposure (center), and after heating (right). Composite photo by R. Khan.

color of the UV/heat-exposed samples. This was most clearly seen after heating, when we observed a darkening of the samples during grading that was due to exposure to light from the fluorescent tubes (grading typically takes up to a couple of minutes per gemstone).

Neither of the two samples we color graded in each of the three states (stable, UV-exposed, heated) showed any change in color grade over several weeks while kept in the dark. From this experiment, we concluded that the samples would not return to their initial (stable) state if kept in the dark indefinitely subsequent to UV exposure or heating. Note that this is different from what is observed in chameleon diamonds, where prolonged storage in the dark may cause a change in color.

Next, the three samples we illuminated under grading lamps for relatively long periods (at least 30 minutes) while they were in each of the three states revealed no change in color for samples in their stable state (as expected), and a return to the initial stable color grade for the UV/heat-exposed samples. We therefore suspect that if CVD synthetics were left lying on a table under normal ambient lighting for more than 30 minutes, they would return to their stable color.

Last, we note that the "initial" state in which a synthetic gemstone is received could be ill-defined, in that it might be affected by the lighting conditions the synthetic gem was exposed to before grading. To obtain a reliable, stable color state prior to grading, we recommend that CVD synthetic gems should be illuminated for a reasonable period of time (we employed >30 minutes but shorter durations might be sufficient) under consistent lighting conditions (e.g., daylight-equivalent lamps at a distance of about 8 in.).

Spectroscopic Analysis. The initial (stable), post-heating, and post-UV-exposure UV-Vis absorption spectra for tabular sample 11 are shown in figure 3. The overall results for sample 10 were similar, but the peaks were weaker. In the spectra of the initial and after-UV states, we observed strong optical absorption features at ~270, 360, and 515 nm.

The feature at ~270 nm has been attributed to neutral single substitutional nitrogen defects (N_S^0), otherwise known as the C form (Chrenko et al., 1971). Although the eye is not sensitive in this area, an increase in the strength of this feature correlates with increased broad absorption over the blue region of the absorption spectrum. A sample possessing strong 270 nm absorption will appear yellow—as do, for example, most type Ib HPHT-grown synthetic diamonds. The features centered at ~360 and 515 nm also have a significant bearing on the color of a CVD synthetic diamond. The 360 nm band is broad and extends into the visible region of the spectrum. The 515 nm feature is particularly important, as the eye is at its most sensitive in this

Figure 3. These UV-Vis-NIR absorption spectra were recorded from a tabular plate of CVD synthetic diamond (sample 11) in its initial (stable) state, after UV exposure, and after heating. The features at 270, 360, and 515 nm increase in strength after UV exposure, while heating reduces their intensity, resulting in the color alterations seen.

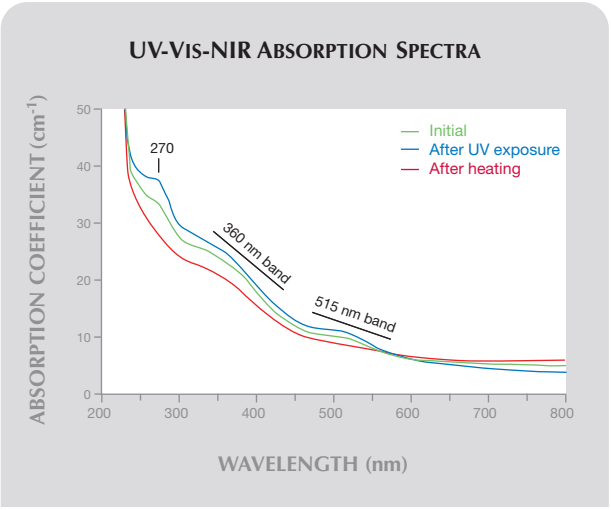

TABLE 2. Changes in the concentration of single-substitutional-nitrogen defects measured with IR spectroscopy in the initial state, after UV exposure, and after heating.

Sample no.	Defect	Spectroscopic feature (cm^{-1})	Concentration (ppm)		
			Initial	After UV exposure	After heating to 550°C
10	N_S^+	1332	0.2 ± 0.2	0.2 ± 0.2	0.5 ± 0.2
	N_S^0	1344	0.5 ± 0.2	0.6 ± 0.2	0.2 ± 0.2
11	N_S^+	1332	2.5 ± 0.4	1.8 ± 0.4	4.7 ± 0.4
	N_S^0	1344	2.4 ± 0.4	3.5 ± 0.4	0.8 ± 0.4

region. Depending on the strength of other absorption features, strong 360 nm absorption will make samples appear more yellow and samples with a strong 515 nm band often appear pinkish.

Comparing the spectra in figure 3, we observe that the 270, 360, and 515 nm bands are much weaker after heating. The 270 and 360 nm features appear to be slightly stronger after UV exposure than when the diamond is in its initial state. Overall, we can conclude that the heating procedure weakened the three main absorption features, and thus reduced the color, which is consistent with our grading results. UV exposure strengthened the three main features, which is consistent with the stronger color recorded in the color grading. Again, via repeating the heating and UV-exposure episodes and re-measuring the samples, we established that these effects were reversible. This suggests that charge transfer between various defects might be responsible (Khan et al., 2009).

The reduction in the strength of the feature at 270 nm provides a clue to the reason for the color alterations. As it corresponds to neutral single substitutional nitrogen (N_S^0) defects, these must have been temporarily converted to another form when the sample was heated. One such form is positively charged single substitutional nitrogen (N_S^+); that is, N_S^0 that has lost an electron. Infrared spectroscopy enables us to investigate both forms of these single nitrogen defects.

Figure 4 shows the FTIR spectra for sample 11 in its initial (stable) state, after UV exposure, and after heating (again, the overall results were similar for sample 10). Both N_S^0 and N_S^+ possess IR-active modes in the region between 1500 and 1200 cm^{-1}. A component of the vibration associated with the N_S^+ defect occurs at 1332 cm^{-1}; likewise, a peak at 1344 cm^{-1} corresponds to N_S^0 defects (Lawson et al., 1998). From figure 4, it is clear that on heating, the intensity of the 1344 cm^{-1} peak decreased and that of the peak at 1332 cm^{-1} increased. This suggests the conversion of single substitutional nitrogen from its neutral to its positively charged state; this charge transfer is consistent with the measurements obtained via UV-Vis spectroscopy. We also note that the stable state lies between the UV-exposed and heated states.

For both tabular plates, we present the changes in concentrations for N_S^0 and N_S^+ derived from the strengths of the 1344 and 1322 cm^{-1} features, respectively, in table 2. We estimate that, between the UV-exposed and heated states, there is a change of ~0.3 parts per million atomic (ppm; sample 10) and ~3 ppm (sample 11) in the single-nitrogen-defect concentration from the neutral to the positively charged state. From table 1, it is also apparent that the magnitude of the color alteration is loosely correlated to the concentration of N_S^0 centers. The synthetic diamond samples that had negligible N_S^0 showed less color alteration. Also note that the

Figure 4. The IR spectra in the region between 1500 and 1200 cm^{-1} recorded from CVD synthetic diamond sample 11 reveal changes in the strengths of the 1344 (N_S^0) and 1332 (N_S^+) cm^{-1} peaks, and variations in the strengths of the peaks at 1371, 1362, and 1353 cm^{-1}. Spectra are shown for the sample in its initial (stable) state, after UV exposure, and after heating.

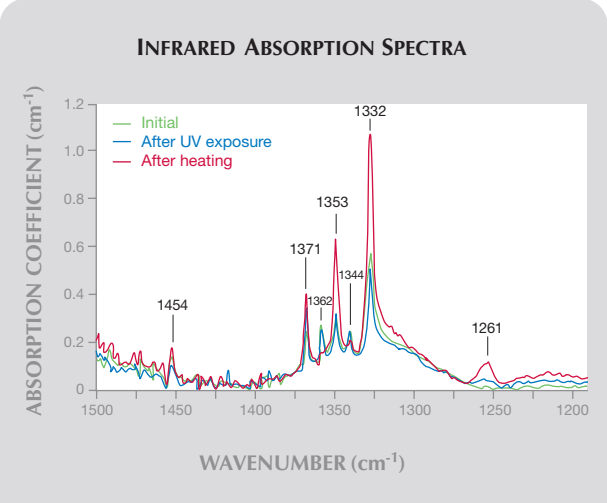

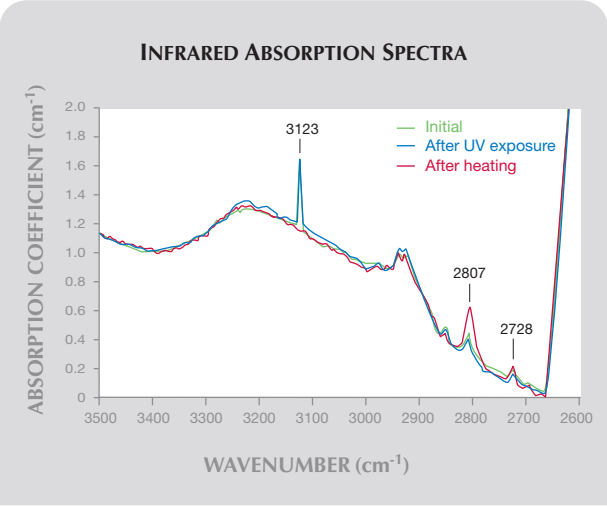

Figure 5. The IR spectra recorded from sample 11 in the 3500–2600 cm^{-1} region illustrate the changes in the strengths of a number of peaks, including the one at 3123 cm^{-1}, which is believed to correspond to the neutral nitrogen-vacancy-hydrogen (NVH^0) defect.

direction of the color alteration was the same in all of the samples, and in no case was the CVD synthetic rendered more colorless by UV exposure.

Similarly, figure 5 shows for sample 11 the region of the IR spectrum between 3500 and 2600 cm^{-1}, which contains various stretch modes of defects in diamond. Here we observe large changes in the strength of an absorption feature at 3123 cm^{-1}: After heating, it is not visible; but after UV exposure and in the initial state, it is clearly observed. This is one of several IR features that reportedly might help identify a diamond as an as-grown CVD synthetic (Wang et al., 2003), and our experiments show that it could be temporarily eliminated via heating. This line is thought to be a vibrational mode of the neutral nitrogen-vacancy-hydrogen center (NVH^0: Glover et al., 2003; Khan et al., 2009). As the CVD process employs a large fraction of hydrogen in the gas feedstock, and because the carbon-containing source gas (methane) also contains hydrogen, it is not at all surprising that hydrogen-containing defects are present in CVD synthetic diamond.

The UV-Vis absorption measurements on sample 11 at liquid-nitrogen temperature allowed us to study the influence of UV exposure and heating on the concentrations of other known defect centers. The results of this experiment are not described in detail here, but we observed relative changes in the strength of the NV^0 and NV$^-$ peaks (at 575 and 637 nm, respectively): The NV$^-$ concentration, calculated by fitting the area and using a known conversion factor (Davies, 1999), decreased from 98 parts per billion atomic (ppb) after heating to 53 ppb following UV exposure, with a concomitant increase in the strength of the NV^0 peak. This suggests that heating also converted NV defects into their negatively charged form, presumably via gain of electrons from the N_S centers, which would be consistent with the reduction in the strength of the 270 nm peak as mentioned above. However, this change in NV concentration is likely to be too small to have a profound effect on color, whereas changes in the strengths of the aforementioned bands (which are not associated with either the 575 or 637 nm features) have produced the observed color alterations.

Several other IR features are also altered with heating and UV exposure. We compared the spectra for sample 11 in its UV-exposed and heated states, and the results are shown in table 3. The spectra for the samples in their stable state consistently fell between those of the two altered states, but they are generally closer to those of the UV-exposed state. Therefore it is not always possible to observe changes in the strengths of lines between the stable and UV-exposed states. Various photoluminescence identification features (e.g., at 467.6 and 532.8 nm) also exist in these samples and have been discussed in a previous publication (Martineau et al., 2004).

Color Alteration Mechanisms. Based on our data and previous work, we propose that the color alterations are due to electron transfer from single substitutional nitrogen centers to electron acceptor defects (Khan et al., 2009). After UV exposure, these defects are neutral and contribute to the color, but after heating they are charged and do not. Some of these defects are of known origin (NVH) and some are of unknown origin. The NVH acceptors are likely to be present in most CVD synthetics doped with nitrogen (Glover et al., 2003). For a large alteration in color, significant concentrations of both N_S and acceptors are required, in which case the initial color of the CVD synthetic would be expected to be darker brown. Note, though, that these various defects are present in practically all types of as-grown CVD synthetic diamond. Even in unintentionally doped material, they can be present in trace concentrations. This means that even nominally pure, near-colorless as-grown CVD synthetic gemstones can show some small changes in color.

Table 1 shows an apparent trend between the single-nitrogen concentration and the strength of the effect, but we have not observed similar color

TABLE 3. Changes in strength of IR spectroscopic features of sample 11 between UV-exposed and heated states.

Position (cm^{-1})	Variation with UV exposure	Variation with heating (550°C)
1332	Decreases	Increases
1344	Increases	Decreases
1353	Decreases[a]	Increases
1362	Increases[a]	Decreases
1371	Decreases[a]	Increases
2728	Decreases	Increases
2807	Decreases[a]	Increases
2900–2950	No change	No change
3123	Increases	Decreases
6451 (1550 nm)[b]	Decreases	Increases
6857 (1458 nm)[b]	Decreases	Increases
7354 (1360 nm)[b]	Decreases	Increases

[a] *No apparent change between stable and UV-exposed state.*
[b] *Not shown in figures 3, 4, or 5.*

alterations in HPHT-grown synthetic diamond samples (which contain appreciable single nitrogen but not these acceptors; Khan et al., 2009).

Last, though large changes in color were observed in the sample that was HPHT-treated to a moderate temperature (no. 8, 1600°C), the sample annealed at the higher temperature (no. 9, 2200°C) showed little color alteration between subsequent heating and UV exposure. In sample 8, HPHT treatment had the effect of removing most of the brown color but leaving the broad absorption feature centered around 515 nm, resulting in a slightly pink hue (for details of this process, see Twitchen et al., 2007). For sample 9, the 515 nm feature was also annealed out, resulting in the removal of much of the visible absorption seen in the as-grown sample. The results for samples 8 and 9 suggest that once the defect responsible for absorption centered at ~515 nm is annealed out, CVD synthetic diamond does not show significant changes in color with subsequent heat or UV exposure. As the 3123 cm^{-1} IR feature anneals out at the same temperature as the 515 nm absorption band, and both display similar charge-transfer dependence, we speculate that the latter may correspond to an optical transition of the NVH^0 defect, though further investigations are required.

CONCLUSIONS

Gemologists should be aware that the color of as-grown CVD synthetic diamond gemstones may not be stable. Some color-causing defects in CVD synthetics doped with nitrogen trap electrons in a way that causes their charge state to change on exposure to UV radiation and heat. UV exposure causes a conversion of these defects to a neutral charge state so they absorb light over the visible range, increasing the apparent color. Conversely, heating to >450°C converts these defects to a charged state where they absorb less light over visible wavelengths, thus reducing the observed color.

These photochromic and thermochromic effects are reversible, and no permanent change occurs. A stable color—which is intermediate between the colors produced by UV exposure and heat—may be induced by illumination with grading lamps (we employed at least 30 minutes' illumination, but shorter durations may be sufficient). However, all three of the states (stable, UV-exposed, and heated) do not change with time if the gemstones are not disturbed by incident light (or heat), such as when they are stored in stone papers in a box at room temperature. The effect is analogous to the Reverse chameleon effect in natural diamond, except that the unstable color in Reverse chameleons can be induced by prolonged storage in the dark (Hainschwang et al., 2005), and it is the opposite of the photochromic and thermochromic changes that occur in some pink natural diamonds (where the more saturated pink coloration is induced by heating and removed by UV exposure).

Although these measurements were only performed on samples grown by Element Six, we suspect that CVD synthetic diamond gemstones from other producers would show similar effects if they were also nitrogen doped and not annealed at high temperature. Note that even the colorless CVD synthetics (which were grown without nitrogen deliberately added), showed some small changes, presumably due to low concentrations of intrinsic defects.

Gemologists should also be aware that a near-colorless CVD synthetic diamond could be heated prior to grading to improve its apparent color. If immediately after heating the synthetic gem was wrapped in thick paper and kept in the dark at room temperature until grading, it might obtain a better grade than merited by its stable color. The color alterations may be significant, in some cases the equivalent of several GIA color grades.

Conversely, a fancy-color CVD synthetic diamond may achieve a more intense color after UV exposure; in this case, too, the color grade might not be a true representation of its stable state. Note, though, that the UV-induced color can be removed by heating, for example, using a suitable furnace or torch to elevate the gemstone to >450°C. A gemolo-

gist can ensure that a synthetic diamond has reverted to a stable intermediate color by illuminating it with a standard daylight-equivalent lamp for a period of time, such as at least 30 minutes as in our study.

Although our experiments involved UV/heat exposures that would not typically occur in a standard diamond-grading environment, some color alteration is possible, and indeed likely, under normal grading conditions. Standard tests applied to diamonds (such as examination in a DiamondView, or using a UV lamp to check for fluorescence) involve exposure to UV radiation, which we have shown may profoundly affect the color. It is also possible that the temperature of gemstones may on occasion—for example, during acid cleaning, polishing, or use of a torch in the repair of jewelry—be raised high enough to cause a temporary color alteration.

Last, some CVD-specific spectroscopic identification features (e.g., a peak at 3123 cm^{-1} in the mid-IR spectrum) may diminish or even disappear on heating or UV exposure, so the absence of such features should not be the sole criterion by which a gemstone is identified as a natural diamond rather than a CVD synthetic.

ABOUT THE AUTHORS

Dr. Khan (riz.khan@dtc.com) is a senior scientist specializing in CVD synthetic diamond, and Dr. Martineau is the head of Physics, both at the DTC Research Centre in Maidenhead, Berkshire, UK. Mr. Cann is a doctoral student, and Dr. Newton is a reader in Experimental Physics, both at the University of Warwick, Coventry, UK. Mrs. Dhillon is an assistant research scientist, and Dr. Twitchen is a principal scientist, both at Element Six, Ascot, Berkshire, UK.

ACKNOWLEDGMENTS

The authors thank Andrew Bennett and Siobhan Woollard at Element Six for their assistance with growing the CVD synthetic diamond samples used in this research. They also acknowledge John Freeth and Chris Kelly (DTC) for preparing the tabular plates and pre-processing of the round brilliant samples, and Jim Nash (DTC) for polishing the round brilliants. Last, spectroscopic assistance from Samantha Sibley and Julia Samartseva (DTC) was much appreciated.

REFERENCES

Achard J., Silva F., Tallaire A., Bonnin X., Lombardi G., Hassouni K., Gicquel A. (2007) High quality MPACVD diamond single crystal growth: High microwave power density regime. *Journal of Physics D: Applied Physics*, Vol. 40, No. 20, pp. 6175–6188.

Chadwick K.M., Breeding C.M. (2008) Lab Notes: First CVD synthetic diamond submitted for dossier grading. *G&G*, Vol. 44, No. 1, pp. 67–69.

Chrenko R.M., Strong H.M., Tuft R.E. (1971) Dispersed paramagnetic nitrogen content of large laboratory diamonds. *Philosophical Magazine*, Vol. 23, pp. 313–318.

Davies G. (1999) Current problems in diamond: Towards a quantitative understanding. *Physica B*, Vol. 273–274, No. 1–4, pp. 15–23.

De Weerdt F., Van Royen J. (2001) Defects in colored natural diamonds. *Diamond and Related Materials*, Vol. 10, No. 3–7, pp. 474–479.

Fritsch E., Massi L., Rossman G.R., Hainschwang T., Jobie S., Dessapt R. (2007) Thermochromic and photochromic behavior of "chameleon" diamonds. *Diamond and Related Materials*, Vol. 16, No. 2, pp. 401–408.

Glover C., Newton M.E., Martineau P., Twitchen D.J., Baker J.M. (2003) Hydrogen incorporation in diamond: The nitrogen-vacancy-hydrogen complex. *Physical Review Letters*, Vol. 90, No. 18, article no. 185507 [4 pp.].

Hainschwang T., Simic D., Fritsch E., Deljanin B., Woodring S., DelRe N. (2005) A gemological study of chameleon diamonds. *G&G*, Vol. 41, No. 1, pp. 20–34.

Khan R.U.A., Martineau P.M., Cann B.L., Newton M.E., Twitchen D.J. (2009) Charge-transfer effects, thermo and photochromism in single crystal CVD synthetic diamond. *Journal of Physics: Condensed Matter*, Vol. 21, No. 36, article no. 364214 [9 pp.].

King J.M., Geurts R.H., Gilbertson A.M., Shigley J.E. (2008) Color grading "D-to-Z" diamonds at the GIA laboratory. *G&G*, Vol. 44, No. 4, pp. 296–321.

Knuth B.G. (1994) *Jeweler's Resource*. Jeweler's Press, Eastlake, CO.

Lawson S.C., Fisher D., Hunt D.C., Newton M.E. (1998) On the existence of positively charged single substitutional nitrogen in diamond. *Journal of Physics: Condensed Matter*, Vol. 10, No. 27, pp. 6171–6180.

Martineau P.M., Lawson S.C., Taylor A.J., Quinn S.J., Evans D.J.F., Crowder M.J. (2004) Identification of synthetic diamond grown using chemical vapor deposition (CVD). *G&G*, Vol. 40, No. 1, pp. 2–25.

Tallaire A., Collins A.T., Charles D., Achard J., Sussmann R., Gicquel A., Newton M.E., Edmonds A.M., Cruddace R.J. (2006) Characterisation of high-quality thick single crystal diamond grown by CVD with a low nitrogen addition. *Diamond and Related Materials*, Vol. 15, No. 10, pp. 1700–1707.

Teraji T., Ito T. (2004) Homoepitaxial diamond growth by high-power microwave-plasma chemical vapor deposition. *Journal of Crystal Growth*, Vol. 271, No. 3–4, pp. 409–419.

Twitchen D.J., Martineau P.M., Scarsbrook G.A. (2007) *Colored Diamond*. U.S. Patent 7,172,655, Feb. 6.

Wang W., Moses T., Linares R.C., Shigley J.E., Hall M., Butler J.E. (2003) Gem-quality synthetic diamond grown by a chemical vapor deposition (CVD) method. *G&G*, Vol. 39, No. 4, pp. 268–283.

Wang W., Hall M.S., Moe K.S., Tower J., Moses T.M. (2007) Latest generation CVD-grown synthetic diamonds from Apollo Diamond Inc. *G&G*, Vol. 43, No. 4, pp. 294–312.

Wang W., Johnson P. (2010) Lab Notes: Red CVD synthetic diamond with multiple treatments. *G&G*, Vol. 46, No. 1, pp. 51–21.

Wang W., Moses T.M. (2008) Gem-quality CVD synthetic diamond with traces of boron. *G&G*, Vol. 44, No. 2, pp. 158–159.

Laminated Reference Charts

The information you need... at a glance!
Perfect for home or office use.

- HPHT-Grown Synthetic Diamonds
- World Gem Localities
- Gem Treatments
- GIA Diamond Cut Grading System
- Pink Diamond Color Chart
- Recognizing Be-Diffused Rubies & Sapphires

Also available:

- Separation of Natural & Synthetic Diamonds
- Identification of Filled Diamonds

Only $16.95 (plus shipping)

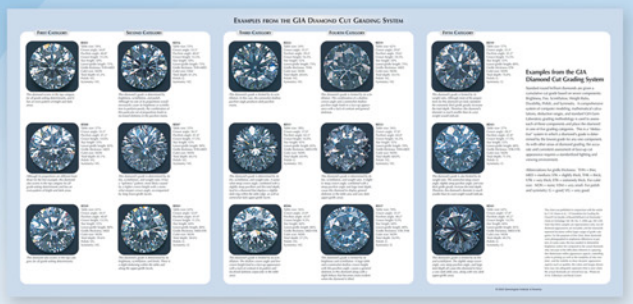

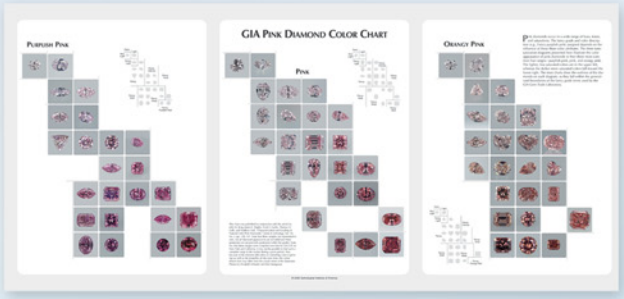

Buy two or more and SAVE!

GEMS & GEMOLOGY®

Order Yours Today!

Visit store.gia.edu

Or call 800-421-7250, ext. 7142
(outside the U.S., 760-603-4000, ext. 7142).

POSSIBLE "SISTER" STONES OF THE HOPE DIAMOND

Scott D. Sucher, Stephen W. Attaway, Nancy L. Attaway, and Jeffrey E. Post

For more than a century, historians have debated the existence of "sister" stones to the Hope diamond, most notably the Brunswick Blue and the Pirie diamonds. The recent discovery of a lead cast of the French Blue, the Hope's precursor, has provided a more accurate model of that diamond, which disappeared in 1792. Computer models of the French Blue and its parent stone, the Tavernier Blue, were used to determine whether other diamonds might have been created when the Tavernier Blue was cut into the French Blue, or when the latter was cut into the Hope. The results show that it was not feasible for other significant diamonds to have been created during any recutting.

The possibility that there might exist "sister" stones to the Hope diamond has long been the subject of speculation (see, e.g., Streeter, 1882; Bapst, 1889; Cattelle, 1911; Patch, 1976; and Balfour, 2009). Many believe that such diamonds could have been created when the Tavernier Blue was cut into the French Blue (at a loss of approximately 46 carats) in the 1670s, or when the French Blue was recut into the Hope (at a further loss of some 24 carats) in the late 18th or early 19th centuries. Streeter (1882) proposed that the 13¾ ct Brunswick Blue and the 1¼ ct Pirie diamonds (which he examined, though both are now long since lost from the public eye) were such byproducts and described in detail how they might have been created. Bapst (1889) also speculated on the connection with the Brunswick Blue. Morel (1988) pointed out errors in Streeter's methodology, rebutting any relationship between these two diamonds and the Hope. More recently, Attaway (2005) corroborated Morel's conclusion.

It is important to note that these earlier conclusions were based on the limited information and technology available at the time. The inherent constraints in modeling these historic diamonds required that assumptions be made about their physical attributes, leaving sufficient margin for error that sister stones might still have been possible (Kurin, 2006). The present study compares a specially created computer model of the Hope diamond with recent computer models of the French Blue (generated from a lead replica of this historical diamond; see Farges et al., 2008, 2009) and the Tavernier Blue (Sucher, 2009) to determine if other stones could have resulted from either recutting.

MATERIALS AND METHODS

Modeling. The French Blue model used in this study (figure 1) is the same one created from a lead cast of the French Blue, as reported by Farges et al. (2008, 2009). The Tavernier Blue model (figure 2), was developed by Sucher (2009) using this French Blue model and drawings published in Tavernier (1676), along with crystallographic information. We also needed an accurate three-dimensional model of the Hope diamond for comparison. Several techniques were considered for determining the Hope's facet angles and index settings, as well as measuring the diamond in three dimensions. Laser scanning, a touch probe, an optical comparator, and photomodelingwere all explored. Photomodeling was selected out of a need

See end of article for About the Authors and Acknowledgments.
GEMS & GEMOLOGY, Vol. 46, No. 1, pp. 28–35.

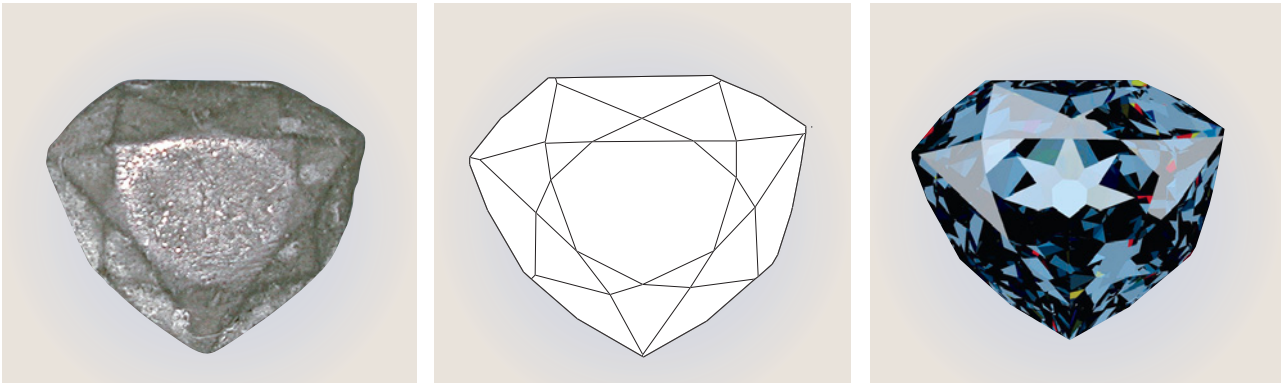

Figure 1. A recently discovered lead cast of the French Blue (left) has allowed more realistic modeling of the original diamond (a wireframe model, center; a photorealistic rendition, right) and, from this, more accurate determinations of how it and the Hope diamond were cut. Both models from Farges et al. (2008, 2009).

for security, cost-effectiveness, and speed. The last was especially important, as the Hope diamond can only be removed from its highly secure storage for a limited time. Many photographs can be taken in a short period and analyzed later, while the other methods would have required much longer periods out of the vault and thus greater security concerns.

Photomodeling is a process in which photographs of an object are taken from many different angles and analyzed using computer software. For this study, the Hope was unmounted and placed on a grid of 10 mm squares (figure 3) developed to provide a modeling reference while the stone was photographed from various angles. The Hope has a large culet that allows it to stand on its own without any supporting structure that could obscure important details from the camera. A series of dots were placed on the grid to maintain a position reference as the cardboard and stone were rotated, and the diamond was placed on the section of the grid framed by the dots. Top, bottom, and side photos were taken at every 45° of rotation with the stone resting on both its culet and table facet. Additional photos were taken perpendicular to both the culet and the table facet for face-up and face-down perspectives.

A Nikon Coolpix 990 digital camera with 3.2 megapixel resolution was used for photography. We took approximately 150 photos of the unset diamond, 30 of which were chosen to characterize the stone. More than 300 points were identified to mark

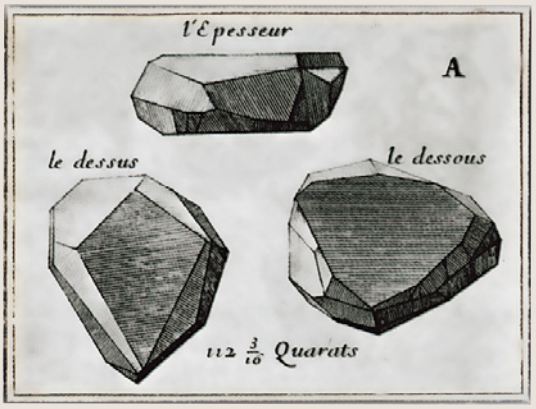

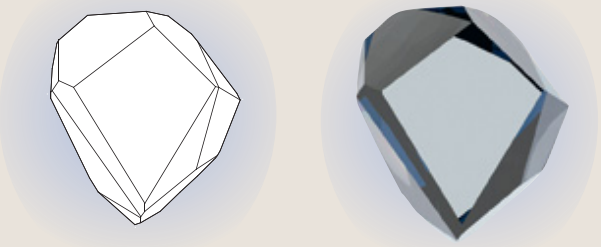

Figure 2. Using the model of the French Blue in figure 1 and Tavernier's drawings of the Tavernier Blue (left), a more accurate computer model (center and right) of the Tavernier Blue could be derived from the crystallographic analysis. Models from Sucher (2009).

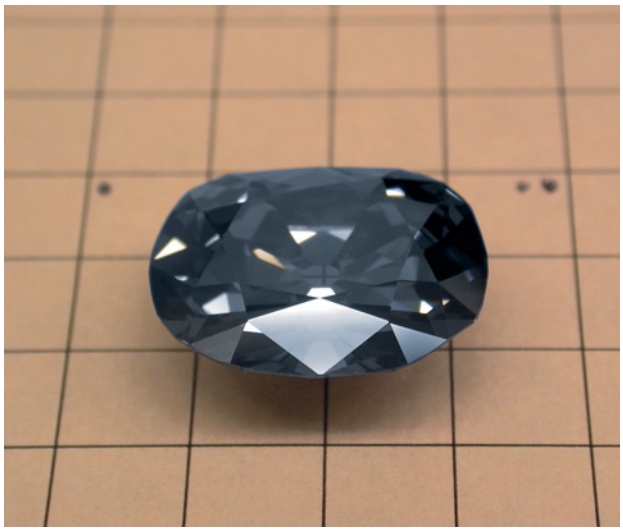

Figure 3. The Hope diamond was placed on a grid designed for photomodeling. The dots served as a fixed point of reference as the stone was rotated. Photo by S. D. Sucher.

the facet intersections. We labeled each facet junction with a unique identifier (figure 4) and plotted the location of all visible junctions in each picture. This process characterized the diamond from every angle to capture details concerning facet size, shape, and placement; girdle size and shape; and overall stone size and shape.

We used PhotoModeler software from Eos Systems to analyze the photos. This Windows-based program allows accurate measurements in three dimensions to be made from a series of photographs; it has been used for preparing forensic evidence in courts of law (Lynnerup and Vedel, 2005). After the software solved for the camera location, all points, lines, and surfaces were plotted in three-dimensional space. The index and angle were computed for each planar surface that defined a facet, and the information was then exported to GemCad to create a computer model.

Error Analysis. Accuracy of photo analysis is dependent on: (1) the quality and resolution of the camera, (2) the geometry of the camera positions, (3) the precision of the photo marking, and (4) how many points are visible in more than one photograph. The background grid in figure 3 provided a consistent geometric reference for accurate plotting, and also served as a check on the accuracy of the modeling solution. Accuracy was based on the number of pixels that spanned a given frame, so a comparison of grid size to frame size provided a measure of the available resolution. Photo dimensions were 2048 × 1536 pixels, with the stone centered in the photo. (A raw format was used, with no correction for optical distortion.) For this resolution, an accuracy of about 1 part in 2,000 was achieved. Error analysis of the computer model showed a facet junction computed error ranging from 0.01 to 0.2 mm.

In addition to labeling the facet junctions in PhotoModeler, we labeled the intersection points of the grid. These points had a known location and spacing that were used to take measurements between any two points on the diamond. After PhotoModeler calculated the simultaneous solutionof the least-squares fit for camera location, camera lens parameters, and point locations, the solution was checked by comparing the solved points on the grid plane with the actual point spacing.

NEED TO KNOW

- Historians have long speculated about sister stones to the Hope diamond.
- An accurate computer model of the Hope diamond was created for comparison with recently developed models of its predecessors, the French Blue and Tavernier Blue diamonds.
- Comparison of this new model of the Hope with those of its predecessors demonstrated that there would have been insufficient material left over—whether cleaved or sawn—to create additional diamonds weighing >1 ct.

Figure 4. Facet junctions were labeled so their locations could be plotted during photo analysis. Photo by S. W. Attaway.

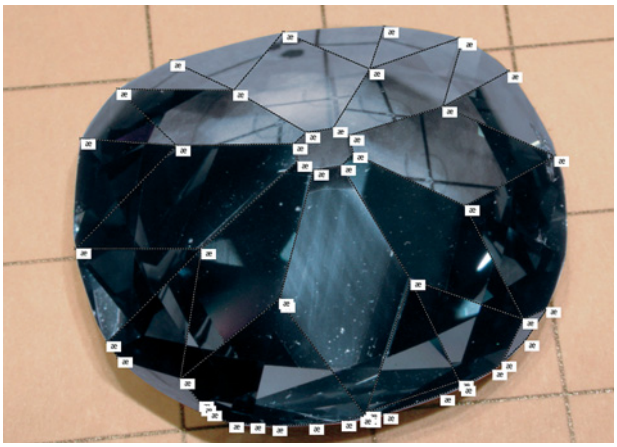

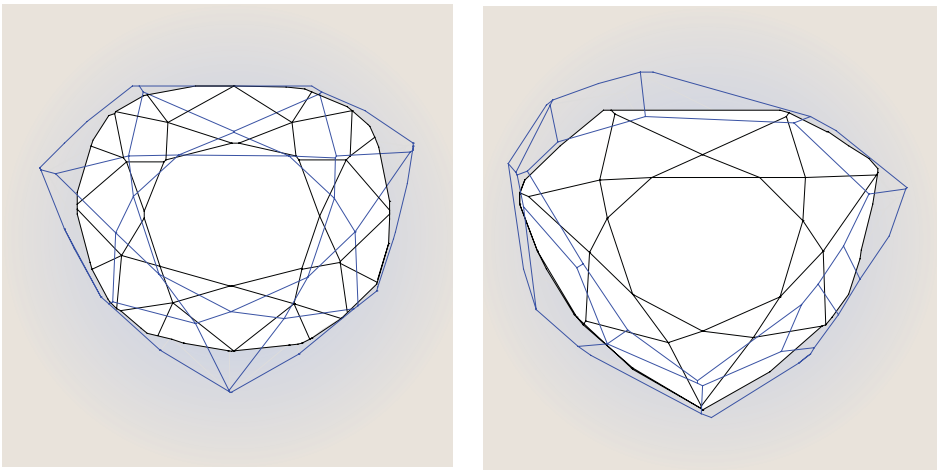

Figure 5. To evaluate the existence of facetable pieces from the Tavernier Blue when cut to become the French Blue—or from the French Blue when cut to become the Hope—the computer model of the Hope was placed inside the model of the French Blue (left), and that of the French Blue within the model of the Tavernier Blue (right).

Other errors to account for were parallax and lens distortion. PhotoModeler corrects for camera lens distortion by solving for focal length and other parameters. Telecentric lenses are frequently used for this process, inasmuch as they are designed so that an object's apparent size does not change as the distance between the lens and the object changes. Object size also remains unchanged if the camera view is slightly out of focus. PhotoModeler also corrects for the use of a non-telecentric lens; the only limitation is that the lens must be fixed at one zoom setting.

A 3D computer model was mathematically generated based on the best fit in three-dimensional space for the points marked on the photos. Once the residual error between the plotted points and the three-dimensional solution was determined, we made position adjustments to selected points at the pixel level to further improve the model's accuracy. The model was considered accurate once the mean square error for all points was at a minimum.

Comparing the Models. The photo model of the Hope was placed inside the updated model of the French Blue in GemCad (figure 5, left) and rotated so that the smaller stone was completely encapsulated by the larger stone, as described in Farges et al. (2008, 2009). There was only one possible orientation, as the tolerances between the two were minimal (in some locations, they were only a fraction of a millimeter). Next, the French Blue model was placed inside the updated Tavernier Blue model by the same process (figure 5, right), as described in Sucher (2009). This process established the position of the "child" stone to its parent, allowing each pairing to be treated as a single unit for crystallographic alignment.

Aligning to an Octahedral Crystal. Using the data from Sucher (2009), the cleavage planes on the Tavernier Blue model were aligned to the cleavage faces ({111} crystal faces) on an idealized model of a hexoctahedral diamond crystal (figure 6). We chose to use a simpler octahedral crystal model for this study, since the orientation of the Tavernier Blue had been established. With the Tavernier Blue model oriented to the octahedral crystal, we then oriented the Tavernier Blue/French Blue model combination. We selected one facet on the Tavernier Blue/octahedral model as a reference (totally arbitrary, as any facet would suffice). The GemCad file

Figure 6. To identify cleavage planes, the Tavernier Blue model was placed inside a model of an idealized octahedral diamond crystal. The top crystal face and table of the Tavernier Blue are "face-up" and aligned with a {111} face.

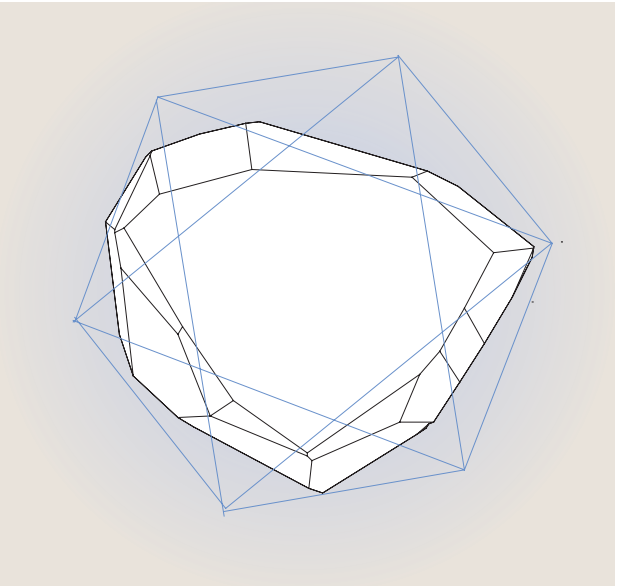

with the Tavernier Blue/French Blue combination was opened, and this composite image was rotated until the reference facet on the Tavernier Blue in each file had the same angle and index settings (as explained in Sucher et al., 2008). The French Blue/Hope model was aligned in similar fashion using a reference facet from the French Blue. All three diamond models were now aligned to each other and the octahedral crystal, with the cleavage planes in any of the diamonds aligned to each octahedral crystal face.

Analyzing the Models. Once the models were aligned to the octahedral crystal, the cleavages in each stone could be established by referring to the facet settings for the {111} octahedral crystal faces. In digitally cleaving the Tavernier Blue in GemCad, these settings were used to remove pieces from the model (as described in Sucher, 2008), with the depth of the cut controlled so that nothing was removed from the French Blue model during the process. Each cleaved fragment from the model was saved as a preform, then analyzed in the GemCad Preform/Edit mode for dimension, weight, and shape. The same process was used to determine the possible cleavages when the French Blue was cut into the Hope. The result of any sawing operation was similarly analyzed.

RESULTS AND DISCUSSION

The Hope Model. The dimensions for the Hope diamond computer model, compared to the actual diamond (as determined by the Smithsonian) are shown in table 1. Dimensional differences between actual measurements and model measurements are artifacts of the measuring process.

Cleaving. There are six possible cleavage planes for a diamond crystal (three on top and three on the bottom) when a cleavage face is oriented "face-up." Only the 120 cleavage plane on the Tavernier Blue digitally removed material of a size that could have been recut (figure 7). This piece weighed 2.2 ct; it was 3.02 mm in depth and irregularly shaped. The cleavage planes on the bottom of the stone were parallel to the lines on the other side. As evident from the drawings, it would not have been possible to remove any material of significant size from any other cleavage direction. The cutter of the Hope maintained even closer tolerances to the French Blue. Of the six possible cleavages, the only piece that could have been digitally cleaved was from the pavilion at the 120 index (figure 8). This piece weighed 0.95 ct and was just 1.14 mm thick. No stones could have been created from a piece of this depth, so as a matter of practicality, no pieces of the French Blue would have been removed by cleaving.

TABLE 1. Measurements of the Hope diamond and its computer model.

	Weight (ct)	Length (mm)	Width (mm)	Depth (mm)
Actual Hope diamond[a]	45.52	25.60	21.78	12.0
Hope model[b]	45.52	25.72	21.86	11.95

[a] *Measurements taken in February 2004 by author JEP.*
[b] *Based on photomodeling for the present study.*

Theoretically, then, the only chance of a sister stone being created from a cleavage piece comes from the 2.2 ct portion of the Tavernier Blue. Again, this is highly unlikely. Ascertaining the cleavage planes in a cut stone is extremely difficult, as crystallographic information contained on the surface of the original crystal is lost. Although we now know that the largest facets on the Tavernier Blue were {111} crystal faces, Jean Pitau (the cutter of the French Blue) would have needed to make an educated guess as to whether they were cubic, dodecahedral, or octahedral. He would have had no way of accurately correlating facets to crystal faces, making the process of locating cleavage planes extremely problematic. This would increase the level of risk during the cleaving operation, as a bad guess might destroy a 115 ct piece of diamond to salvage (at best) 2.2 ct of rough.

Sawing. Could the Tavernier Blue or the French Blue have been sawn? De Boodt (1604) mentioned the use of a bow saw to cut gemstones (figure 9). He used the phrase "*crassiries laminae secans lappides*" (p. 77), which translates to a "thin sheet of metal for cutting gems." A mixture of water and grit would be constantly applied as the saw was drawn back and forth, until the stone was completely sawn through. This passage was written decades before the Tavernier Blue was cut (1671–1673), so we know that Pitau had access to stone sawing technology (though not necessarily *diamond* sawing technology). De Boodt specifically mentioned *smiri* as grit for cutting large ornamental stones such as jasper and marble. He did not indicate its use for cutting diamonds, or that diamond grit was ever used to cut any stone. Nor did he refer to cutting diamonds with such equipment, making it highly doubtful that it was used for this purpose.

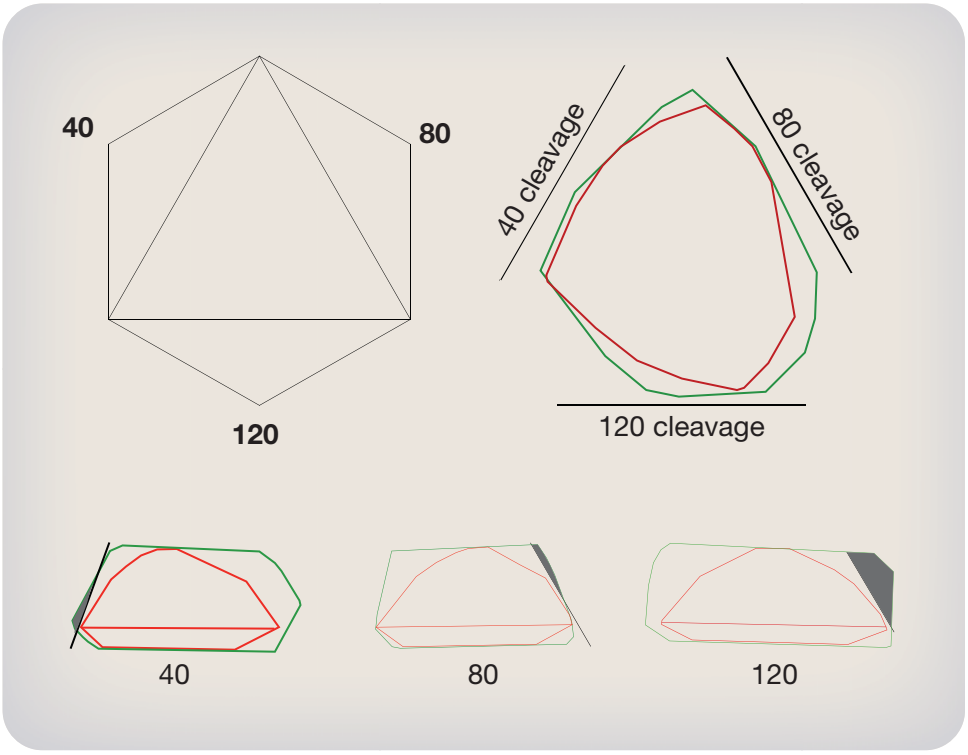

Figure 7. These outlines of the Tavernier Blue upper view (green) and the French Blue (red) show the orientation of cleavage planes (top right). Index settings are on the perimeter. Only one of the cleavage planes, from the 120 index setting, could have produced a cuttable fragment (bottom right). The side views oriented at the 40, 80, and 120 index settings at an angle of 70.5° show that there are no significant cleavage pieces at the 40 and 80 settings.

Dr. Nebenjab Grepp (Grepp, 1681, pp. 282–283) mentioned the use of a saw for diamonds made of "a very small iron Wyre, and having daubed it with Oil and Powder of Diamonds; draw it upon the Diamond, by a Tool, to and fro like a Saw." This is the earliest known documentation of a wire saw used for diamond sawing. But does it mean that this technology existed in 1671, 10 years earlier, when Pitau created the French Blue? This can only be a point of conjecture until other evidence is discovered.

Even assuming diamond sawing was practiced in 1671, the largest piece of the Tavernier Blue that theoretically could have been removed would have been 6.6 mm in depth, yielding a 5.3 ct piece (figure 10). This conclusively eliminates the possibility of the Brunswick Blue as a sister stone. Two other fragments could have resulted, but they would have been only 4 mm in depth and steeply tapered with no reasonably expected yield. The thickest piece of the French Blue theoretically removed by sawing (the very tip) would have resulted in a 2.8-mm-deep piece weighing 3.46 ct (figure 11). Thus, two pieces of both the Tavernier Blue and the French Blue could—*theoretically*—have been removed by sawing. But were any of these pieces *actually* removed, even if the technology existed? More than likely not, for the following reasons:

1. Grepp's statement indicates a very simple process. Would this process have been sufficiently sophisticated to saw off the tip of the Tavernier Blue, and accurate enough so that any part of the future French Blue was not removed? This is certainly not indicated.

2. Kerf (width of cut) losses must be considered. Grepp does not provide a wire diameter, but there is invariably some loss of material as the wire is drawn through the diamond. The cut must be wider than the wire diameter, as Grepp infers the saw is handheld. If the width of the cut was just 2 mm, resulting in a sawn piece 4.6 mm thick, this reduces the largest sawn piece of the Tavernier Blue to 1.5 ct, which likely eliminates the 1¼ ct Pirie as well. Kerf considerations completely preclude getting any usable pieces when the French Blue was cut into the Hope.

3. Starting a cut on the sloped polished surface of the Tavernier Blue would have been extremely difficult. The cutter would have wanted to err on the side of caution and move the blade away from the planned bodies of the French Blue or Hope, further reducing the thickness and weight of the sawn piece.

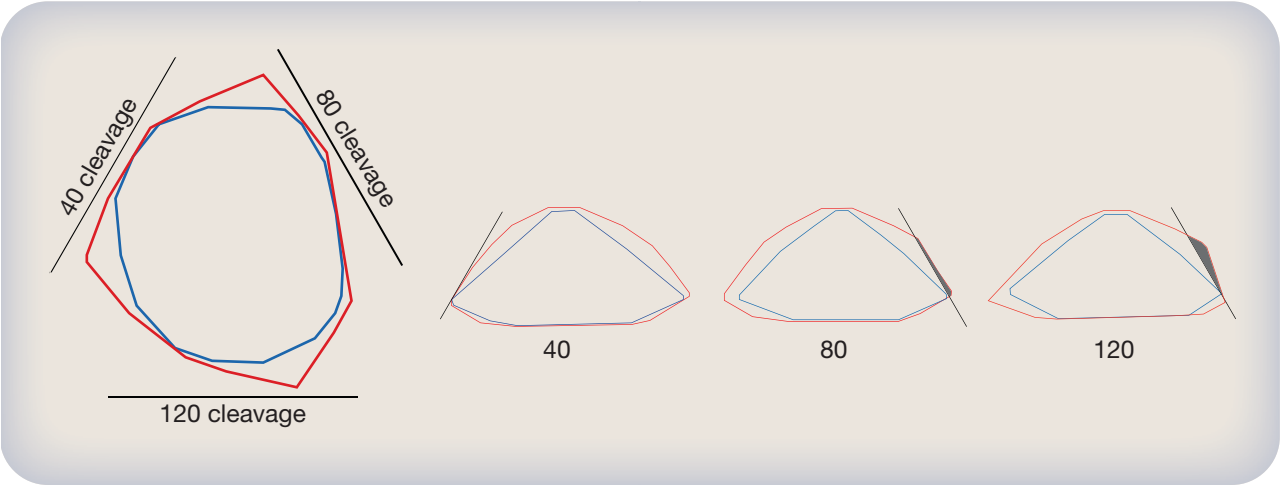

Figure 8. Like figure 7, these outlines of the French Blue (red) and Hope (blue) show the orientation of cleavage planes. Only a tiny fragment could have been cleaved from the 120 index (far right).

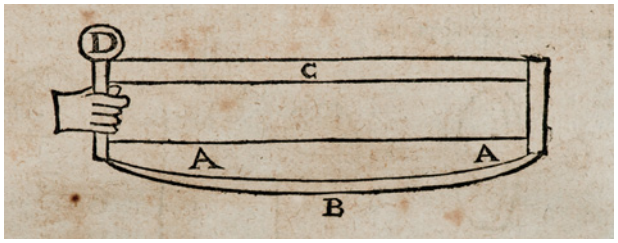

Figure 9. De Boodt's 1604 drawing shows the bow saw he described for cutting gemstones. It is doubtful this could have been used to saw diamonds.

4. Maintaining a cut at the precise angle needed and following the proper track would have been difficult. Neither De Boodt nor Grepp mentions the use of any guides.
5. Perhaps most importantly, Jean Pitau's charter for recutting the Tavernier Blue was to create a stone of regal size and appearance (Farges et al., 2008, 2009), not maximize yield. It is difficult to imagine King Louis caring about preserving such small fragments, and it would of course have been a crime for Pitau to have kept any pieces without the king's permission. Thus, it is doubtful Pitau would want to take the risk when a mistake could literally have been fatal.

In summary, it is highly unlikely that either the Tavernier Blue or the French Blue was cleaved, due to the difficulty of locating the cleavage planes and the inherent danger of destroying the parent stone. Sawing the two diamonds is historically and technically questionable. Even if sawing was possible, the existence of residual fragments of any significant size is not likely. The most reasonable conclusion is that both diamonds were reduced by grinding alone.

Figure 10. Under ideal theoretical circumstances, a 5.3 ct piece could have been sawn from the Tavernier Blue. Shown here is the model with the cutting plane viewed edge-on (left). The possible sawn piece is in black. The center model shows the same view rotated 80°. At right is the model with the sawn piece removed, showing the French Blue model inside.

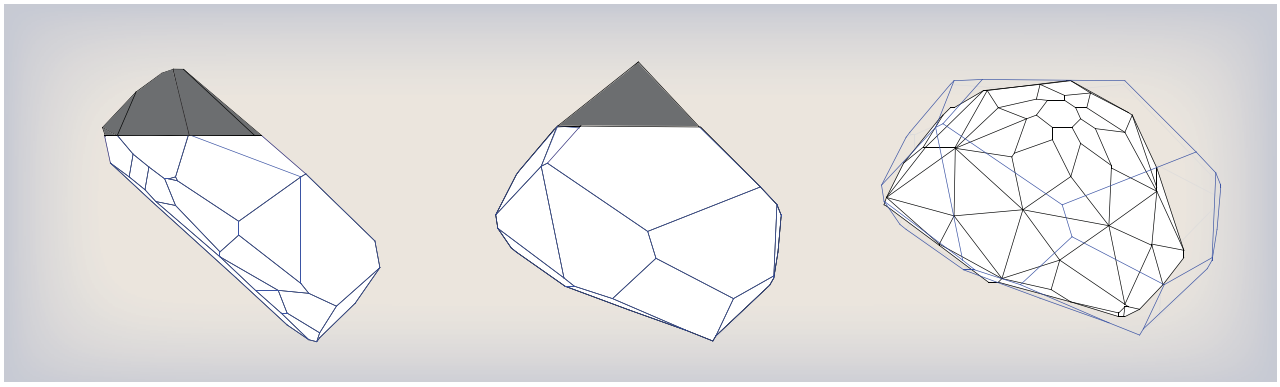

CONCLUSIONS

The possibility that the 13¾ ct Brunswick Blue and 1¼ ct Pirie diamonds might be sister stones to the Hope has been a somewhat romantic notion since Streeter's proposal in the late 19th century. Previous modeling efforts to address this issue were constrained by the limited information available on both the Tavernier Blue and French Blue diamonds, with historical line drawings the only viable references to their appearance. This led to uncertainty and error in modeling these stones.

The recent discovery of a lead cast of the French Blue at the Muséum National d'Histoire Naturelle in Paris provided the best possible computer model of this diamond. It was subsequently used to refine the latest Tavernier Blue model, and a computer model of the Hope was generated for this study by photomodeling. When the three diamond models were compared and analyzed, it was evident that sister stones could not have been created. Cleavage would have been too risky for such a minimal return. Pieces of the size needed to create the Brunswick Blue are physically impossible, and while creating the Pirie would have theoretically been possible from a sawn piece, it would have been impractical, even if the technology existed. This corroborates earlier assertions by Morel and Attaway that no sister stones to the Hope resulted from the cutting of the Tavernier Blue or French Blue diamonds.

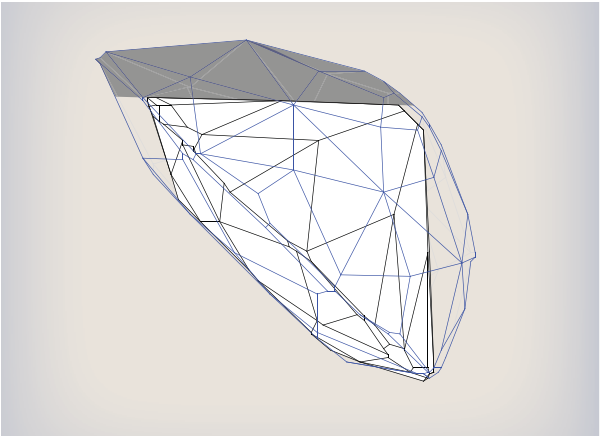

Figure 11. It is theoretically possible that a 3.46 ct piece (shaded area) could have been sawn from the French Blue along one of the pavilion facets.

ABOUT THE AUTHORS

Mr. Sucher (scott@museumdiamonds.com) is principal of The Stonecutter in Tijeras, New Mexico. Dr. and Mrs. Attaway are the principals of High Country Gems in Tijeras. Dr. Post is curator of the National Gem and Mineral Collection at the Smithsonian Institution's National Museum of Natural History in Washington, DC.

ACKNOWLEDGMENTS

The authors thank Jeff Kaufman of the Discovery Channel for making this project possible. Dr. François Farges, professor of mineralogy and curator of minerals and gems at the Muséum National d'Histoire Naturelle (MNHN) in Paris, provided insights regarding the cutting of the French Blue. They also thank Karen Sucher for her support and advice on stone cutting. Ms. Julianne Terrill of Rio Grande High School, Albuquerque, kindly translated Anselmus de Boodt's Latin text.

REFERENCES

Attaway N. (2005) The French connection. *Lapidary Journal*, June, pp. 24–28.

Balfour I. (2009) *Famous Diamonds*, 5th ed. Antique Collectors' Club, Woodbridge, Suffolk, UK.

Bapst C.G. (1889) *Histoire des Joyaux de la Couronne de France* [*History of the French Crown Jewels*]. Hachette, Paris.

Bion J.-M., Delattre F.-P., Christin C.-G.-F. (1791) Inventaire des diamants de la couronne, perles, pierreries, tableaux, pierres gravées, et autres monumens des arts & des sciences existans au garde-meuble (…) [Inventory of diamonds of the crown, pearls, precious gems, paintings, engraved stones, and other monuments of arts & sciences in the royal storehouse]. Imprimerie Nationale, Paris.

de Boote A. (1604) *Gemmarum et Lapidum Historia*. Joannis Maire, Leiden.

Cattelle W. (1911) *The Diamond*. John Lane Co., New York.

Farges F., Sucher S., Horovitz H., Fourcault J.-M. (2008) Deux découvertes majeures autour du "diamant bleu de la Couronne" [Two major discoveries about the "Blue Diamond of the Crown"]. *Revue de Gemmologie*, No. 165, pp. 18–24.

Farges F., Sucher S., Horovitz H., Fourcault J.-M. (2009) The French Blue and the Hope: New data from the discovery of a historical lead cast. *G&G*, Vol. 45, No. 1, pp. 4–19.

Grepp N. (1681) *Catalogue and Description of the Natural and Artificial Rarities Belonging to the Royal Society and Preserved at Gresham College*. W. Rawlins, London.

Kurin R. (2006) *Hope Diamond: The Legendary History of a Cursed Gem*. Harper Collins, New York.

Lynnerup N., Vedel J. (2005) Person identification by gait analysis and photogrammetry. *Journal of Forensic Sciences*, Vol. 50, No. 1, pp. 112–118.

Morel B. (1988) *The French Crown Jewels*. Fonds Mercator, Antwerp.

Patch S.S. (1976) *Blue Mystery: The Story of the Hope Diamond*. Smithsonian Institution Press, Washington, DC.

Streeter E.W. (1882) *The Great Diamonds of the World*. George Bell and Sons, London.

Sucher S., Carriere D. (2008) The use of laser and X-ray scanning to create a model of the historic Koh-i-Noor diamond. *G&G*, Vol. 44, No. 2, pp. 124–141.

Sucher S.D. (2009) A crystallographic analysis of the Tavernier Blue diamond. *G&G*, Vol. 45, No. 3, pp. 178–185.

Tavernier J.B. (1682) *Travels in India*, Vol. II. Translated by V. Ball (1889), Macmillan and Co., London.

CONFOCAL MICRO-RAMAN SPECTROSCOPY: A POWERFUL TOOL TO IDENTIFY NATURAL AND SYNTHETIC EMERALDS

Le Thi-Thu Huong, Tobias Häger, and Wolfgang Hofmeister

More than 300 natural and synthetic emeralds from various sources were examined with confocal Raman spectroscopy. This method identifies different water types in the beryl channel sites, making it possible to determine whether an emerald is natural or synthetic. In addition, this approach can provide information regarding geographic origin or synthesis technique (flux or hydrothermal).

To separate natural from synthetic emeralds, or determine the geographic origin of a natural stone or the growth technique of a synthetic, a gemologist can use microscopy, chemical analysis, and FTIR spectroscopy. Although there are varying degrees of overlap in features seen or analyzed, in many cases each method can lead to a good identification. Here we introduce another tool for determining emerald origin—confocal Raman spectroscopy. This method provides some distinct advantages over previous techniques. For example, traditional FTIR analysis requires that 2 mg of material be pulverized and mixed with KBr powder (Schmetzer and Kiefert, 1990), and then the powder needs to be pressed into a thin disk, making this a destructive and time-consuming technique. Microscopic determination requires a trained and experienced gemologist, and is only effective if the sample contains diagnostic inclusions. Chemical analysis can sometimes determine geographic origin as well as synthesis technique based on the concentrations of some minor or trace elements (e.g., Hänni, 1982; Schrader, 1983; Stockton, 1984; Yu et al., 2000). However, there is chemical overlap among some origins.

This article describes the use of confocal micro-Raman spectroscopy to classify water types in the structural channels of emeralds, to differentiate natural vs. synthetic emeralds (including the form of synthesis), and to investigate geographic origin (figure 1). Raman spectrometers with confocal capability are available in many gemological laboratories, and the analysis is rapid and nondestructive.

BACKGROUND

Beryl—$Be_3Al_2Si_6O_{18}$—has a structure that is composed of six-membered rings of $[SiO_4]^{4-}$ tetrahedra. The Si_6O_{18} rings are aligned precisely over one another, forming open channels parallel to the c-axis of the crystal (figure 2). The diameter of the channels is large enough to hold large ions and molecules such as alkalis and water (Goldman et al., 1978; Aines and Rossman, 1984).

For more than 40 years, water molecules in the structural channels of beryl have been classified by infrared spectroscopy. According to Wood and Nassau (1967, 1968), *type I* water molecules occur independently in the channels with their symmetry axis positioned perpendicular to the c-axis of the beryl crystal. *Type II* water molecules associate with nearby alkalis (mainly sodium) in the channels (again, see figure 2); as a result, the water molecule symmetry axis is parallel to the c-axis of the host

See end of article for About the Authors and Acknowledgments.
GEMS & GEMOLOGY, Vol. 46, No. 1, pp. 36–41.

Figure 1. Natural and synthetic emeralds are available in the marketplace from a variety of sources. Shown here are a Gilson synthetic emerald crystal group (top left, 11.5 g, GIA Collection no. 30490), a faceted Biron synthetic emerald (bottom left, 2.38 ct, GIA Collection no. 23523), a 10.9 g emerald crystal from Colombia (top right, courtesy of William Larson/Palagems.com), and a 4.50 ct faceted emerald from Colombia's Chivor mine. Composite photo by Robert Weldon.

crystal (Schmetzer, 1989; Schmetzer and Kiefert, 1990). Aurisicchio et al. (1994) confirmed the existence of type I and type II water, and they also indicated that, in addition to Na^+, the alkalis K^+ and Cs^+ can occupy the channel positions of the beryl structure. The type and amount of water and associated

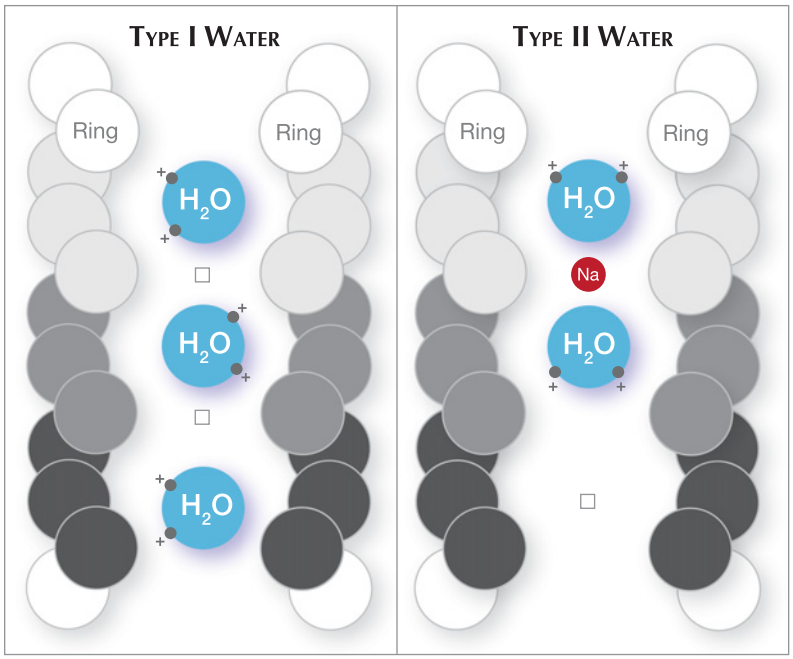

Figure 2. This view of the emerald structure looking approximately perpendicular to the c-axis shows the Si_6O_{18} rings aligned precisely over one another, forming continuous, open channels that may hold large ions or molecules. Water molecules in the channels are classified as type I *or* type II *according to their orientation relative to the beryl structure. Modified from Aurisicchio et al. (1994).*

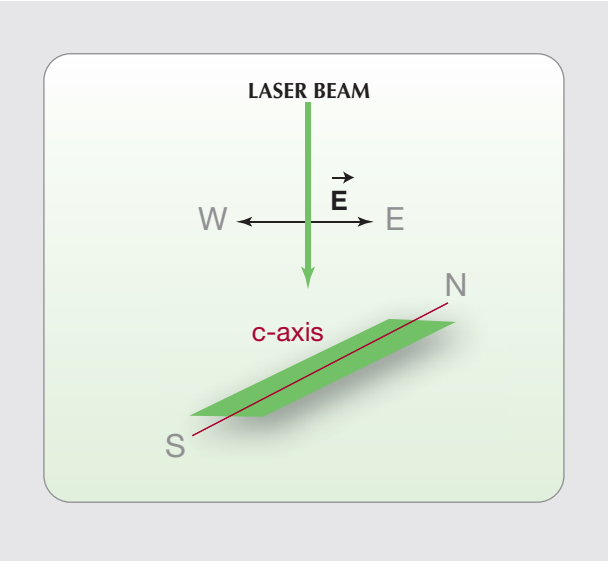

Figure 3. For Raman analysis, the sample is oriented so the c-axis of the crystal is perpendicular to the electric vector (E) of the laser beam.

alkalis in the beryl channel sites can provide valuable information for assessing the natural vs. synthetic origin of emeralds, as well as their geographic origin or method of manufacture.

MATERIALS AND METHODS

We collected 326 samples for Raman measurements, including 260 emerald crystals obtained directly from mines in Brazil (Carnaiba—15 samples, Capoeirana—15, Itabira—15, Santa Terezinha—20, and Socotó—15), Colombia (Chivor—30), Austria (Habachtal—10), Russia (Ural Mountains—10), Madagascar (Mananjary—30), South Africa (Transvaal—30), Zambia (Kafubu—30), Nigeria (Gwantu—30), and China (Malipo—10). In addition, 66 faceted synthetic emeralds consisting of hydrothermally grown (Tairus—15 and Biron—10) and flux-grown (Gilson—20, Chatham—20, and Lennix—1) samples were provided by the producers.

Raman spectra were collected from all samples at room temperature in the confocal mode. Confocal capability is necessary for Raman analysis of individual layers of a sample on a micron scale (0.2–0.5 μm). We used a Jobin Yvon (Horiba group) LabRam HR 800 spectrometer equipped with an Olympus BX41 optical microscope and a Si-based CCD (charge-coupled device) detector. Spectra were collected in the range of OH^- and water molecule vibrations (3700–3500 cm^{-1}). The instrumentation used an Ar^+ ion laser (514 nm emission), a grating of 1800 grooves/mm, and a slit width of 100 mm. These parameters, and the optical path length of the spectrometer, yielded a resolution of 0.8 cm^{-1}. The spectral acquisition time was set at 240 seconds for all measurements, and sample orientation was carefully controlled. The electric vector of the polarized laser beam was always perpendicular to the c-axis (see figure 3). The polarization degree of the laser was about 98%. Peak analysis was performed with an OriginLab 7.5 professional software package, and the peaks were fitted using a Gauss-Lorentz function.

Thirty-one of the crystals were chosen for chemical analysis of major and minor elements by electron probe microanalysis (EPMA; microprobe), and of minor/trace elements (including alkalis) by laser ablation–inductively coupled plasma–mass spec-

TABLE 1. Chemical data of natural and synthetic emeralds by LA-ICP-MS.

Source	Na (wt.%)	K (wt.%)	Na+K (wt.%)
Natural			
Colombia/Chivor 1	0.315	0.008	0.323
Colombia/Chivor 2	0.296	0.041	0.337
Colombia/Chivor 3	0.501	0.006	0.507
Colombia/Chivor 4	0.657	0.021	0.678
Colombia/Chivor 5	0.349	0.047	0.396
Nigeria/Gwantu 1	0.093	0.090	0.183
Nigeria/Gwantu 2	0.064	0.069	0.133
Nigeria/Gwantu 3	0.070	0.052	0.122
Nigeria/Gwantu 4	0.066	0.029	0.095
Nigeria/Gwantu 5	0.070	0.053	0.123
China/Malipo 1	0.773	0.123	0.896
China/Malipo 2	0.962	0.084	1.046
Brazil/Santa Terezinha	1.452	0.102	1.554
Brazil/Socotó	1.466	0.224	1.690
Brazil/Capoeirana	1.329	0.316	1.645
Brazil/Carnaiba	1.533	0.112	1.645
Brazil/Itabira	1.466	0.323	1.789
Russia/Ural 1	1.035	0.712	1.747
Russia/Ural 2	1.394	0.456	1.850
Austria/Habachtal 1	1.281	0.167	1.448
Austria/Habachtal 2	1.327	0.230	1.557
Madagascar/Mananjary 1	1.053	0.057	1.110
Madagascar/Mananjary 2	1.035	0.575	1.610
Zambia/Kafubu 1	1.053	0.392	1.445
Zambia/Kafubu 2	1.065	0.481	1.546
South Africa/Transvaal 1	1.065	0.610	1.675
South Africa/Transvaal 2	1.327	0.525	1.852
Synthetic (hydrothermal)			
Biron 1	0.015	0.008	0.023
Biron 2	0.016	0.004	0.020
Tairus 1	0.007	0.005	0.012
Tairus 2	0.001	0.002	0.003

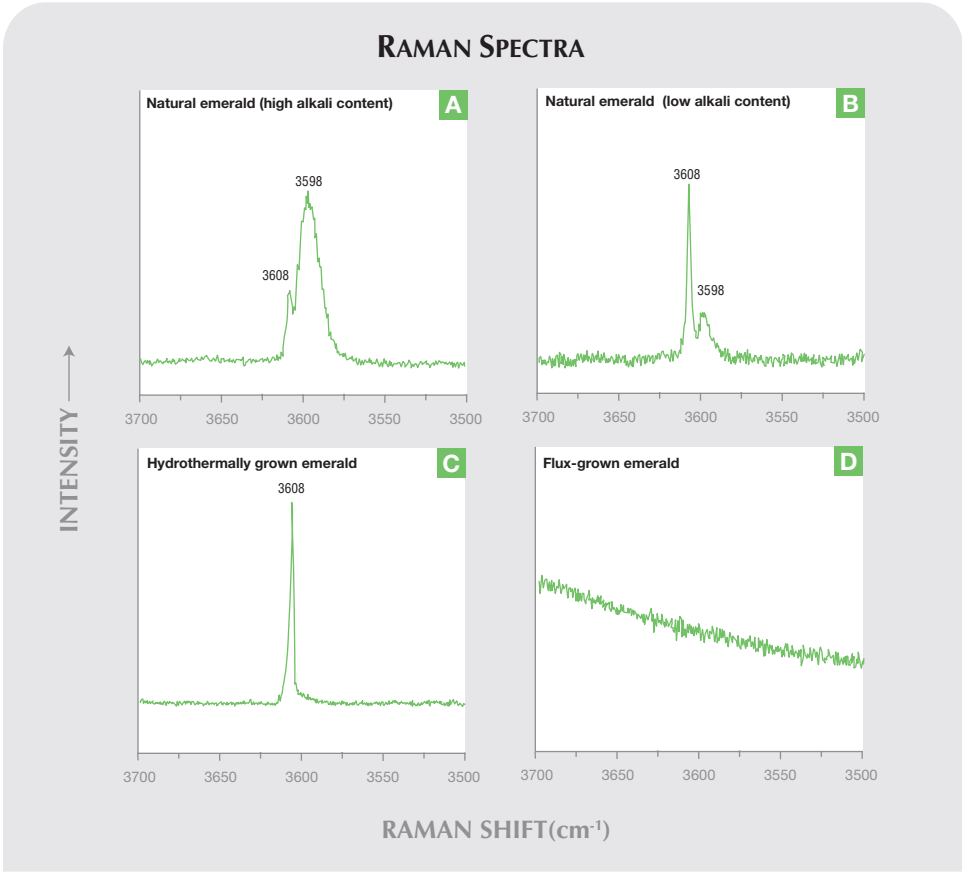

Figure 4. The Raman spectra of emeralds in the water range from 3700 to 3500 cm^{-1} (E⊥c) are shown here. Natural emeralds (A and B, representing samples from Austria and Nigeria, respectively) show two Raman bands, at 3608 and 3598 cm^{-1}, with different intensities depending on alkali content. Hydrothermally grown synthetic emeralds (C) show one Raman band, at 3608 cm^{-1}, while flux-grown samples (D) do not display any Raman signal in this range other than the luminescence signal.

NEED TO KNOW

- Natural and synthetic emeralds from a variety of sources were examined with confocal Raman spectroscopy.
- The presence of Raman bands at 3608 and 3598 cm^{-1} is diagnostic of natural emeralds.
- Hydrothermal synthetics have only the 3608 cm^{-1} band, and flux-grown synthetics show neither band.
- The relative intensity of the two Raman bands in natural emeralds is determined by water type and alkali contents, and may be useful for assigning geographic origin.

trometry (LA-ICP-MS; table 1). No flux-grown samples were chemically analyzed because synthetic emeralds grown by this technique are devoid of channel constituents. Ablation was achieved with a New Wave Research UP-213 Nd:YAG laser ablation system, using a pulse repetition rate of 10 Hz and 100 µm crater diameters. Analyses were performed with an Agilent 7500ce ICP-MS in pulse counting mode (one point per peak and 10 milliseconds dwell time). Data reduction was carried out using Glitter software. The amount of material ablated in laser sampling varied in each spot analysis. Consequently, the detection limits were different for each spot and were calculated for each individual acquisition. Detection limits generally ranged between 0.001 and 0.5 ppm. Silicon (determined with the microprobe) was used as the internal standard. Analyses were calibrated against the silicate glass reference material NIST 612 using the values of Pearce et al. (1997), and the U.S. Geological Survey (USGS) glass standard BCR-2G was measured to monitor accuracy.

RESULTS AND DISCUSSION

As shown in figure 4, bands at 3608 and 3598 cm^{-1} were seen in the Raman spectra of all the natural emeralds, with varying relative intensity. The hydrothermally grown synthetic samples showed just

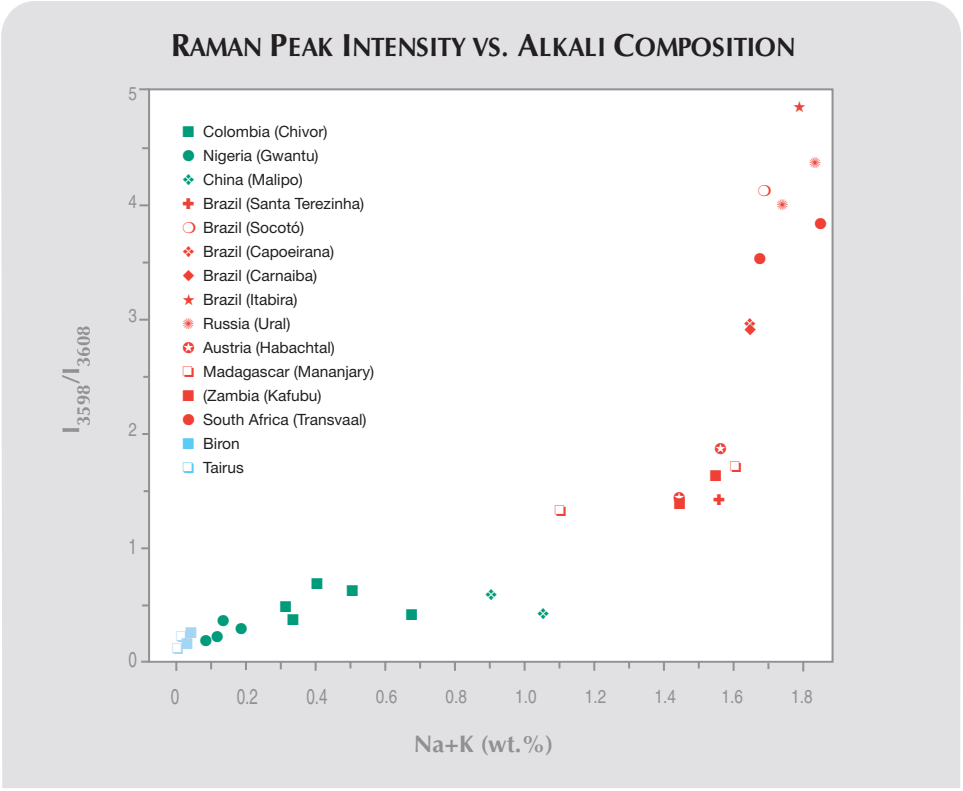

Figure 5. This diagram shows the intensity ratios of the two Raman peaks assigned to the two water types versus the alkali contents in the 31 samples for which chemical analysis was performed. The higher the alkali content in the sample, the greater the intensity ratio of the band at 3598 cm^{-1} to that at 3608 cm^{-1}. This confirms that the 3598 cm^{-1} band is generated by water molecules associated with alkalis (type II), while the 3608 cm^{-1} band is related to water molecules without alkalis (type I).

one band, at 3608 cm^{-1}. None of the flux-grown synthetic samples showed distinct Raman bands in this range because they were anhydrous.

In the samples from Colombia and Nigeria, the band at 3598 cm^{-1} was less intense than that at 3608 cm^{-1}—that is, the I_{3598}/I_{3608} ratio (where I is the peak intensity) was <1—while in samples from all other localities, the I_{3598}/I_{3608} ratio was >1 (figure 5). The Chinese samples had I_{3598}/I_{3608} ratios close to 1.

From the chemical data reported by Hänni (1982), Schrader (1983), and Stockton (1984), and our data obtained by LA-ICP-MS (table 1), it was obvious that the presence and strength of the band at 3598 cm^{-1}, as well as the I_{3598}/I_{3608} ratio, depend on the amount of alkali ions. The 3598 cm^{-1} band was detected only in the alkali-containing (natural) emeralds. In the nearly alkali-free samples (hydrothermal synthetics), this band disappeared while the 3608 cm^{-1} band persisted.

Figure 5 provides a good illustration of how the 3598 cm^{-1} band increased in intensity (relative to the 3608 cm^{-1} band) according to alkali content. For example, in high-alkali samples such as emeralds from Brazil's Socotó mine, with up to 1.7 wt.% alkalis, the I_{3598}/I_{3608} ratio exceeded 4. In low-alkali samples, such as emeralds from Colombia's Chivor mine, with ~0.4 wt.% alkalis, the I_{3598}/I_{3608} ratio was about 0.7. Since emeralds from different localities contain different amounts of alkalis, this Raman technique appears useful for fingerprinting geographic origin (although there was some overlap in our samples from certain localities).

The Raman band at 3598 cm^{-1} is therefore here assigned to the vibration of type II water molecules, because it occurred exclusively in samples containing alkalis, and the Raman band at 3608 cm^{-1} is ascribed to the vibration of type I water. These Raman signals from the different types of water molecules in the beryl channels appear to provide diagnostic evidence for establishing if a sample is natural, flux grown, or hydrothermally grown: In natural emeralds both bands are visible, in hydrothermally grown samples only the 3608 cm^{-1} band is seen, and in flux-grown synthetic emeralds neither of these bands is visible.

CONCLUSION

This study used nondestructive confocal micro-Raman spectroscopy to distinguish natural and synthetic emeralds as well as emeralds synthesized by flux and hydrothermal methods. The technique also appears useful for investigating the geographic origin of natural emeralds, although additional samples from various known localities should be investigated to further evaluate its effectiveness.

ABOUT THE AUTHORS

Dr. Le Thi-Thu Huong (letth@vnu.edu.vn) is a lecturer in mineralogy at the Faculty of Geology, Hanoi University of Science, Vietnam. Prof. Dr. Hofmeister is dean of the Faculty of Chemistry, Pharmacy and Geosciences, and head of the Centre for Gemstone Research, at Johannes Gutenberg University, Mainz, Germany. He is also head of the Institute of Gemstone Research in Idar-Oberstein, Germany. Dr. Häger is senior scientist at the Centre for Gemstone Research at Johannes Gutenberg-University, lecturer in the Gemstone and Jewellery Design Department at the University for Applied Sciences in Idar-Oberstein, and managing director of the Institute of Gemstone Research in Idar-Oberstein.

ACKNOWLEDGMENTS

This research was financed by the Johannes Gutenberg University Fund for Gemstone Research. Analytical facilities were provided by the Institute of Geology at Johannes Gutenberg University. The authors are grateful for the support.

REFERENCES

Aines R.D., Rossman G.R. (1984) The high temperature behavior of water and carbon dioxide in cordierite and beryl. *American Mineralogist*, Vol. 60, pp. 319–327.

Aurisicchio C., Grubessi O., Zecchini P. (1994) Infrared spectroscopy and crystal chemistry of the beryl group. *Canadian Mineralogist*, Vol. 32, pp. 55–68.

Goldman D.S., Rossman G.R., Parkin K.M. (1978) Channel constituents in beryl. *Physics and Chemistry of Minerals*, Vol. 3, pp. 225–235.

Hänni H.A. (1982) A contribution to the separability of natural and synthetic emeralds. *Journal of Gemmology*, Vol. 18, No. 2, pp. 138–144.

Pearce N.J.G., Perkins W.T., Westgate J.A., Gorton M.P., Jackson S.E., Neal C.R., Chenery S.P. (1997) A compilation of new and published major and trace element data for NIST SRM 610 and NIST SRM 612 glass reference materials. *Geostandards Newsletter*, Vol. 21, pp. 115–144.

Schmetzer K. (1989) Types of water in natural and synthetic emerald. *Neues Jahrbuch für Mineralogie, Monatshefte*, No. 1, pp. 15–26.

Schmetzer K., Kiefert L. (1990) Water in beryl—A contribution to the separability of natural and synthetic emeralds by infrared spectroscopy. *Journal of Gemmology*, Vol. 22, No. 4, pp. 215–223.

Schrader H.W. (1983) Contribution to the study of the distinction of natural and synthetic emeralds. *Journal of Gemmology*, Vol. 19, No. 6, pp. 530–543.

Stockton C.M. (1984) The chemical distinction of natural from synthetic emeralds. *G&G*, Vol. 23, No. 2, pp. 141–145.

Wood D.L., Nassau K. (1967) Infrared spectra of foreign molecules in beryl. *Journal of Chemical Physics*, Vol. 47, No. 7, pp. 2220–2228.

Wood D.L., Nassau K. (1968) The characterization of beryl and emerald by visible and infrared absorption spectroscopy. *American Mineralogist*, Vol. 53, pp. 777–800.

Yu K.N., Tang S.M., Tay T.S. (2000) PIXE studies of emeralds. *X-ray Spectrometry*, Vol. 29, pp. 267–278.

BASTNÄSITE-(CE) AND PARISITE-(CE) FROM MT. MALOSA, MALAWI

Alessandro Guastoni, David Kondo, and Fabrizio Nestola

Large crystals of the rare-earth carbonates bastnäsite-(Ce) and parisite-(Ce) have been collected from alkaline pegmatites at Malawi's Mt. Malosa, where they occur associated with aegirine, microcline, and several other unusual accessory minerals. Only small portions of some crystals are suitable for cutting into attractive gems, because most of the material is opaque or heavily fractured. This report presents the gemological and chemical properties of Mt. Malosa bastnäsite-(Ce) and parisite-(Ce) gemstones. This area shows good potential for future production of these rare-earth carbonates, although cut stones will continue to be rare.

Bastnäsite-(Ce), which has the chemical formula (Ce,*RE*)(CO_3)(F,OH), and parisite-(Ce), or Ca(Ce,*RE*)$_2$(CO_3)$_3$(F,OH)$_2$, are cerium-dominant rare-earth (*RE*) carbonates. Although they very rarely form as crystals large and clean enough for faceting, one locality in Pakistan (Zagi or Zegi Mountain) has produced bastnäsite-(Ce) that has been faceted into stones up to 20 ct (Johnson, 1999; Obodda and Leavens, 2004). Gem-quality parisite-(Ce) has been reported very rarely, usually associated with Colombian emeralds such as those from Muzo (Henn et al., 1992). In fact, the mineral is named in honor of J. I. Paris, one of the first managers of the Muzo mine (Palache et al., 1963). This note reports on bastnäsite-(Ce) and parisite-(Ce) from Malawi's Mt. Malosa, where these minerals occur as well-formed crystals that locally may contain clear, gem-quality portions (e.g., figure 1). One of the authors (AG) visited the deposit in 2002 for research purposes, and has documented the geology and mineralogy of the area in other publications (e.g., Guastoni et al., 2007, 2009).

See end of article for About the Authors and Acknowledgments.
GEMS & GEMOLOGY, Vol. 46, No. 1, pp. 42–47.

LOCATION AND ACCESS

The Zomba-Malosa massif is located in southern Malawi, ~250 km southeast of the capital city of Lilongwe (figure 2). Pegmatites containing bastnäsite-(Ce) and parisite-(Ce) are located close to the summit of Mt. Malosa (elevation ~2,000 m) and along the slopes flanking the Zomba-Malosa massif. The steep terrain makes mining dangerous and restricts accessibility in the area (figures 3 and 4). Lake Valley Minerals Ltd. (Lilongwe) is sponsoring and training local farmers in mining techniques, and assisting them with obtaining nonexclusive licenses for commercially recovering mineral specimens from this deposit.

GEOLOGIC SETTING

The pear-shaped Zomba-Malosa pluton (again, see figure 2) is composed of a central core of syenite and an outer ring of peralkaline granite (Bloomfield, 1965). This suite was emplaced ~113 ± 4 million years ago (Eby et al., 1995), and belongs to the Chilwa alkaline belt, which includes several smaller Cretaceous plutons outcropping along the East African rift (Woolley, 1987). The bastnäsite-(Ce) and parisite-(Ce) crystals are hosted by miarolitic alkaline pegmatites and are associated with albite, aegirine, arfvedsonite, Ce-bearing pyrochlore, fluorite, hingganite-(Y), microcline, several Nb-Ta-Y oxides and Be-Na-Y-Zr-Ba-silicates, the niobophyl-

Figure 1. Some gem-quality portions can be seen in this 2 cm parisite-(Ce) crystal from Mt. Malosa, which is sitting on a matrix of aegirine. Courtesy of the Natural History Museum of Milan, catalog no. 37800; photo by R. Appiani.

lite-astrophyllite mineral series, quartz, synchysite-(Ce), xenotime-(Y), and zircon (e.g., Guastoni et al., 2007). For the most part, these pegmatites outcrop within the central syenite portion of the Malosa intrusion, and they often contain large miarolitic cavities of decimeter-to-meter dimensions that are lined with the aforementioned minerals and RE-carbonates.

DESCRIPTION OF THE CRYSTALS

Bastnäsite-(Ce) and parisite-(Ce) from Mt. Malosa form prismatic or barrel-shaped crystals up to 20 cm long. The bastnäsite-(Ce) crystals are brownish orange and interlayered with opaque yellow-brown parisite-(Ce). The parisite-(Ce) crystals are fractured (again, see figure 1) and commonly consist of an inner transparent brownish orange core that is surrounded by an opaque crust composed of yellow-brown bastnäsite-(Ce) + rhabdophane-(Ce) + cerianite. However, the parisite-(Ce) crystals may be completely replaced by goethite + microcline. A detailed description of the mineralogy of these two carbonates is provided by Guastoni et al. (2009).

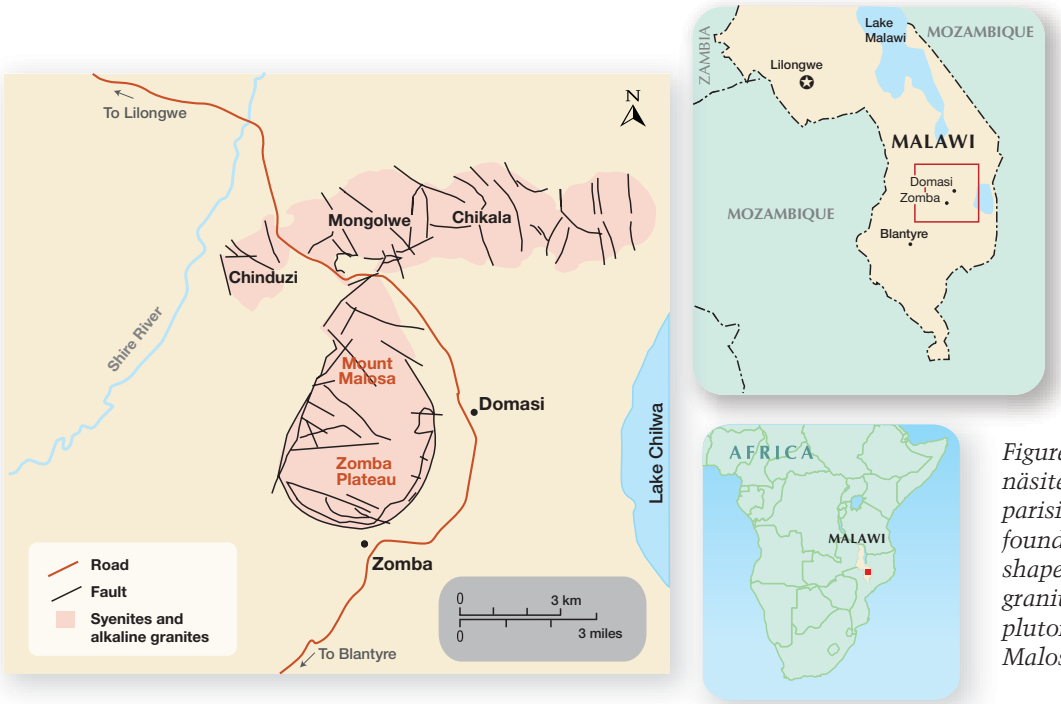

Figure 2. Bastnäsite-(Ce) and parisite-(Ce) are found in the pear-shaped syenitic-granitic alkaline pluton at Mt. Malosa.

Figure 3. The pegmatite mining area is located within steep terrain, as seen here from the summit of Mt. Malosa. Photo by A. Guastoni.

MATERIALS AND METHODS

We studied four faceted samples of bastnäsite-(Ce) and one faceted parisite-(Ce), all from Mt. Malosa (see table 1 and figure 5), from the gem collection of the Natural History Museum of Milan. All five samples were characterized by standard gemological methods and Raman spectroscopy at GIA in New York. Chemical analyses were performed at the University of Padua.

Color appearance was assessed in a Macbeth Judge II light box and in incandescent light. We determined specific gravity hydrostatically, and measured refractive indices using a standard gemological refractometer. Fluorescence was tested using standard long- and short-wave UV lamps, and internal features were observed with a gemological binocular microscope. Ultraviolet-visible–near infrared (UV-Vis-NIR) absorption spectra were observed with a double-beam spectrophotometer. Raman spectra were collected with a Renishaw inVia microspectrometer.

Chemical data were obtained from two rough samples (nos. 79815 and 79819) before they were faceted. Electron microprobe analyses were performed using a Cameca Camebax SX 50 instrument with wavelength-dispersive spectrometers (16–18 spot analyses per sample). The F^- and OH^- contents were measured with a CE-Instruments EA 1110 automatic CHNS elemental analyzer, and CO_2 content was obtained with thermogravimetric profiles (Guastoni et al., 2009).

Figure 4. Small tunnels follow miarolitic cavities in the alkaline pegmatites on Mt. Malosa. Photo by A. Guastoni.

NEED TO KNOW

- Bastnäsite-(Ce) and parisite-(Ce) are cerium-dominant rare-earth carbonates.
- Both minerals are mined from alkaline pegmatites in Malawi, but very rarely in gem quality.
- As gems, both have a similar brownish orange color, but they are easily separated by their standard gem properties.

RESULTS AND DISCUSSION

Visual Appearance and Physical Properties. These properties are summarized in table 1. The faceted bastnäsite-(Ce) and parisite-(Ce) samples generally resembled one another, with face-up colors ranging from slightly brownish orange to very slightly brownish yellowish orange; they appeared slightly more brownish when examined with incandescent vs. daylight-equivalent illumination. The RI values for bastnäsite-(Ce) were $n_o = 1.718–1.719$ and $n_e =$ over the limits of the refractometer (>~1.81); the parisite-(Ce) had RIs of $n_o = 1.669$ and $n_e = 1.769$. Both RE-carbonates were uniaxial positive and strongly birefringent. The SG of bastnäsite-(Ce) ranged from 5.05 to 5.23; Guastoni et al. (2009) found that this variability is related to the abundance of lanthanides, particularly

TABLE 1. Gemological properties for the Malawi bastnäsite-(Ce) and parisite-(Ce) samples studied.

Sample no.	Species	Weight (ct)	Color	Refractive index		Specific gravity	Raman vibrational bands (cm^{-1})
				n_o	n_e		
79815	Bastnäsite-(Ce)	1.55	Slightly brownish orange	1.718	>1.81	5.13	3588, 1743, 1442, 1097, 352, 259, 166
79816	Bastnäsite-(Ce)	0.82	Slightly brownish orange	1.719	>1.81	5.05	3598, 1743, 1441, 1097, 737, 349, 259, 166
79817	Bastnäsite-(Ce)	0.79	Slightly brownish orange	1.719	>1.81	5.23	3586, 1742, 1431, 1097, 738, 353, 260
79818	Bastnäsite-(Ce)	0.34	Very slightly brownish yellowish orange	1.719	>1.81	5.07	3586, 1743, 1433, 1097, 738, 353, 260
79819	Parisite-(Ce)	0.22	Very slightly brownish yellowish orange	1.669	1.769	3.79	1740, 1567, 1431, triplet at 1101/1093/1083, 741, 398, 269

the ratio Ce/(Y+La+Pr+Nd+Sm). The SG of the parisite-(Ce) was measured at 3.79. All the samples were inert to both long- and short-wave UV radiation. All samples showed "rare-earth" spectral features, consistent with descriptions by Johnson (1999) and Massi (2007). The hardness of bastnäsite-(Ce) and parisite-(Ce) are reported to be 4–4.5 and 4.5, respectively (Gaines et al., 1997).

Our bastnäsite-(Ce) samples showed properties comparable to those in gems from Pakistan reported by Johnson (1999) and Massi (2007). Our single parasite-(Ce) sample had similar RI values to those reported for two samples from Muzo (Fryer, 1982), but our SG of 3.79 was markedly different from the 4.18 value measured for the Colombian sample.

Internal Features. Microscopy revealed the presence of numerous "fingerprints" and fractures in all samples (e.g., figure 6). The fingerprints in the bastnäsite-(Ce) gemstones were composed of multiphase inclusions, frequently displaying a large gas bubble and in some cases a very minute transparent solid phase. The fingerprints in the parisite-(Ce) sample were composed of finer two-phase (fluid-gas) inclusions.

None of our bastnäsite-(Ce) samples contained the needle-like inclusions that are common in material from Pakistan, which were identified as astrophyllite by Niedermayr (2001).

Figure 5. These samples (from left to right, 79818, –16, –15, –17, and –19; see table 1) were examined for this study. The faceted round stone on the right is parisite-(Ce), and the other four stones are bastnäsite-(Ce). Photo by J. Liao.

Raman Spectra and Chemical Composition. Figures 7 and 8 show the Raman spectra of the bastnäsite-(Ce) and parisite-(Ce) samples, respectively. The main feature of the bastnäsite-(Ce) spectra (which were quite similar for the four samples studied) is the intense vibrational band at ~1097 cm^{-1}, which is consistent with symmetric CO_3 stretching. Further characteristic bands were recorded at approximately

Figure 6. These "fingerprints" in bastnäsite-(Ce) are composed of two- and three-phase inclusions. Photomicrographs by D. Kondo; image widths 2.1 (left) and 1.1 mm (right).

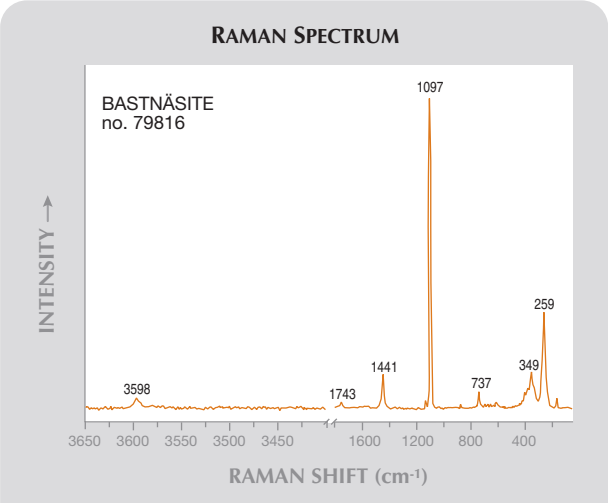

Figure 7. The Raman spectrum for bastnäsite-(Ce) displays the most intense vibrational band at ~1097 cm^{-1}.

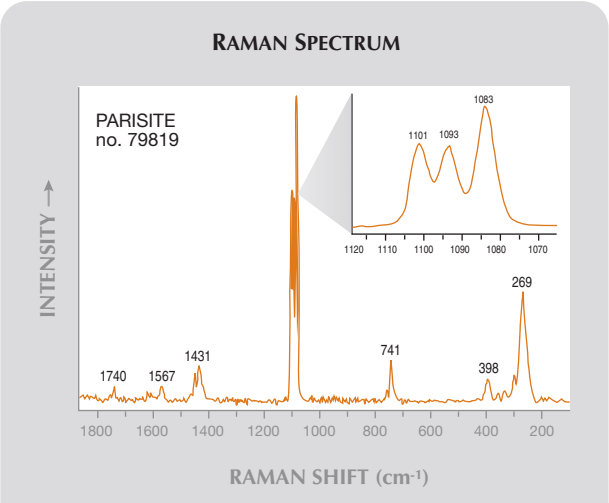

Figure 8. The Raman spectrum for parisite-(Ce) displays the strongest vibrational band at 1083 cm^{-1}.

259 cm^{-1} [translational lattice mode T(Ce,CO_3)], 737 cm^{-1} (symmetric CO_3 deformation), and 1441 cm^{-1} (asymmetric CO_3 stretching; see Gunasekaran et al., 2006). In addition, a clear band at ~3600–3585 cm^{-1} can be assigned to OH^- (Guastoni et al., 2009). The Raman spectrum of the parisite-(Ce) sample recorded a main vibrational band at 1083 cm^{-1}, similar to bastnäsite-(Ce). However, the inset in figure 8 clearly shows a marked split of the band at three slightly different wavenumber values (1101, 1093, and 1083 cm^{-1}), which is due to different crystal structure features.

Representative electron microprobe analyses of bastnäsite-(Ce) and parisite-(Ce) are presented in table 2. The bastnäsite-(Ce) samples were rather homogeneous in composition, and the parisite showed a similar makeup—except for a significantly higher Ca content, as expected from the chemical formula. The minor Sm and traces of Ca in our bastnäsite-(Ce) samples have not been reported in the material from Pakistan (e.g., Johnson, 1999).

TABLE 2. Chemical composition of bastnäsite-(Ce) and parisite-(Ce) from Mt. Malosa, Malawi.

Oxide (wt.%)	Bastnäsite-(Ce) (no. 79815)	Parisite-(Ce) (no. 79819)
CaO	nd[a]–0.2	9.3–9.8
Y_2O_3	0.2–0.6	0.5–1.1
La_2O_3	17.2–20.5	14.8–17.0
Ce_2O_3	34.4–36.9	30.4–32.3
Pr_2O_3	3.1–3.6	2.5–3.5
Nd_2O_3	8.8–9.5	7.8–8.9
Sm_2O_3	1.6–2.1	1.3–1.7
CO_2	20.9–21.2	23.9–24.7
F	6.5–7.2	5.6–6.3
H_2O	0.7–0.9	0.3–0.6
Total	99.6–99.8	99.7–99.9

[a] *nd = not detected*

Identification. Bastnäsite-(Ce) and parisite-(Ce) from Malawi can be easily separated by their RI and SG values, as well as by Raman analysis and chemical composition. Parcels of bastnäsite-(Ce) from Pakistan have been mixed with similar-colored grossular and sphene, but these can be easily separated by their standard gemological properties (Blauwet and Hyršl, 2001), as well as their rare-earth spectral features observable with a spectroscope or spectrophotometer.

CONCLUSION

Bastnäsite-(Ce) and parisite-(Ce) are rare accessory minerals from alkaline pegmatites at Mt. Malosa, and only small portions of these materials are suitable for faceting. Parisite-(Ce) gemstones are particularly rare, because most of the rough is opaque or heavily fractured. Although production of both minerals is still less than 20 grams per year, the deposit appears to be extensive. Most faceted RE-carbonates are sold to private collectors because they are too soft to be set in jewelry.

ABOUT THE AUTHORS

Dr. Guastoni (alessandro.guastoni@unipd.it) is museum curator in the Department of Geosciences, and Dr. Nestola is assistant professor of mineralogy and crystallography, at the University of Padua, Italy. Mr. Kondo is gemological research associate at the GIA Laboratory in New York.

ACKNOWLEDGMENTS

The authors thank Dr. Federico Pezzotta of the Museum of Natural History of Milan, Italy, for loaning the samples used in this study.

REFERENCES

Blauwet D., Hyršl J. (2001) Gem News International: Brownish red to orange gems from Afghanistan/Pakistan misrepresented as bastnäsite and other materials. *G&G*, Vol. 37, No. 2, p. 144.

Bloomfield K. (1965) *The Geology of the Zomba Area*. Geological Survey of Malawi Bulletin 16, 193 pp.

Eby G.N., Roden-Tice M., Krueger H.L., Ewing W., Faxon E.H., Woolley A.R. (1995) Geochronology and cooling history of the northern part of the Chilwa alkaline province, Malawi. *Journal of African Earth Sciences*, Vol. 20, pp. 275–288.

Fryer C., Ed. (1982) Gem Trade Lab Notes: Parasite. *G&G*, Vol. 18, No. 4, p. 230.

Gaines R.V., Skinner H.C.W., Foord E.E., Mason B., Rosenzweig A. (1997) *Dana's New Mineralogy: The System of Mineralogy of James Dwight Dana and Edward Salisbury Dana*, 8th ed. John Wiley and Sons, New York, pp. 476 and 480.

Guastoni A., Pezzotta F., Zorzi F. (2007) Neufunde aus Alkalipegmatiten am Mount Malosa, Malawi: Die weltbesten Zektzeritkristalle und interessante Pseudomorphosen. *Lapis*, Vol. 33, No. 3, pp. 38–41.

Guastoni A., Nestola F., Giarretta A. (2009) Mineral chemistry and alteration of rare earth element (REE) carbonates from alkaline pegmatites of Mount Malosa, Malawi. *American Mineralogist*, Vol. 94, pp. 1216–1222.

Gunasekaran S., Anbalagan G., Pandi S. (2006) Raman and infrared spectra of carbonates of calcite structure. *Journal of Raman Spectroscopy*, Vol. 37, pp. 892–899.

Henn U., Vonplaten H., Hofmesiter W., Bank H. (1992) Physical and chemical properties of gem parisite from Muzo, Colombia. *Neues Jahrbuch für Mineralogie, Monatshefte*, Vol. 6, pp. 258–264.

Johnson M. (1999) Gem Trade Lab Notes: Bastnäsite, a rare faceted sample. *G&G*, Vol. 35, No. 2, pp. 136–137.

Massi L. (2007) Gem News International: Color-change bastnäsite-(Ce) from Pakistan. *G&G*, Vol. 43, No. 2, pp. 165–166.

Niedermayr G. (2001) Bastnaesit aus Pakistan – ein neuer Schmuckstein? *Mineralien Welt*, Vol. 12, No. 3, p. 51.

Obodda H., Leavens P. (2004) Zagi Mountain, Northwest Frontier Province, Pakistan. *Mineralogical Record*, Vol. 35, pp. 205–220.

Palache C., Berman H., Frondel C. (1963) *Dana's System of Mineralogy*, 7th ed., Vol. 2, John Wiley and Sons, New York, pp. 282–285.

Woolley A.R. (1987) Lithosphere metasomatism and the petrogenesis of the Chilwa Province of alkaline igneous rocks and carbonatites, Malawi. *Journal of African Earth Sciences*, Vol. 6, pp. 891–898.

DIAMOND

Coated and Fracture-Filled Orangy Red Diamond

The New York lab recently examined a 1.09 ct round brilliant diamond with an evenly distributed, highly saturated orangy red color (figure 1, left). Extremely rare in nature, such high saturation is typically seen only in treated or synthetic diamonds. Viewed with magnification, though, it lacked the color zoning or graining seen in such stones. Further investigation with reflected light revealed colorless spots along the pavilion facets and facet junctions (figure 1, right), which indicated the presence of a coating.

Viewed face-up, the diamond fluoresced weak blue to long-wave ultraviolet (UV) radiation, and very weak yellow to short-wave UV. Both appeared patchy throughout the diamond. Viewed face-down, however, the diamond appeared inert, indicating that the fluorescence was being masked.

Infrared (IR) spectroscopy showed features typical of a type Ia diamond.

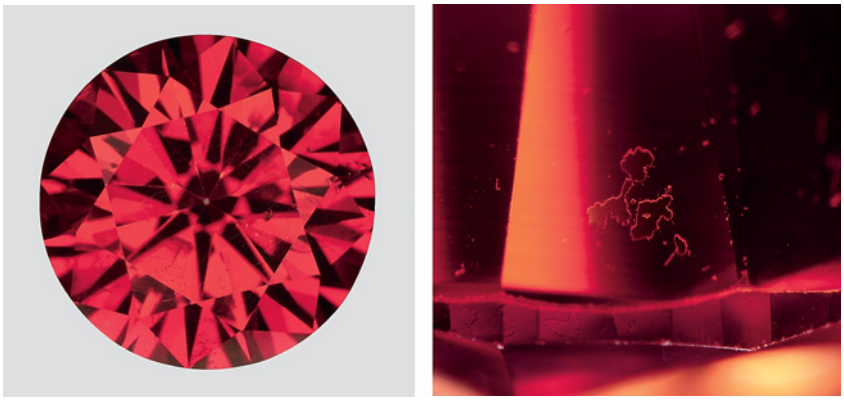

Figure 1. This coated and fracture-filled 1.09 ct diamond displayed a vivid orangy red color (left). In reflected light, small colorless spots were evident on the pavilion (magnified 60×).

The UV-visible-near infrared (UV-Vis-NIR) spectrum (figure 2) revealed a broad band centered at ~480 nm, typical for an orangy yellow to yellowish orange diamond, rather than a strong orangy red one such as this. With the ultra-short-wave (~225 nm) radiation of the DiamondView (figure 3), we could see patches of blue fluorescence where the coating had been damaged; no coating was evident on the crown facets.

Further examination with magnification produced evidence of a second treatment. Looking at the stone through the pavilion, we saw numerous cracks that appeared to contain trapped bubbles, often the first indication that a diamond has been glass filled (S. F. McClure and R. C. Kammerling, "A visual guide to the identification of filled diamonds," Summer 1995 *G&G*, pp. 114–119). Although the flash effect would normally be easy to see in a glass-filled diamond such as this one that had many large feathers, the orangy red coating masked the effect. Only with strong fiber-optic lighting could we see flash effects in this diamond, but they appeared in several areas when viewed through the crown and the pavilion. Energy-dispersive X-ray fluorescence (EDXRF) spectroscopy detected lead, which confirmed the presence of a glass filling.

As this stone illustrates, we are now seeing combinations of diamond treatments. Since neither coating nor fracture filling is permanent, only an identification report was issued for this diamond.

Sharon Cybula and Paul Johnson

Editors' note: All items were written by staff members of the GIA Laboratory.

GEMS & GEMOLOGY, *Vol. 46, No. 1, pp. 48–57.*

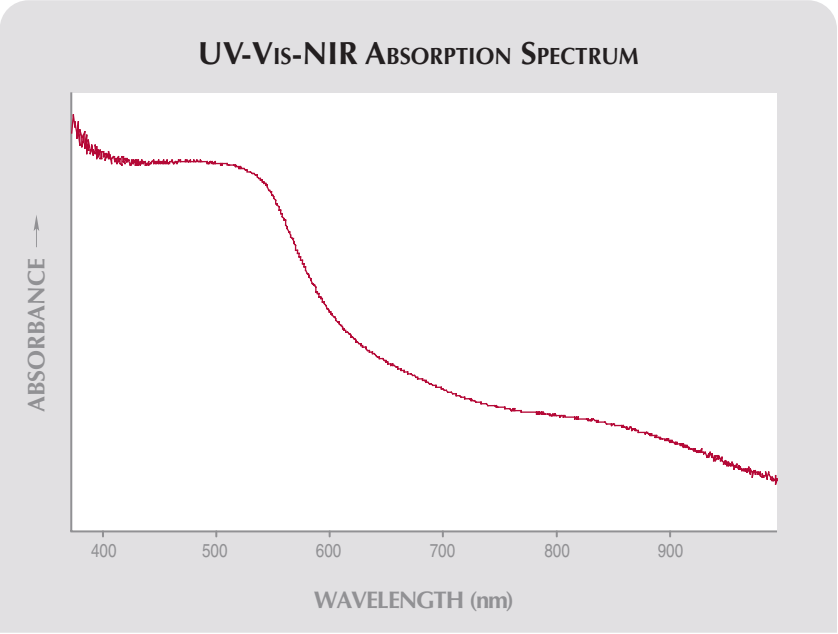

Figure 2. The UV-Vis-NIR absorption spectrum of the coated orangy red diamond is typical of a diamond with an orangy yellow to yellowish orange color.

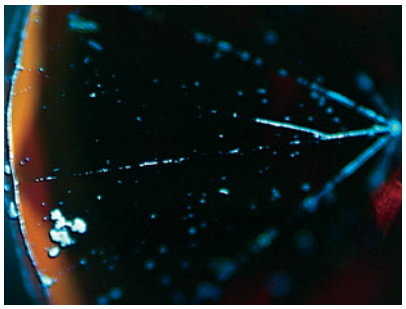

Figure 3. In the DiamondView, the pavilion of the 1.09 ct treated diamond fluoresced only in those areas where the coating was not present.

Diamond with Rare Green Fluorescence

Some gem-quality diamonds fluoresce when exposed to UV radiation. The majority exhibit blue fluorescence, which is produced by the N3 center (a group of three nitrogen atoms surrounding a vacancy) found in type Ia diamonds (see, e.g., T. M. Moses et al., "A contribution to understanding the effect of blue fluorescence on the appearance of diamonds," Winter 1997 *G&G*, pp. 244–259). Other fluorescence colors may also be observed, depending on the type of optical centers present. For example, the strong orange-pink fluorescence associated with rare type IIa diamonds (often referred to as "Golconda pinks") is produced by nitrogen-vacancy (NV) centers.

A 2.39 ct round brilliant-cut diamond (figure 4) submitted to the New York lab showed unusual green fluorescence. It received a color grade of E and a clarity grade of Internally Flawless (IF). IR absorption spectroscopy confirmed the diamond was type IIa, with no detectable N-related absorption. It fluoresced moderate-to-strong green to long-wave UV radiation, and strong green to short-wave UV; the green fluorescence was also visible in the DiamondView (figure 5).

Green fluorescence is produced by the H3 center, which was detected in the UV-Vis absorption spectrum of this diamond. The H3 center is also responsible for the strong green luminescence emitted to visible light by type Ia "green transmitters" (e.g., E. Fritsch et al., "Detection of treatment in two unusual green diamonds," Fall 1988 *G&G*, pp. 165–168). To find a natural-color type IIa diamond with this strong, evenly distributed green fluorescence is extremely rare, especially in the colorless (D-E-F) range. The characteristic pattern of the dislocation network seen in the DiamondView (figure 6) was—combined with other spectroscopic and gemological features—a clear indication that the color was natural. This green fluorescence provided an added rarity factor to an already very unusual type IIa diamond with excellent color and clarity.

Paul Johnson

Figure 4. This 2.39 ct E-color diamond was notable for its evenly distributed green fluorescence to both long- and short-wave UV radiation.

Figure 5. The DiamondView image of the 2.39 ct diamond shows the strong green fluorescence.

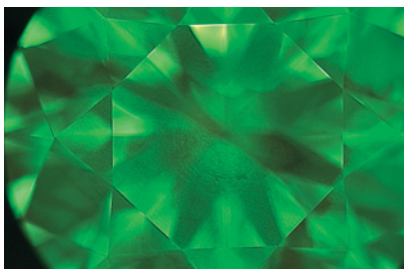

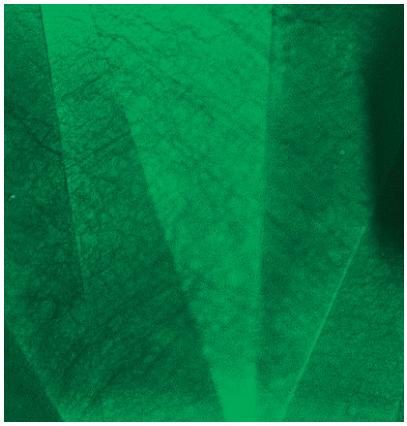

Figure 6. As seen in this DiamondView image of the E-color diamond, the pavilion facets displayed a distinct pattern of dislocations.

Identification of Irradiated Black Diamonds

Irradiating diamonds to change their color is not a new practice, especially for black stones. In fact, nearly six decades ago F. H. Pough and A. A. Schulke noted that overexposure to cyclotron radiation caused diamonds to turn black ("The recognition of surface irradiated diamonds," Spring 1951 *G&G*, pp. 3–11). The identification of laboratory-irradiated black diamonds has historically been conducted mainly through standard gemological testing (i.e., examination with a microscope and handheld spectroscope). With technological advances, we now have sophisticated testing protocols that help provide more conclusive evidence for the cause of color in such stones.

The two round brilliants in figure 7 were recently submitted to the New York laboratory for origin-of-color reports. Both were identified as type Ia diamonds and were color graded Fancy black. Viewed with an overhead light source, they appeared opaque, with a high luster despite numerous pits and polish marks.

With microscopic examination and fiber-optic illumination, the 0.65 ct stone appeared dark green and the 2.10 ct diamond was deep blue (again, see figure 7). The larger sample had numerous graphitized inclusions. The dark green color of the smaller stone was typical of "black" diamonds colored by artificial irradiation (see, e.g., R. C. Kammerling et al., "An investigation of a suite of black diamond jewelry," Winter 1990 *G&G*, pp. 282–287). Both diamonds were inert to both long- and short-wave UV radiation, and we detected no radioactivity in either of them with a Geiger counter. Today, most diamonds are irradiated in an electron accelerator, which typically leaves no residual radioactivity.

UV-Vis-NIR spectroscopy at liquid-nitrogen temperature showed no distinct absorptions in the 0.65 ct stone but a 741 nm cutoff in the 2.10 ct diamond. In addition, high-resolution UV-Vis-NIR spectroscopy of the 2.10 ct diamond showed weak and broad absorption peaks at 464, 470, and 545 nm. The 464 and 470 nm peaks are thought to be radiation-related, while the 545 nm peak suggests the presence of hydrogen. Photoluminescence (PL) spectra collected with a 633 nm laser revealed a clear emission peak at 741 nm in both diamonds, due to the GR1 carbon vacancy defect.

The combination of gemological and spectroscopic features indicated that these diamonds were artificially irradiated. The high concentration of the GR1 defect is responsible for the extremely dark color of both "black" diamonds; the "tail" of this absorption system extended throughout the visible range of the spectrum. Although the GR1 defect may be present in both natural and artificially irradiated diamonds, the intensity of this peak further corroborated observations that these diamonds underwent laboratory irradiation to induce their black appearance.

Jason Darley, Sally Chan, and Michelle Riley

Figure 7. The extremely dark bodycolors of these two "black" diamonds (0.65 ct, left; 2.10 ct, right) were created by laboratory irradiation.

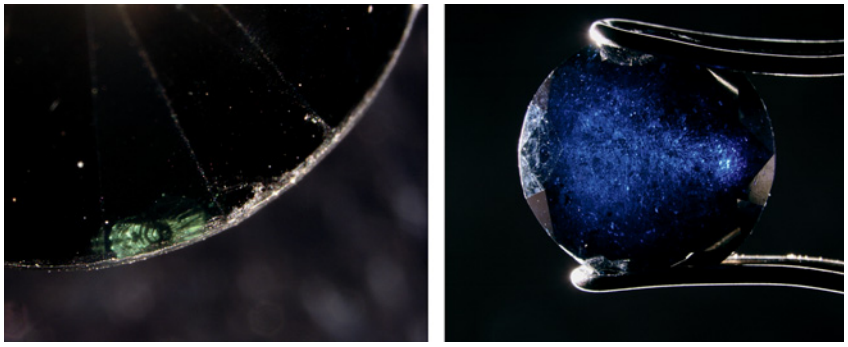

Large HPHT-Treated Type IIb Blue Diamond

Type IIb diamonds are well known for their blue color and electrical semiconductivity, both of which are caused by boron impurities. Yet only a small portion of type IIb diamonds have a pure, strong blue color. Gray and even brown hues are commonly present and sometimes dominate the color appearance. However, high-pressure, high-temperature (HPHT) treatment can remove these unwanted gray and brown components, resulting in a more attractive blue bodycolor. This treatment technique has been used to improve diamond colors for more than a decade, and recently the New York laboratory tested one of the largest HPHT-treated type IIb diamonds we have seen to date (figure 8).

This 6.46 ct pear-shaped diamond (15.31 × 10.48 × 5.71 mm) was color graded Fancy Intense blue, with no gray or brown modifier. The clarity

Figure 8. This 6.46 ct Fancy Intense blue diamond is one of the largest HPHT-treated type IIb diamonds seen in the GIA lab.

was IF; unlike many other HPHT-treated type IIa and IIb diamonds, it displayed no internal graining. One relatively large pavilion facet was only partially polished, with remnants of the frosted surfaces created by HPHT treatment still evident. Microscopic observation with crossed polarizers revealed only a weak gray-brown interference color in a wavy pattern. The diamond was electrically conductive.

Examination with the DiamondView showed moderately strong blue fluorescence and strong blue phosphorescence. The mid-IR spectrum had strong, broad absorptions at ~2930, ~2800, and ~2460 cm^{-1}, which confirmed this diamond was type IIb. Based on the intensity of these absorption bands, the boron concentration was estimated at ~0.24 ppma. The UV-Vis-NIR spectrum showed smoothly decreasing absorption from the near-IR to the UV region, typical of a pure type IIb blue diamond. Photoluminescence spectroscopy at liquid-nitrogen temperature with laser excitations from UV to IR, together with other gemological properties, confirmed this diamond was HPHT treated.

Type IIb diamonds are extremely rare in nature and highly valued in the jewelry market. The existence of an HPHT-treated type IIb diamond of such size and quality underscores the importance of having gems identified by a properly equipped laboratory.

Wuyi Wang, Ren Lu, and Tom Moses

Pink Diamonds Colored by Multiple Treatment Processes

Natural pink-to-red diamonds derive their color from two types of lattice defects: one referred to as the 550 nm band and the other known as NV centers. In most such diamonds, including those from the Argyle mine in Australia, the cause of color is attributed to the 550 nm band. While the importance of this absorption feature has been known for some time, the physics of this defect are not fully understood, and to date there is no known technique that can create it artificially.

NV centers, however, are better understood and can be introduced in a laboratory, mainly through a combination of multiple treatment processes. A large number of orange-pink-red diamonds, colored by artificially induced NV centers, have recently become available in the jewelry market. The New York lab has tested 63 such treated diamonds, all with strong pink coloration (most the equivalent of Fancy to Fancy Vivid).

The largest stone was an 8.44 ct pear shape (18.02 × 11.21 × 6.41 mm), color graded Fancy Vivid orangy pink (figure 9). Weak color concentration was observed at the culet and along the keel. The stone fluoresced strong orange with weak green zones to long-wave UV radiation and strong orange to short-wave UV. Aside from some minor fractures, there were no notable internal features.

The mid-IR spectrum displayed weak absorptions at 1332 and 1170 cm^{-1}, but no peaks at ~1360 cm^{-1} (platelets) or ~1280 cm^{-1} (A-form nitrogen). These features indicated a pure type IaB diamond, with an estimated 2.3 ppma of nitrogen based on the intensity of the absorption at 1280 cm^{-1}. In addition, very weak absorptions at 1450 cm^{-1} (the H1a defect) and 1344 cm^{-1} (attributed to isolated nitrogen) were recorded. Also observed were moderately strong hydrogen-related absorptions at 3107 and 1405 cm^{-1} (intensities of 0.35 and 0.09 cm^{-1}, respectively).

UV-Vis-NIR spectra collected at liquid-nitrogen temperature showed strong absorptions from NV centers, with sharp zero-phonon peaks at 575.0 and 637.0 nm, as well as their related sidebands. These absorptions effectively block green and yellow light and partially block orange light, resulting in the intense orangy pink color. Moderately strong absorptions were observed at 594.3 and 741.2 (GR1) nm, which are typical features of irradiation and/or annealing in diamond. Weak absorptions from ND1 (393.3 nm), N3 (415.2 nm), H4 (496.0 nm), and H3 (503.1 nm) were also confirmed.

All 63 diamonds had very similar features. The gemological and spectroscopic observations strongly suggest that they were treated by multiple processes, which may include HPHT annealing and subsequent irradiation and annealing at relatively low temperatures.

This combination of techniques has resulted in an influx of treated-

Figure 9. This 8.44 ct diamond, color graded Fancy Vivid orangy pink, was treated by multiple processes, which may include irradiation and HPHT annealing.

color pink diamonds into the jewelry industry.

Wuyi Wang

Type IIa Greenish Yellow Diamond Colored by IR-Inactive Nitrogen

Type IIa diamonds have no detectable nitrogen-related absorptions in the mid-IR region, and they are most commonly colorless, near-colorless, or brown with varying saturation (attributed to "vacancy cluster" defects in connection with plastic deformation). N-related lattice defects rarely contribute to the color of a type IIa diamond, except for a few very light pink "Golconda" diamonds, which are colored by NV centers. Recently, the New York laboratory examined a greenish yellow type IIa diamond colored by an IR-inactive nitrogen defect.

The color of this 0.90 ct Fancy greenish yellow diamond (5.86 × 5.54 × 3.30 mm; figure 10) was distributed evenly throughout the stone. The mid-IR spectrum showed no absorption in the one-phonon region—which classified it as type IIa—and no hydrogen-related 3107 cm^{-1} band. (A weak 3107 cm^{-1} band is commonly observed when a type IIa diamond contains a trace amount of nitrogen that is barely detectable in the IR spectrum.) When examined with a standard UV lamp, the diamond fluoresced strong blue to long-wave UV radiation and moderate yellow to short-wave UV. Examination with the DiamondView showed strong green fluorescence and the well-developed polygonal pattern, caused by lattice dislocations, that is characteristic of natural type II diamonds (figure 11).

Figure 10. The greenish yellow color of this 0.90 ct type IIa diamond is caused by an IR-inactive nitrogen-related defect.

The UV-Vis-NIR absorption spectrum, collected at liquid-nitrogen temperature, revealed the relatively high concentration of the H3 defect, with its zero-phonon line (ZPL) at 503.2 nm, that is responsible for the greenish yellow color (e.g., figure 12). The H3 defect—composed of two nitrogen atoms and a nearby vacancy—absorbs blue and violet light and emits green light. Also recorded was a moderately strong absorption from the N3 defect (ZPL at 415.2 nm) and a weak but sharp peak at 637.0 nm from the NV^- center, as well as their sidebands related to the ZPLs. The N3 defect and the NV^- center contributed little, if anything, to the diamond's color, since N3 is outside the visible light region and absorption from NV^- was very weak. An E-color type IIa diamond with strong green fluorescence to UV radiation attributed to the N-bearing H3 defect is reported by P. Johnson on pp. 49–50 of this section.

Figure 11. The DiamondView image of the 0.90 ct diamond showed strong green fluorescence and the well-developed polygonal pattern typical of a type II stone.

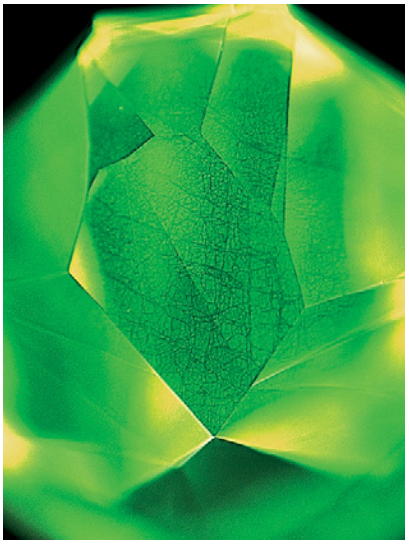

Both gemological and spectroscopic features ruled out any possibility of treatment. It is interesting to encounter a type IIa diamond that contains a substantial amount of IR-inactive nitrogen, especially since the greenish yellow color is caused by a nitrogen-related defect.

Ren Lu and Wuyi Wang

Red CVD SYNTHETIC DIAMOND with Multiple Treatments

As noted above, natural diamonds with strong pink-to-red colors are very rare and highly valued. Various techniques have been developed to create such colors in the laboratory, including the use of synthetic diamonds as the starting material.

The New York lab recently received a 0.74 ct red rectangular modified brilliant (figure 13) for grading. The Fancy red color was slightly more concentrated in the culet area and in the pavilion corners. The stone contained some nearly linear arrays of tiny black inclusions with irregular morphology that were oriented parallel to the table. The sample fluoresced moderate and strong orange to long- and short-wave UV radiation, respectively. In the DiamondView, it displayed intense red fluorescence and darker parallel banding in the pavilion, as well as moderately strong red phosphorescence.

The mid-IR spectrum revealed weak absorptions at 1450 cm^{-1} (H1a), 1344 (isolated nitrogen), and 1332 cm^{-1}. In addition, weak but sharp absorptions related to hydrogen were observed at 3107 and 1405 cm^{-1}. One notable feature was a very weak band recorded at 3123 cm^{-1}, which is specific to synthetic diamonds grown by chemical vapor deposition (CVD). No absorption features were detected in the near-IR region, except for a very weak band at 5892 cm^{-1}.

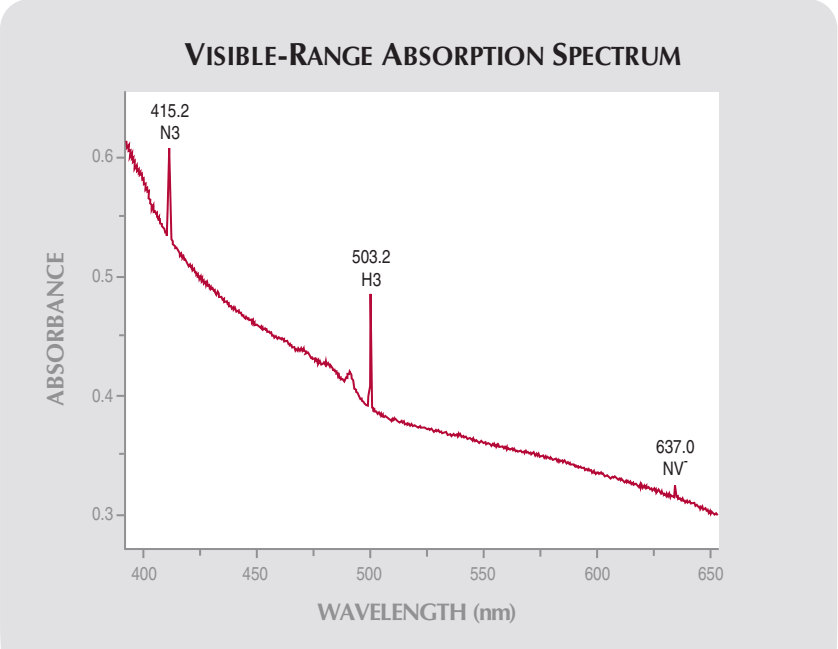

Figure 12. As this visible-range absorption spectrum demonstrates, the greenish yellow color of the 0.90 ct diamond was caused by the H3 defect.

The UV-Vis-NIR spectrum (figure 14), recorded at liquid-nitrogen temperature, included strong NV absorptions with zero-phonon lines at 574.9 and 637.0 nm and their corresponding sidebands. Absorptions observed at 594.3 ("595 nm center") and 741.2 (GR1) nm are typical of diamonds that have undergone an irradiation/annealing process. An absorption doublet at 736.6/737.0 nm was attributed to the $[Si\text{-}V]^-$ defect, which appears almost exclusively in CVD synthetic diamonds. In addition, several very weak but sharp absorptions were detected in the 420–505 nm region, including those from the H3 and H4 defects. Photoluminescence (PL) spectra collected with various laser excitations at liquid-nitrogen temperature detected many additional features, including a weak line from the N3 defect at 415.2 nm and the characteristic radiation-related 389 nm center.

Annealing experiments on CVD synthetic diamonds have demonstrated that the 3123 cm^{-1} band is stable up to ~1600°C, while the 3107 cm^{-1} band is not generated until the temperature reaches 2200°C. Annealing at temperatures above 1600°C will cause diamond to graphitize unless the heating

Figure 13. This 0.74 ct Fancy red diamond (4.85 × 4.41 × 3.67 mm) was identified as a CVD synthetic. Multiple treatments were applied after the initial growth to produce this color.

Figure 14. The UV-Vis-NIR absorption spectrum revealed that the red color of the CVD synthetic diamond in figure 13 was produced by a relatively high concentration of NV centers. Also detected were the 594.3 nm and GR1 irradiation/annealing features.

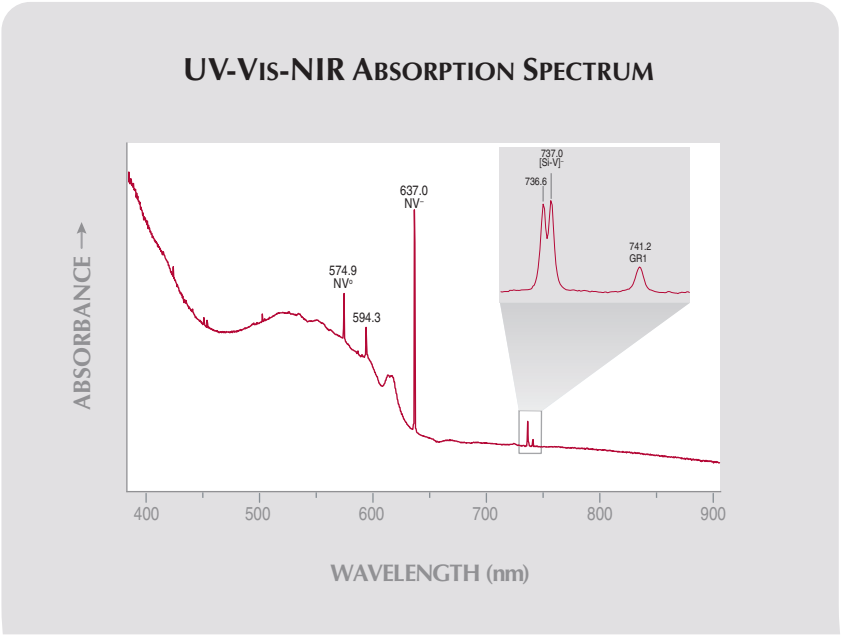

Figure 15. The remarkable transparency of this jadeite bangle is due to impregnation with a polymer that has an RI very close to that of the host material.

is done at high pressures. Therefore, we believe the present sample underwent high-pressure, high-temperature annealing, which would have removed the brown hue common in nitrogen-doped CVD synthetic diamonds, as well as increased the concentration of isolated nitrogen.

With low-temperature PL spectroscopy, NV centers are commonly detected in as-grown CVD synthetic diamonds, except for rare high-purity samples. While NV emissions may be dominant in PL spectra, typically they are virtually undetectable or very weak in UV-Vis absorption spectra and have little, if any, effect on body-color. Concentrations of NV centers in as-grown CVD synthetic diamonds decrease significantly after HPHT annealing, so the high concentrations of NV centers in this red CVD-grown sample cannot be the direct result of HPHT annealing alone. Instead, the strong absorptions from NV centers, which are responsible for the red color, were likely introduced by additional treatment processes, such as irradiation followed by annealing at relatively low temperatures. Vacancies, produced by high-energy irradiation, will migrate and combine with pre-existing isolated nitrogen impurities to form NV centers when the stones are annealed at relatively low temperatures. During this process, other irradiation-related defects, such as the absorptions at 594.3 nm and 1450 cm^{-1} will be produced. The high concentration of NV centers strongly absorb light in the green-to-orange region, creating a transmission window in the red region. The intensity of the resulting pink-to-red coloration depends on the concentration of these optical centers.

W. Wang et al. ("Latest generation CVD-grown synthetic diamonds from Apollo Diamond Inc.," Winter 2007 *G&G*, pp. 294–313) described some CVD synthetic diamonds with intense pink color that was mainly attributed to a broad absorption band at ~520 nm. However, we have not previously detected typical radiation-related optical centers (e.g., 594.3 nm and the GR1) and the 3107 cm^{-1} absorption in pink CVD samples.

This is the first red CVD synthetic diamond with multiple treatments submitted to the GIA Laboratory for grading. We do not know the manufacturer.

Wuyi Wang and Paul Johnson

Figure 16. The jadeite bangle is so transparent it is possible to read through it.

Exceptionally Transparent Treated JADEITE

Jadeite jade is an aggregate material and therefore easy to treat; in fact, dyeing of jadeite has been performed for centuries. In the early 1990s, it was discovered that the undesirable natural brown staining often seen in jadeite could be removed with acid, leaving purer white, green, or purple colors. Unfortunately, this acid treatment also damaged the structure of the jadeite, which then had to be impregnated with polymers to make it usable. This treatment is now commonplace, and labs routinely test for it.

Two main factors determine the value of jadeite: color and transparency. Jadeite is never completely transparent, but the closer it gets the more desirable it becomes. This is true even if a specimen has no color at all. In fact, colorless, semitransparent jadeite is highly sought after.

It was with interest, then, that the Carlsbad laboratory examined the bangle bracelet shown in figure 15. Gemological testing confirmed that it was jadeite, but we were immediately struck by its exceptional transparency. The bangle was not particularly thin, yet it was still possible to read through it (figure 16). Further testing showed that the bangle was impregnated with a foreign substance, and microscopic examination gave us clues to its remarkable appearance.

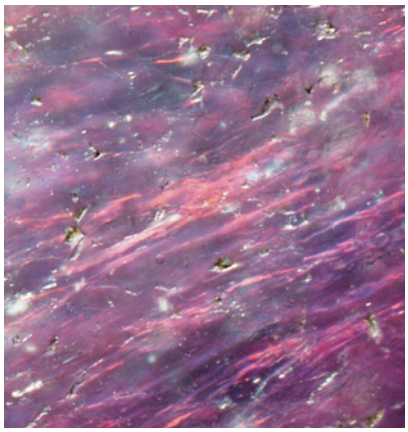

Figure 17. Microscopic examination of the jadeite bangle revealed the tell-tale flash effect produced by fracture filling. Field of view 1.4 mm.

In darkfield illumination, the piece looked purplish, even though it had no apparent purple coloration in normal light. Higher magnification showed that the purple actually represented "flashes" from the areas between the crystal grains of the aggregate, with orange flashes also evident as the piece was tilted (figure 17). We have seen this flash effect in a number of gem materials over the last two decades, most notably glass-filled diamonds (see, e.g., the first entry in this Lab Notes section), and we know of only one explanation for it: a filling substance with a refractive index very close to that of its host.

These observations pointed to impregnation with a polymer that has an RI close to that of jadeite (~1.66), which masked the voids between the crystal grains and thus made the bangle appear much more transparent than it would have been otherwise. The jadeite had apparently been treated not only to enhance the color and stabilize the material, but also to improve its transparency.

This was the first time we had seen this variation on impregnated jadeite, but several more examples have since appeared at the lab.

Shane F. McClure

Large Pair of Natural Freshwater PEARLS

The New York laboratory recently received a pair of large pink pearls (figure 18) for identification. This was our second look at both pearls, which were submitted separately the first time. The pearls were undrilled and measured 17.67 × 17.24 mm (37.85 ct) and 17.46 × 17.05 mm (35.72 ct).

Using microradiography and X-ray luminescence, we confirmed that they were natural freshwater pearls with no indication of treatment, and that they originated from a mollusk in the Unio family. Even with subtle differences in hue and overtone, the pearls were fairly well matched. The first was classified as orangy pink with no overtone, and the second was light pink with orient. This similarity in color, and their matching size and shape, made for a visually appealing set.

Most natural freshwater pearls of this shape and color have been found in rivers in the United States, particularly the Mississippi River. We have seen a number of pearls in this hue range that were reportedly recovered in Texas, though they were much smaller.

When we next saw the two pearls, they had been set in a pair of pendant earrings. While a single near-round natural freshwater pearl of such size is unusual in itself, a matched pair is truly remarkable.

Akira Hyatt

Blockage-Induced Growth Tubes in TOURMALINE

The Carlsbad laboratory recently examined an interesting watermelon tourmaline from the Governador Valadares area of Minas Gerais, Brazil. A window polished parallel to the optic axis revealed several growth tubes induced by inclusions that had blocked the growth of the tourmaline. While this is not especially unusual in tourmaline, this particular specimen provided an extremely good example of blockage-induced growth tubes.

Figure 18. These large pearls (37.85 and 35.72 ct) were identified as natural freshwater pearls from the Unio family. Courtesy of Mr. and Mrs. Mohammed Idris Jabir.

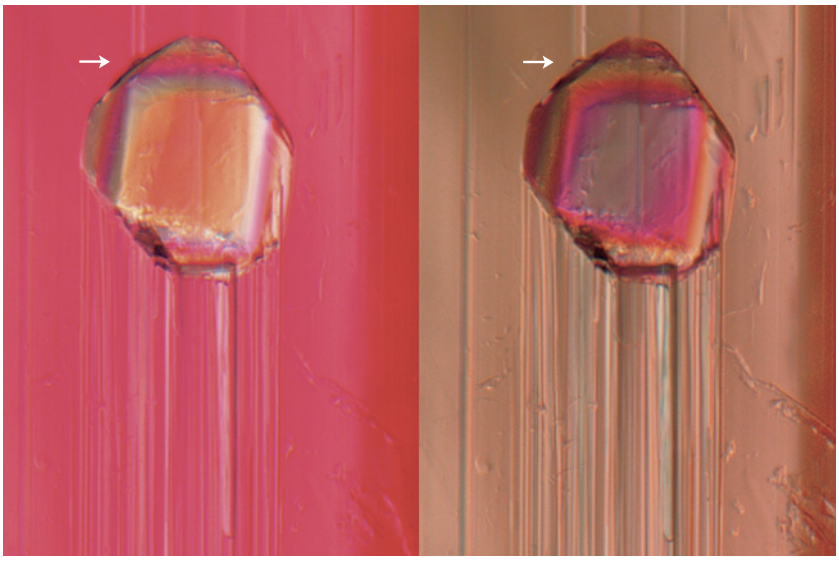

Figure 19. This feldspar crystal interrupted crystal growth in a watermelon tourmaline, creating growth tubes, which have a dramatic appearance in the pleochroic colors seen here with polarized light. Magnified 113×.

The first thing we noticed, using magnification and polarized light, was the pleochroism of the tourmaline itself (figure 19). The growth tubes extended above and below the included feldspar crystal (identified by Raman spectroscopy), as evident in this figure.

During rapid growth of elongated crystals such as tourmaline, small foreign bodies that land on the host may create a localized blockage of necessary nutrients that prevents growth of the host mineral in that area. While the rest of the host is still growing rapidly, the foreign crystal is pushed up along the tourmaline's length until it is sufficiently lodged in place or until growth slows enough to encapsulate the inclusion. The disruptive presence of the protogenetic crystal leaves behind a void, or growth tube, as the host tourmaline continues to grow (R. V. Dietrich, *The Tourmaline Group*, Van Nostrand Reinhold Co., New York, 1985).

Figure 20. Growth tubes are clearly visible only in the green portion of the watermelon tourmaline, originating from the pink/green color boundary. Magnified 20×.

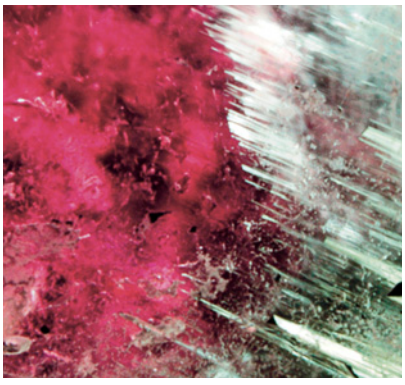

Also evident was a small growth tube extending upward from a defect on the upper left edge of the feldspar crystal (see arrows in figure 19). This defect on the surface of the inclusion was enough to disrupt the growth of the tourmaline host. The growth tube tapered to a sharp point and terminated within the tourmaline (just outside the field of view in figure 19).

Another interesting feature was the correlation between the color boundary and the growth tubes. In the pink core crystal, there were typical trichites and two-phase inclusions, but no growth tubes. This suggests a more stable growth environment during the pink stage of crystal formation. At the boundary between the pink and overlying green zones is where we first see blockage-induced growth tubes (figure 20), and we speculate from this correlation that the event that caused a change in the nutrient solution was sufficiently turbulent to deposit protogenetic debris, such as tiny feldspar crystals, onto the surface of the growing tourmaline crystal.

Because of the rapid growth environment, and the presence of protogenetic debris and growth tubes within the outer green zone, we are left with a story about this tourmaline's growth. As gemologists, it is up to us to read and understand it.

Nathan Renfro and John Koivula

Treated Green TURQUOISE

Because of its porosity, turquoise is routinely impregnated with polymers to make low-quality material more stable. It is not uncommon to see turquoise dyed blue to improve an otherwise feeble color. This is often accomplished with a blue polymer, in effect impregnating and dyeing the material at the same time.

Green turquoise is much rarer than blue turquoise and considered by some to be more desirable. We have recently seen a spike in the amount of green turquoise submitted to the GIA Laboratory, and there is an abundance of it for sale on the Internet, so it was noteworthy when we discovered an interesting modification of the treatment mentioned above (figure 21).

Three cabochons (5.62, 6.28, and 9.58 ct) were submitted to the Carlsbad laboratory for identification. They had an unusual patchy yellowish green to bluish green color, but with the structure and overall appearance of natural turquoise. The RI and SG values were low but consistent with impregnated turquoise. All three

Figure 21. The gem material in this necklace and earrings set shows a composite turquoise structure with a yellow bonding agent. The rondelles in the necklace range from 4 × 8 mm to 8 × 18 mm. Jewelry courtesy of April Logan.

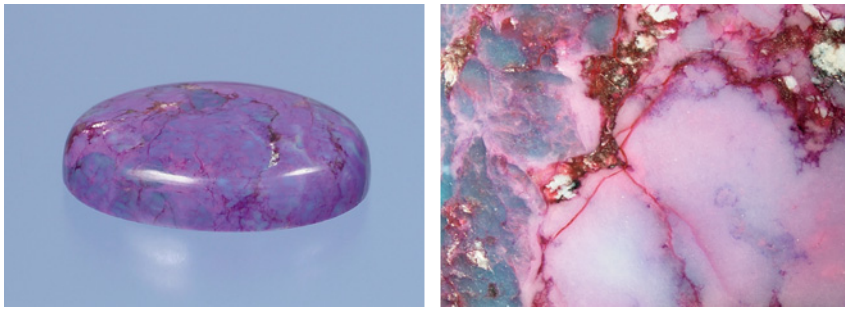

Figure 23. Also seen is turquoise in which the filler is red, making the originally blue stone appear purple. The stone on the left is 5.18 ct; field of view for the photomicrograph on the right is 4.5 mm.

stones fluoresced moderate yellow to greenish yellow to long-wave UV radiation and were inert to short-wave UV. IR spectroscopy confirmed they were turquoise and revealed the presence of a polymer.

Microscopic examination showed that the 5.62 and 9.58 ct cabochons were composites made of multiple pieces of turquoise combined using pressure and a bonding agent. Turquoise composites are not unusual, but in this case the bonding agent (some type of epoxy resin) was yellow, as evidenced by the numerous transparent yellow veinlets (filled fractures) and small filled cavities seen throughout the stones (figure 22). This yellow color was far more saturated than the yellowish tint inherent in many epoxies. The 6.28 ct stone did not appear to be a composite and the bodycolor was predominantly yellowish green, but it also was permeated with fractures filled with a transparent yellow epoxy.

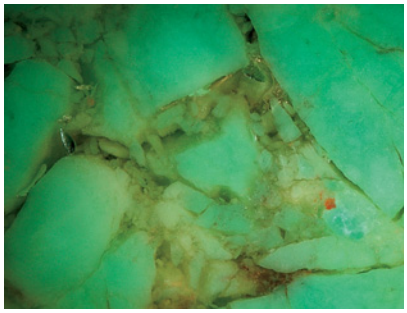

Figure 22. The bonding agent's yellow color is readily apparent in the filled cavities and fractures within the host turquoise. Field of view 3.3 mm.

We realized we were looking at a new scenario. The only explanation for the use of a yellow polymer was to make the originally blue turquoise appear green. We do not recall seeing this particular treatment in turquoise before, but it was readily identified by examination with magnification.

Since encountering those first three cabochons, we have seen several more examples of this material. We also have seen instances where a red filler was used, turning the originally blue stones purple (figure 23).

Shane McClure and Philip Owens

PHOTO CREDITS

Jian Xin (Jae) Liao—1 (left), 4, 8–10, and 13; Sharon Cybula—1 (right); Paul Johnson—3, 5, and 6; Sally Chan—7; Wuyi Wang—11; Don Mengason—15, 16, and 23 (left); Shane F. McClure—17, 22, and 23 (right); Sood-Oil (Judy) Chia—18; Nathan Renfro—19 and 20; Robison McMurtry—21.

GEM NEWS International

2010 TUCSON

Dealers at this year's Tucson gem and mineral shows had low sales expectations, but many were pleasantly surprised given the slow recovery from the global economic downturn. Although attendance was rather low, vendors with unusual and/or attractive merchandise at good prices were typically successful. The shows featured a vast array of crystals, jewelry, and gems, and particularly widespread were Tanzanian spinels (e.g., figure 1). A relatively new product consisted of "Soufflé" cultured freshwater pearls from China, which were notable for their large size, varied colors, and relatively light heft, leading some people to suspect they were hollow (see report on pp. 61–63 of this issue). Several other items seen in Tucson are described in the following pages and will also be documented in future issues of *G&G*.

The theme of this year's Tucson Gem and Mineral Society show was of particular interest to gemologists: "Gems and Gem Minerals." The theme of next year's TGMS show will be "Minerals of California."

G&G appreciates the assistance of the many friends who shared material and information with us this year, and also thanks the American Gem Trade Association for providing space to photograph these items during the AGTA show.

Figure 1. Spinel from Tanzania was prevalent at this year's Tucson gem shows. These attractive pieces from Mahenge each weigh ~20 ct. Courtesy of Dudley Blauwet Gems, Louisville, Colorado (left), and Evan Caplan and Omi Gems Inc., Los Angeles (right); photo by Robert Weldon.

COLORED STONES AND ORGANIC MATERIALS

Update on ametrine from the Yuruty mine, Bolivia. During the Tucson gem shows, Hugo Marancenbau (Steinmar Ltd., Santa Cruz, Bolivia) provided an update on ametrine from the Yuruty mine in Bolivia (see Summer 2000 Gem News, p. 163). This deposit was initially claimed in the mid-1990s and is located ~50 km north of the famous Anahí ametrine mine. Mining at Yuruty has been intermittent, although commercial production was resumed during the past two years. The deposit is exploited by ~100 people in underground workings consisting of a 90 m shaft and four horizontal tunnels up to 200 m long. The mine produces an average of ~40 tonnes/month of mixed-grade material, approximately 3% of which is facetable. Although Mr. Marancenbau's company plans to sell the ametrine in the rough form only, they have test faceted a few thousand carats (weighing 3–30 ct each) that

Editor's note: Interested contributors should send information and illustrations to Brendan Laurs at blaurs@gia.edu or GIA, The Robert Mouawad Campus, 5345 Armada Drive, Carlsbad, CA 92008. Original photos will be returned after consideration or publication.

GEMS & GEMOLOGY, Vol. 46, No. 1, pp. 58–72.

Figure 2. This ametrine (6.46–35.59 ct) was recently mined from the Yuruty deposit in Bolivia. Photo by Robert Weldon.

were sold at the JOGS show. He indicated that it was the first time ametrine from this mine was sold in Tucson.

Mr. Marancenbau kindly donated several rough and cut pieces of ametrine to the GIA Collection. The faceted stones (figure 2) contained varying amounts of purple and yellow, with a sharp color boundary visible face-up in one of the samples. None of them had the distinctive smoky layers seen previously in Yuruty material (see the Summer 2000 Gem News entry).

With several tonnes of rough material stockpiled and good reserves that are inferred to remain underground, the Yuruty deposit appears poised to become an important supplier of ametrine.

Brendan M. Laurs

Andradite from China. At the 2009 and 2010 AGTA shows in Tucson, Eric Braunwart (Columbia Gem House, Vancouver, Washington) had andradite from what he believed to be a new find in China. According to his supplier, the material was initially mined in late 2007 by hand methods in a remote region of western China. The rough consists of well-formed crystals that were apparently derived from a skarn-type deposit. Although referred to as "demantoid" by the miners, none of the garnet appeared green enough to be considered as such.

Mr. Braunwart reported that he faceted ~5,000 carats from his first shipment of rough. Although stones up to 4 ct have been cut, smaller gems up to 1.5 ct typically show the best color and brilliance. Most of the material averages 0.75 ct (5 mm diameter) and ranges from medium greenish yellow to dark brownish yellow to brown and brownish red. At Mr. Braunwart's factory in China, the cutters typically seek the largest size that should yield an attractive stone, and then recut any over-dark gems until their appearance is optimized.

Six faceted samples of the andradite (0.30–1.58 ct; figure 3) were loaned to GIA for characterization, and the following properties were recorded: color—green-yellow to greenish yellow-brown; RI—over the limits of the standard refractometer; hydrostatic SG—3.91 (on the largest stone only); and strong absorption below 450 nm visible with a desk-model spectroscope. These properties are consistent with those reported for andradite by M. O'Donoghue (*Gems*, 6th ed., Butterworth-Heinemann, Oxford, UK, 2006, pp. 206–210), except the SG values in that publication are somewhat lower (3.82–3.85). The fluorescence of the samples ranged from inert to very weak red under long-wave UV, and inert to weak red under short-wave UV radiation. Microscopic examination revealed scattered metallic black crystals (figure 4), randomly oriented transparent colorless needles, and "fingerprints." Two stones also contained low-relief fractures that showed evidence of clarity enhancement. The reaction of the filler to hot-point testing suggested some type of oil.

In the spring of 2009, Mr. Braunwart's supplier provided another parcel of rough, which was very similar to the original material. The individual pieces were significantly smaller, but the supplier indicated that more of the andradite could be produced to meet market demand.

Nathan Renfro (nrenfro@gia.edu)
GIA Laboratory, Carlsbad

Brendan M. Laurs

Figure 3. These andradites (0.30–1.58 ct), reportedly from a new deposit in western China, were selected to show the material's typical range of color. Photo by Robert Weldon.

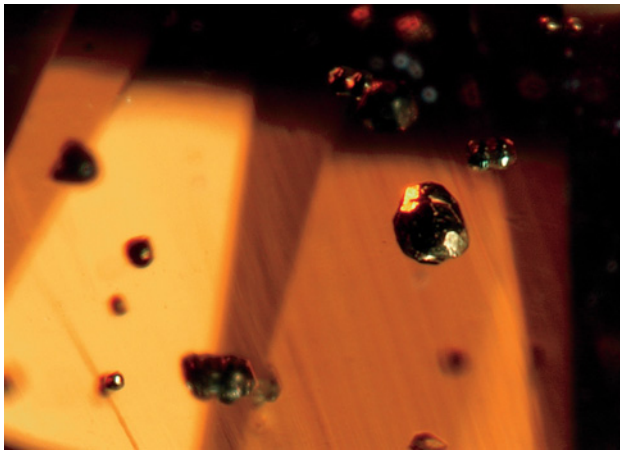

Figure 4. Scattered metallic black inclusions were seen in the Chinese andradite. Photomicrograph by N. Renfro; magnified 60×.

Barite from Brazil. Barite ($BaSO_4$) is a common mineral that is rarely faceted due to its typically opaque appearance, low hardness (Mohs 3–3½), and two good cleavage directions. It was surprising, therefore, to see large clean faceted barites in a variety of colors in Tucson this year. These stones were offered by Luciana Barbosa (Gemological Center, Belo Horizonte, Brazil) at the Gem & Jewelry Exchange (GJX) show, and by Dilermando Rodrigues de Melo Filho (Geometa Ltda., Governador Valadares, Brazil) at the Arizona Mineral & Fossil Show (Hotel Tucson City Center, formerly Inn Suites).

Figure 5. Barite from a new deposit in Acre State, Brazil, is notable for its large size and range of colors. The crystal has a distinct blue zone in the lower right (and an iron stain on the lower left); the cut stones weigh 25.9–51.7 ct. Courtesy of Gemological Center; photo by Robert Weldon.

According to Mr. Rodrigues, the barites came from a new deposit in Acre State, in Brazil's Amazon region. He was told that the stones were mined in August–September 2009 by local *garimpeiros*, and that ~30 kg of mixed-grade material was produced. Although both dealers reported that only a small percentage of the barite was facetable, some large stones have been cut (up to 700 ct), in colors ranging from near-colorless to pale brownish yellow ("champagne") and pale gray, green, and blue. Sharp color boundaries were displayed in some of the bicolored stones (e.g., figure 5). However, only a few bicolored gems were cut because the material is not commonly color zoned, or the color boundary is located near the outer edge of the crystals.

The potential for additional production of this interesting barite is unknown at this time.

Brendan M. Laurs

Hanksite as a gem material. At the GJX show, rare-stone specialist Arthur Birago (Freakingcat.com, Bangkok) had several pieces of faceted hanksite from Searles Lake in Trona, San Bernardino County, California. The stones typically weighed >10 ct, although one rather large one was >250 ct. In addition, faceted hanksite from Searles Lake has been offered for sale on various web sites. As hanksite is a soft and highly water-soluble evaporite mineral, its use in jewelry seems unlikely. In October 2009, this contributor visited Searles Lake and collected several hanksite crystals to investigate the feasibility of using this material as a gem.

Searles Lake—a dry lake bed located in Southern California's Mojave Desert—has produced industrial minerals such as borax for more than 100 years. It is also the source of other evaporite minerals such as halite, hanksite, trona, and sulfohalite. Hanksite, $Na_{22}K(SO_4)_9(CO_3)_2Cl$, contains both sulfate and carbonate groups, which makes it difficult to classify; most mineralogical texts group it with sulfates (see, e.g., E. S. Dana and W. E. Ford, *Textbook of Mineralogy*, 4th ed., John Wiley & Sons, New York, 1932, p. 755).

Because of ongoing commercial mining operations, the site is open to mineral collecting by the public for only one weekend each year, through the cooperation of Searles Valley Minerals. Although hanksite crystals up to several centimeters long can be found, smaller well-formed crystals are typically cleaner and more appropriate for faceting (e.g., figure 6).

This contributor faceted two samples (5.06 and 8.91 ct) of hanksite using standard lapidary techniques. The only modification was that, because of the material's solubility, water could not be used to remove swarf buildup from the lap; a saturated solution of dissolved hanksite was used instead. The stones were polished using 0.5 µm diamond abrasive and mineral oil as a lubricant. A satisfactory pol-

Figure 6. These four crystals (1.3–7.0 g) and faceted gems (5.06 and 8.91 ct) are hanksite from Searles Lake, California. Photo by Robert Weldon.

ish and well-defined facet junctions were achieved using this method, but it was almost impossible to avoid some scratching due to the mineral's low hardness (Mohs 3.5).

Not surprisingly, microscopic examination revealed chips, abrasions, scratches, and cleavage breaks on some surfaces of the faceted stones. Both samples contained similar inclusions, which mostly consisted of pale green angular crystals (figure 7). Raman analysis identified them as gaylussite, a hydrous Na-Ca-carbonate.

Standard gemological testing of the two stones gave the following properties, which were consistent with those published for hanksite in mineralogical textbooks: RI—1.469–1.481; SG (determined with a Sarin device, again because of the material's solubility)—~2.58; fluorescence—weak greenish yellow to long-wave UV and moderate greenish yellow to short-wave UV, with phosphorescence from the latter lasting ~3–5 seconds. Raman analysis confirmed the stones' identity as hanksite.

Because of hanksite's solubility, softness, and typically abundant inclusions, it is poorly suited for jewelry use. Nevertheless, hanksite can be appreciated as a very unusual collector's gem.

Nathan Renfro

Figure 7. Pale green masses of gaylussite were the predominant inclusion in the faceted hanksite specimens. Photomicrograph by N. Renfro; magnified 60×.

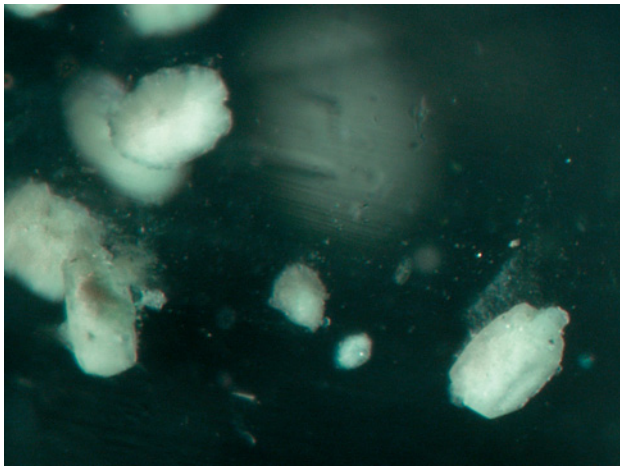

Lepidolite beads from Mozambique. Micas such as muscovite and lepidolite are not commonly used as gem materials, although they have been polished into cabochons and even faceted stones when found in attractively colored fine-grained masses (e.g., Fall 1993 Gem News, pp. 210–211; Spring 2006 Gem News International [GNI], pp. 65–66). At the Arizona Mineral & Fossil Show held at Hotel Tucson City Center, Giuseppe Agozzino (Geofil, Cascais, Portugal) showed this contributor some purple lepidolite beads from the Naipa mine in the Alto Ligonha region of Mozambique (figure 8). The beads were notable for their coarse-grained texture, which produced shiny reflections when viewed from certain directions. Mr. Agozzino indicated that ~200 strands of the beads had been manufactured, in diameters from 12 to 20 mm. In addition, some of the lepidolite was polished into spheres up to 12 cm in diameter.

While most coarse-grained lepidolite lacks the toughness necessary for a gem material, these beads were fashioned from compact spherical radial aggregates. The lepidolite "balls" may attain dimensions exceeding 14 cm (M. Battencourt Dias and W. Wilson, "The Alto Ligonha pegmatites, Mozambique," *Mineralogical Record*, Vol. 31, No. 6, pp. 459–497). The rough material was recovered several years ago from mine dumps. The Naipa deposit continues to be worked today for gem-quality tourmaline, beryl, and other minerals.

Brendan M. Laurs

"Soufflé" freshwater cultured pearls. At the AGTA show, Jack Lynch (Sea Hunt Pearls, San Francisco) had an attractive new product that he sold as "Soufflé pearls." They were notable for their size, up to 20 mm; their high luster; and their wide range of reportedly natural colors (figure 9). According to Mr. Lynch, they debuted with one supplier as "hollow keshi" at the September 2009 Hong Kong Jewellery and Gem Fair. This name probably came from their relatively light heft, leading the dealer to assume they were hollow. Yet other Chinese dealers insisted that producing such large hollow pearls was impossible. Mr. Lynch cut a few samples in half and found that the interiors indeed contained voids, with a dark matter lining the walls. However, when he returned to the United States

Figure 8. These beads (12 and 20 mm in diameter) were fashioned from coarse-grained lepidolite, such as the spherical aggregate shown here. Photo by Jeff Scovil.

and drilled some of the other pearls, he noticed that a black liquid bled from the drill holes. He speculated that they were produced by a new cultivation process, whereby an unconventional type of nucleus was inserted into pre-existing pearl sacs in the mollusks.

Mr. Lynch sent two undrilled samples and one sliced sample to each of these authors for examination. They ranged from 17.7 to 18.6 mm in maximum dimension and were white, light orangy pink, and light pink; all were baroque shaped. Microradiography by both authors revealed large irregular areas of a relatively uniform gray color in their interiors—that is, areas more translucent to X-rays than the surrounding nacre, along with smaller darker, more X-ray transparent areas (e.g., figure 10).

When one of the samples was cut in half, a dark, viscous liquid was noted that quickly dried into the gray matter that filled the pearl's interior (figure 11, left). It could easily have fallen out or been removed during drilling, leaving a void (lined with organic substance) and an irregular nacre thickness of 1.2 to 4 mm. The gray matter, totally separate from the outer layers of the pearl, displayed a brittle, mortar-like structure when viewed with a gemological microscope as well as a scanning electron microscope (SEM; figure 11, right). Energy-dispersive spectroscopy of the gray matter with the SEM showed that the major components were Si and Al, with traces of K, Fe,

Figure 9. These new "Soufflé" freshwater cultured pearls are relatively large (here, ~14 to 20 mm) and come in a wide range of hues with highly lustrous surfaces. Photo by Jack Lynch.

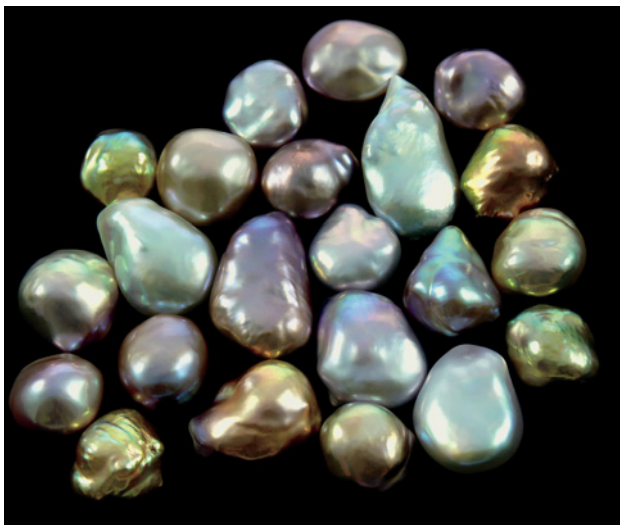

Figure 10. This microradiograph of a "Soufflé pearl" (18 mm long) shows a central gray area that also contains a darker spherical area to the right (possibly a gaseous or liquid phase).

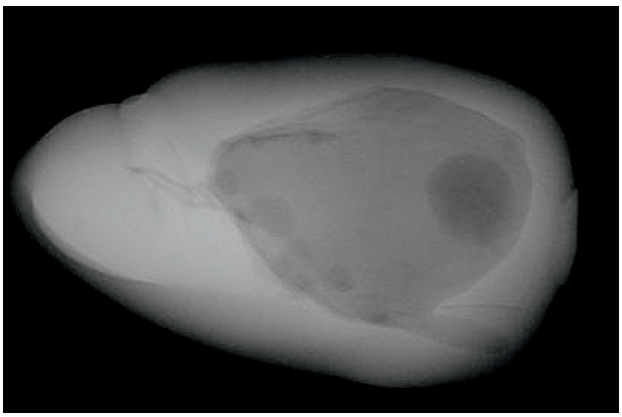

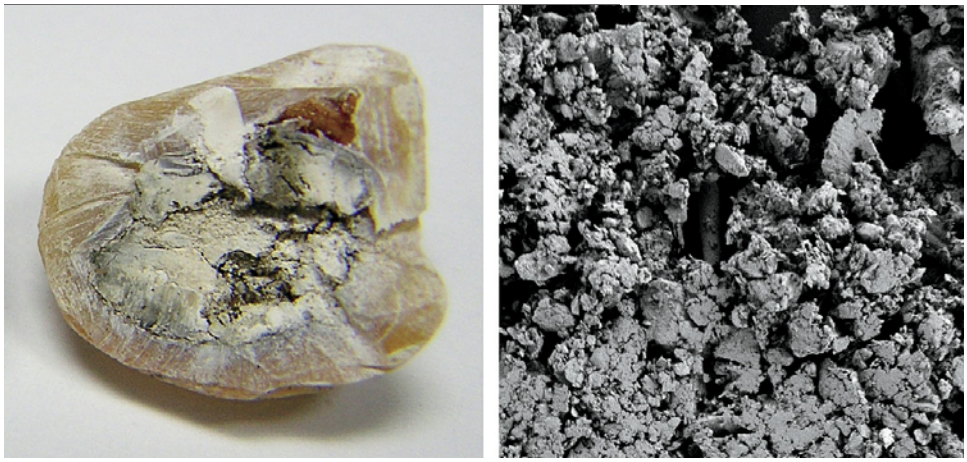

Figure 11. A mud-like core is evident in this section of a "Soufflé pearl" (left, 13.7 × 11.1 mm; photo by E. Strack), with the porous, powdery texture evident in the SEM image (right, magnified 2000×).

Mg, and Na. While this did not identify the material, it did prove that the substance was not a calcium carbonate or organic material connected to pearls or mollusks.

Mr. Lynch's supplier subsequently informed him that "muck," possibly pond mud, had been used to initiate pearl growth. Since this material was deliberately placed within existing pearl sacs in the host mollusks, the resulting cultured pearls cannot be classified as "keshi." Instead, they appear to represent an interesting twist on pearl cultivation. The "nuclei" are unstable to drilling and may not be present in the drilled cultured pearls. This would explain why the strands have a relatively low heft, a fact that—among other attributes—prompted Mr. Lynch to embark on further testing.

Nick Sturman (nicholas.stu@giathai.net)
GIA Laboratory, Bangkok

Elisabeth Strack
Gemmologisches Institut Hamburg, Germany

"Churrasco quartz" with tourmaline and chamosite inclusions from Brazil. In May 2009, Denilson Henrique Salomão (Hercules Gems, Teófilo Otoni, Brazil) recovered 700 kg of colorless-to-smoky quartz containing black needles and hexagonal crystals from the Chapada Diamantina area in Bahia State. The parcel included broken pieces and prismatic crystals; only a few had their natural terminations. Approximately 100 kg were suitable for cutting into cabochons and faceted gems (e.g., figure 12), while the remaining 600 kg were reserved for carving. Mr. Salomão sold the material in Tucson at the GJX show, and he also donated some samples to the Mineralogy Museum at the University of Rome "La Sapienza" that were examined for this report.

Two cabochons were characterized using standard gemological techniques, an FEI Quanta 400 scanning electron microscope, and a Cameca SX 50 electron microprobe at the Italian National Research Council's Institute of Environmental Geology and Geoengineering (IGAG-CNR) in Rome, as well as with a Seifert MZIV X-ray diffractometer at the University of Rome "La Sapienza." The gemological properties were consistent with quartz. The black needles ranged from 0.1 to 5 cm long and 50 to 150 μm in diameter. The hexagonal inclusions were tabular and 0.1–1 cm in diameter. Electron microprobe analyses (see G&G Data Depository at www.gia.edu/gandg) identified the needles as schorl tourmaline and the hexagonal inclusions as chamosite (an Fe-rich chlorite-group mineral that forms a series with clinochlore). Since the chamosite contained an unusually low amount of Mg, powder X-ray diffraction analysis was used to confirm its identity.

The tourmaline needles commonly intersected the chamosite inclusions. The resemblance to *churrasco* Brazilian cuisine, in which meat is grilled on a skewer, led Mr. Salomão and one of these authors (MM) to call the material "Churrasco quartz." To the best of our knowledge, this is the first report of chamosite in quartz. The unusually low Mg content of the chamosite inclusions, and their association with tourmaline, are also noteworthy.

Simona Mazziotti Tagliani, Michele Macrì,
Stefano Stellino, and Adriana Maras
Department of Earth Sciences
University of Rome "La Sapienza"

Marcello Serracino
IGAG-CNR, Rome

Figure 12. This 17.44 ct cabochon of "Churrasco quartz" contains a chamosite crystal that is intersected by a needle of schorl. Photo by M. Macrì.

Figure 13. This cat's-eye rhodonite (6.93 ct) from Brazil shows good chatoyancy. Photo by Robert Weldon.

Cat's-eye rhodonite. Rhodonite ($MnSiO_3$) is an attractive pink-to-red mineral that is often sold as mineral specimens or ornamental material, but seldom as a gemstone, since it is typically opaque and has perfect cleavage in two directions. Facetable material is very rare, and small amounts are occasionally produced from just two localities—Broken Hill, Australia, and Minas Gerais, Brazil (see, e.g., P. W. Millsteed, "Faceting transparent rhodonite from Broken Hill, New South Wales, Australia," Summer 2006 *G&G*, pp. 151–158; and Fall 2004 GNI, pp. 260–261). Some polished rhodonite has a saturated color that resembles fine spinel or rhodochrosite.

At the GJX show, Luciana Barbosa had some attractive rhodonite cabochons showing good chatoyancy (e.g., figure 13). She reported that the material was found in 2009 at Morro da Mina, near Conselheiro Lafaiete in Minas Gerais. The rhodonite is recovered as a byproduct of manganese mining, in a large open pit that is operated by Companhia Vale do Rio Doce. Ms. Barbosa knew of ~30 pieces of the cat's-eye rhodonite (ranging from ~2 to 40 ct), and she had not seen the material previously. To her knowledge, the stones were all untreated. She indicated that the identity of the rhodonite had been confirmed by X-ray diffraction analysis.

We believe this is the first report of cat's-eye rhodonite.

Brendan M. Laurs

GNI Regular Features

DIAMONDS

A large hydrogen-rich diamond with a cuboid phantom cloud. In late 2009, the Gübelin Gem Lab received a 41.54 ct brownish greenish yellow brilliant-cut diamond for routine analysis (figure 14). The cushion-shaped stone measured ~24.4 × 21.4 × 12.0 mm. The client informed us that it was purchased in the early 1970s.

Microscopic examination revealed a cuboid-shaped phantom cloud, which was particularly evident with dark-field illumination (figure 15). The cuboid shape, rarely seen with optical microscopy, is more often noted using X-ray topography; it results from the growth of undulating surfaces with an average orientation corresponding to a cube face. This growth is typically associated with unusually high concentrations of hydrogen (e.g., E. Fritsch et al., "Hydrogen-related optical centers in natural diamond: An update," *New Diamond and Frontier Carbon Technology*, Vol. 17, No. 2, 2007, pp. 63–89). Hydrogen-rich diamonds often have distinctive gemological properties, such as desaturated colors and pinpoint inclusions, typically with yellow UV luminescence. This diamond weakly fluoresced chalky yellow to long-wave UV and faint orange to short-wave UV, with no phosphorescence.

Hydrogen-rich diamonds also have a well-documented

Figure 14. This 41.54 ct brownish greenish yellow diamond is the second-largest documented member of the brown to grayish yellow to green "family" of H-rich diamonds. Photo by Evelyne Murer.

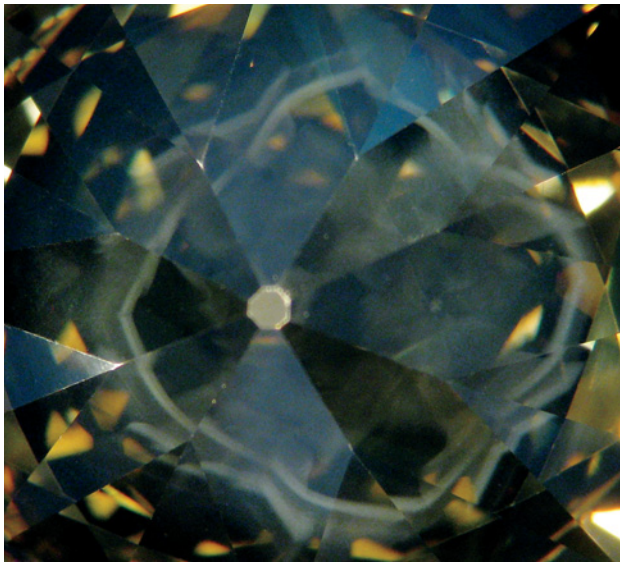

Figure 15. With darkfield illumination, the diamond in figure 14 displays a cuboid phantom cloud (5 mm wide) typical of H-rich diamonds. Photomicrograph by P. Hardy.

set of UV, visible, and IR absorption features. They have been grouped into three "families" according to their UV-visible absorption: (1) brown to grayish yellow to green, (2) gray to blue to violet, and (3) chameleon (see again Fritsch et al., 2007). The UV-Vis-NIR spectrum of this stone showed the N3 (~415 nm) and N2 (~478 nm) bands, which together caused the yellow color. Also present was a continuum of absorption throughout the visible spectrum, giving the brown color component. A broad band centered at ~730 nm was responsible for the green color component, and there was an additional broad band at ~830 nm. This spectrum is typical of diamonds from the brown to grayish yellow to green family. Because it was similar in appearance to some chameleon diamonds, the stone was tested for chameleon behavior, but no change in color was observed when it was placed on a hot plate.

The FTIR spectrum obtained with the beam positioned through the girdle indicated a type IaAB diamond with high nitrogen and hydrogen content (figure 16). The H-related bands associated with the 3107 cm^{-1} system were present, including the elusive 5555 cm^{-1} band. Until now, this weak band has been found only in small diamonds of the gray-to-blue-to-violet family. Nevertheless, this is the most well-defined 5555 cm^{-1} band documented so far (figure 16, inset), presumably due to the diamond's size. Also, this is the second-largest documented member of the H-rich brown to grayish yellow to green family of diamonds, after the 61 ct brown Eye of the Tiger.

Figure 16. The FTIR spectrum shows the H-related absorptions of the 3107 cm^{-1} system. In the inset, the elusive 5555 cm^{-1} band is well resolved. The presumed N-H band at 3236 cm^{-1} is also seen.

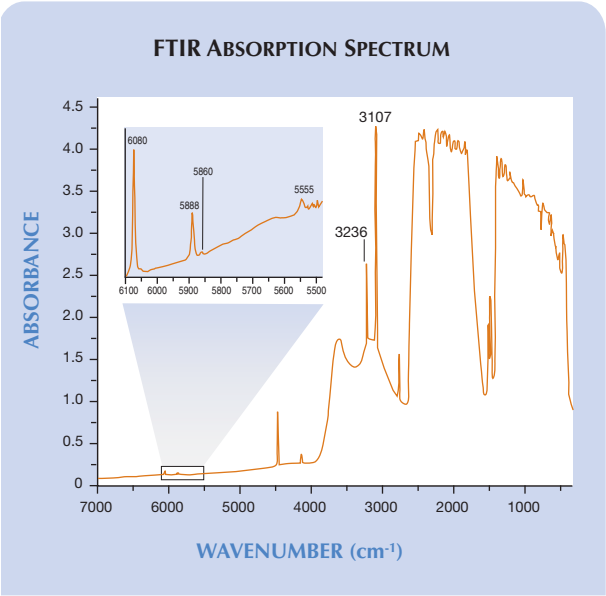

Stefanos Karampelas (s.karampelas@gubelingemlab.ch) and Pierre Hardy
Gübelin Gem Lab, Lucerne, Switzerland
Emmanuel Fritsch

COLORED STONES AND ORGANIC MATERIALS

Diopside from Ihosy, Madagascar. Several "olive" green samples were brought to our attention by gem dealer Farooq Hashmi (Intimate Gems, Jamaica, New York). The material was reportedly mined from the Ihosy region of south-central Madagascar. It was purchased in early 2007 as kornerupine, which is known to come from the same area of the country, but Mr. Hashmi's supplier was later informed that it was diopside. The parcel consisted of ~500 g of rough, in pieces weighing 5–20+ g, and about half of the material was facetable.

Two faceted samples, two well-formed prismatic crystals, and several small pieces of rough were loaned to GIA for gemological observation (e.g., figure 17). Examination of the two cut stones (5.93 and 6.50 ct) and some of the rough pieces showed the following properties: color—medium-dark yellowish green; pleochroism—very weak; RI—1.676–1.700; birefringence—0.024; hydrostatic SG—3.27–3.30; no reaction to the Chelsea filter; inert to long- and short-wave UV radiation; and absorption lines at 490 and 505 nm visible with the desk-model spectroscope. These properties were consistent with diopside (R. Webster, *Gems*, 5th ed., rev. by P. G. Read, Butterworth-Heinemann, Oxford, UK, 1994, pp. 330–331).

The two faceted samples contained only minor inclusions, consisting of a few "fingerprints" and some small

Figure 17. These samples of diopside were recovered from south-central Madagascar. The gemstones, faceted by Robert Buchannan, weigh 5.93 and 6.50 ct. Photo by Robert Weldon.

fractures. Iron-stained fractures and strings of pinpoints were visible in the rough material. Laser ablation–inductively coupled plasma–mass spectrometry (LA-ICP-MS) analysis of one faceted sample showed major amounts of Si, Ca, and Mg, and minor Fe—as expected for diopside ($CaMgSi_2O_6$), which forms a series with hedenbergite ($CaFeSi_2O_6$). The relatively low RI values are consistent with a near–end member diopside composition (see W. A. Deer et al., *Rock-Forming Minerals—Single-Chain Silicates*, Vol. 2A, 2nd ed., John Wiley & Sons, New York, 1978, pp. 198–293).

Although gem-quality diopside from Madagascar has been reported previously in the literature (e.g., U. Henn and C. Milisenda, "The gemstone occurrences of Madagascar," *Australian Gemmologist*, Vol. 21, 2001, pp. 76–82), to our knowledge this is the first description of this material.

Riccardo Befi (riccardo.befi@gia.edu)
GIA Laboratory, New York

Garnet and zircon from the Solomon Islands. Islands of the South Pacific are not known as sources of gem minerals, but in late 2007 GIA learned about new finds of garnet and zircon from the Solomon Islands. According to Brian Pepperall (BR Gemstones, Queensland, Australia), the gems come from the island of Malaita, where they have been gathered by hand as waterworn pebbles from stream gravels. The garnets are dark red and weigh up to 8 g, although the rough is commonly fractured. The zircon is colorless, and eye-clean pieces weigh up to 4 g. Mr. Pepperall estimates that the local people have collected no more than a few kilograms of the garnet and zircon. Although they are interested in pursuing a commercial venture, there are no plans for organized mining because the stones are so easily found on the surface, and they wish to preserve the integrity of their watercourse. A small amount of rough has been sold to Australian faceters, and some of the gems have been set in jewelry to test-market the material. To the best of Mr. Pepperall's knowledge, the stones have not been treated in any way.

Mr. Pepperall had several stones faceted in Australia, and he loaned some of each gem to GIA for examination. A study of three of the garnets (0.94–1.39 ct; figure 18) showed the following properties: color—dark red, RI—1.748, hydrostatic SG—3.73–3.79, fluorescence—inert to long- and short-wave UV radiation, and a dark diffuse band from the violet to the blue region visible with the desk-model spectroscope. These properties are generally consistent with those reported for pyrope-almandine by C. M. Stockton and D. V. Manson ("A proposed new classification for gem-quality garnets," Winter 1985 *G&G*, pp. 205–218). Microscopic examination revealed very small transparent crystals, fractures, and transparent growth features. Chemical analysis with LA-ICP-MS showed major amounts of Al, Si, Mg, and Fe (expected for pyrope-alman-

Figure 18. These garnets (0.94–1.39 ct) from the Solomon Islands proved to be pyrope-almandine. Photo by Robert Weldon.

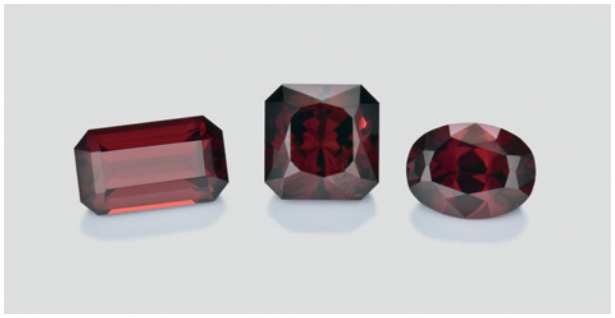

Figure 19. Also recovered from the Solomon Islands are colorless zircons (here, 0.79–2.50 ct). Photo by Robert Weldon.

dine), minor Ca, and significant traces of Mn, Ti, Cr, and V.

Examination of three of the zircons (0.79–2.50 ct; figure 19) showed the following properties: color—colorless; RI—>1.81; hydrostatic SG—4.71–4.72; fluorescence—moderate white to short-wave UV radiation, and moderate yellowish orange to long-wave UV; and just two lines (in the red region, stronger at 653.5 nm) visible with the desk-model spectroscope. These properties are generally consistent with those reported for zircon by R. Webster (*Gems*, 5th ed., revised by P. G. Read, Butterworth-Heinemann, Oxford, UK, 1994, pp. 176–179). Magnification revealed a cloud of minute particles in two of the stones. LA-ICP-MS analyses showed major Si and Zr, minor Hf, and significant traces of Ti and Sc.

Although the Solomon Islands have the potential to become a supplier of dark red pyrope-almandine and colorless zircon, these gems will probably remain uncommon in the marketplace until further efforts are made for organized recovery.

Kamolwan Thirangoon (kamolwan.thi@giathai.net)
GIA Thailand, Bangkok

Tsavorite mining at Namalulu, northern Tanzania. In late August 2009, these contributors visited a relatively new tsavorite deposit located 110 km south of Arusha. The mines were situated 13 km south of the village of Nabarera, near Namalulu Village, at coordinates 4°18′57″ S, 36°56′42″ E, and 1550 m elevation. Tsavorite was reportedly discovered there in August 2008 by Masai herders. We were told mining activities peaked in December 2008 when there were ~500 people working the deposit, but this number soon decreased after the near-surface deposits were exhausted and underground hard-rock mining became necessary. In addition, at the end of 2008 most of the miners moved to the former Swala Gem Traders tsavorite mine at Lemshuku, near Komolo village, also in northern Tanzania (03°51′36″ S 36°51′34″ E), when Mark and Eric Saul decided not to renew their claims and stopped mining there.

We were guided to Namalulu by local miner Rafael Manyosa and gem broker Abdul M'sellem. Upon our arrival we were met by several members of the Masai tribe (figure 20), who were dealers as well as miners there. We estimated that ~150 people were active in tsavorite mining or trading during our visit. The workings were confined to a narrow band ~100 m wide and 1 km long, oriented in the north-south direction. The geology of the area was described by J. Feneyrol et al. ("Lemshuku and Namalulu 'tsavorites,' Tanzania," poster presentation at the 31st International Gemmological Conference, Arusha, Tanzania, October 8–14, 2009), who visited there in October 2008. They found that the tsavorite crystallizes in veins associated with folded and metasomatized graphitic gneisses near dolomitic marbles.

Most of the mining has taken place during the dry season, from May to November. We visited three pits, which ranged from ~10 to 100 m deep. The largest pit consisted of a shaft and horizontal tunnels with an estimated total length of ~250 m. The shafts were accessible by ropes and followed the near-vertical graphitic gneiss layers downward. The excavations were mainly done using hand tools and explosives, except for one shaft where a compressor and a jackhammer were present.

Figure 20. Masai traders offer a parcel of rough tsavorite at Namalulu, Tanzania. Photo by V. Pardieu.

The miners reported finding good tsavorite every two days, on average, and we saw many attractive parcels while visiting the area. Most of the rough was vividly colored in yellowish green to deep green (figure 21), with some bluish green. We were told that pieces larger than 2 g had been recovered, but we only saw 0.6–0.8 g pieces that had fine color and acceptable clarity. After faceting, the tsavorites typically weigh <2 ct and contain eye-visible inclusions. Although clean material is rare, the deposit appears to show good potential for producing attractive smaller-sized tsavorite gems.

Vincent Pardieu (vincent.par@giathai.net)
GIA Laboratory, Bangkok
Stephane Jacquat (Geneva, Switzerland)
Lou Pierre Bryl (Gaspé, Canada)

Figure 21. Tsavorite from Namalulu shows good color and moderate transparency. Photo by V. Pardieu.

SYNTHETICS AND SIMULANTS

Treated CVD-grown pink synthetic diamond melee. The Gemmological Association of All Japan (GAAJ) – Zenhokyo Laboratory recently examined 48 small orangy pink round brilliants that were submitted for color origin identification (e.g., figure 22). They were represented as natural diamonds treated by a high-pressure, high-temperature (HPHT) process. Six were in the 0.20–0.27 ct range, and the remainder were melee size (<0.20 ct). Color grades ranged from Fancy Intense orangy pink to Fancy pinkish orange and Light pinkish orange. Thirteen pieces ≥0.10 ct were graded for clarity; of these, three were VVS_2, four VS_1, three VS_2, two SI_1, and one SI_2.

Microscopic examination revealed a few pinpoints in most of the samples. Several had black graphitization in cleavages and frosty etching on the surface—both signs of HPHT treatment. The pink color was evenly distributed. Most samples showed a streaked pattern of anomalous double refraction (ADR) that ran parallel to the growth direction of the {100} crystal face (figure 23), but some revealed a cross-hatched "tatami"-like pattern when observed in other directions. The samples fluoresced strong orange to long- and short-wave UV radiation, with no phosphorescence. In the DiamondView, the samples luminesced bright orange, and seven showed parallel laminated growth structures (figure 24). Cathodoluminescence imaging confirmed this structure in 15 of 26 samples. The streaked ADR pattern, fluorescence, and growth structures are consistent with CVD-grown synthetic diamonds.

Results from UV-Vis-NIR, FTIR, and photoluminescence (PL) spectroscopy of all samples are summarized in table 1. UV-Vis-NIR spectra (collected at room temperature) showed a broad absorption centered at ~500 nm (related to NV centers at 575 and 637 nm) that was the cause of the pink color and orange fluorescence. FTIR spectra (collected at room temperature with 1 cm^{-1} resolution) indicated that all samples were type IIa. Twenty-nine samples showed weak absorptions in the 3150–2700 cm^{-1} region, presumably caused by hydrogen impurities; a C-H absorption at 3107 cm^{-1}, common in natural diamond, was vaguely present in only some samples. An absorption at 3123 cm^{-1}, which has been reported as characteristic of

Figure 22. These eight representative samples of treated-color pink CVD synthetic diamonds range from 0.01 to 0.25 ct. Photo by M. Sasahara.

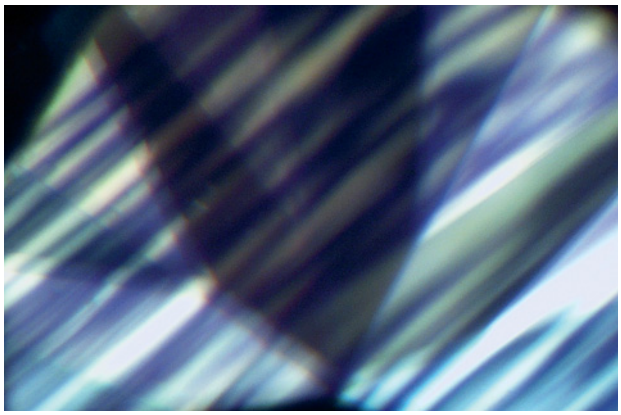

Figure 23. A characteristic streaked ADR pattern was observed in most of the CVD synthetic diamonds between crossed polarizing filters. The streaks run parallel to the growth direction of the crystal and are likely caused by dislocations during growth. Photomicrograph by A. Abduriyim; magnified 50×.

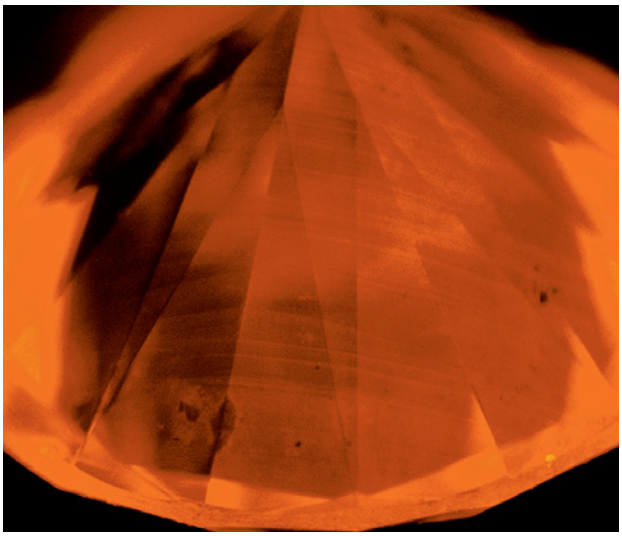

Figure 24. All the CVD-grown synthetic diamonds displayed strong orange fluorescence in the DiamondView. Parallel laminated growth structures also were observed in seven samples. Photo by J. Kawano; magnified 30×.

CVD synthetic diamond but annealed out by HPHT treatment (P. M. Martineau et al., "Identification of synthetic diamond grown using chemical vapor deposition [CVD], Spring 2004 *G&G*, pp. 2–25), was not detected. In all samples, PL spectroscopy with 633 nm excitation at liquid nitrogen temperature recorded Si-related defects (737 nm)—which are characteristic of CVD synthetic diamonds—as well as GR1 centers (741 nm) that are related to irradiation. Radiation-related features were also recorded in all samples with 325 nm excitation: a 389 nm line accompanied by numerous weak peaks in the 400–440 nm region. With 514.5 nm excitation, all samples showed NV centers at 575 and 637 nm.

The NV centers were apparently formed by irradiation and annealing of N-containing CVD synthetic diamonds (nitrogen gas is used to accelerate the growth rate). In addition, HPHT treatment was indicated by the lack of the 3123 cm^{-1} absorption in the FTIR spectra, as well as the graphitized cleavages and frosty surface etching. While these small treated pink CVD synthetic diamonds have not yet become common in the marketplace, material with similar properties was also recently documented by GIA (see W. Wang and P. Johnson, pp. 51–52 of this issue), and gemologists must be wary of them. A combination of growth-structure observations, pinpoint inclusions, strain patterns, specific IR absorption peaks in the 3150–2700 cm^{-1} range, and PL lines at 575, 637, and 737 nm, can be used to separate these CVD synthetics from natural pink diamonds.

Hiroshi Kitawaki, Ahmadjan Abduriyim (ahmadjan@gaaj-zenhokyo.co.jp), Jun Kawano, and Makoto Okano
Gemmological Association of All Japan – Zenhokyo, Tokyo

TABLE 1. Characteristics of 48 treated-color pink CVD synthetic diamonds.

Weight	0.01–0.27 ct
Cut	Round brilliant
Color	Orangy pink to pinkish orange
Clarity	VVS_2 to SI_2 (≥0.10 ct)
Microscopic features	Pinpoints, graphitized cleavages, frosty surface etching, streaked and tatami-like ADR
UV fluorescence	
Long-wave	Strong orange
Short-wave	Strong orange
DiamondView	Bright orange luminescence; parallel growth layers in seven samples
UV-Vis-NIR spectroscopy	Broad absorption at 500 nm; peaks at 575 (NV^0), 595, 637 (NV^-), 741 (GR1) nm; some showed very weak peaks at 268 and 271 (isolated N), 392 (ND1), and 503 (H3) nm; no 737 nm peak detected in these room-temperature spectra
FTIR spectroscopy	Very weak bands at 3136, 3118, 3107, 3028, 2925, 2885, 2855, 2846, 2837, 2788, 2773, 2747, and 2724 cm^{-1} detected in some samples only; the N-related 1344 cm^{-1} band was not found
PL spectroscopy	
633 nm laser	740.9/744.3 nm doublet, 737 ($[Si\text{-}V]^-$) nm
514.5 nm laser	575 (NV^0) and 637 (NV^-) nm Very weak 737 nm in four samples, very weak 741 nm in six samples
325 nm laser	389, 409, 411, 413, 435, 438, 453, 496 (H4), 498, 503 (H3), and 505 nm; 415 (N3) nm in six samples

Figure 25. This 2.16 ct brownish orange sapphire displays a color typically associated with Be-diffusion treatment. Photo by G. Choudhary.

TREATMENTS

A Be-diffused sapphire with interesting zoning patterns. The Gem Testing Laboratory of Jaipur often receives gem materials with interesting and unusual internal features. One example was a 2.16 ct brownish orange sapphire, notable for its zoning pattern.

The oval mixed-cut stone, which measured 7.81 × 6.81 × 4.29 mm, had a color reminiscent of beryllium-diffused sapphire (figure 25). It was readily identified as corundum by RI readings of 1.760–1.768 and a hydrostatic SG of 3.98. In addition, weak lines in the red region of the spectrum were observed with the desk-model spectroscope, and the stone fluoresced a weak orange-red to long-wave UV radiation.

With magnification, fine surface-reaching fingerprint-like inclusions were observed. Some had whitish bubble-like textures, such as those associated with high-temperature heat treatment, which suggested the presence of a foreign substance such as borax. Notably, fiber-optic lighting revealed a few zones of fine minute particles that formed nested patterns with unusual square/rectangular profiles, rather than the hexagonal or pseudohexagonal shapes that are expected in corundum. Viewed in some directions, the sides of some of the zones appeared oblique, forming slightly rhomboid shapes (e.g., figure 26).

Since this sapphire's color suggested beryllium diffusion, we expected to see surface-conformal color zoning. Immersion in methylene iodide in diffused lighting indeed revealed such color layers. (Additional evidence for beryllium diffusion was provided by some areas of recrystallization remaining on the surface of the sample, which are associated with the elevated temperatures used for this treatment.) The color zones were arranged in unusual concentric oval to cushion-shaped zones (figure 27). This contributor has never seen these concentric patterns in a natural sapphire, nor were any such reports found in the literature. Although similar curved color bands may be present in flame-fusion synthetic sapphires, the natural origin of this stone was demonstrated by the zones of minute particles described above.

In the absence of any other inclusion feature, the presence of the concentric colored bands in this Be-diffused natural sapphire could lead to its misidentification by an inexperienced gemologist as a flame-fusion synthetic.

Gagan Choudhary (gtl@gjepcindia.com)
Gem Testing Laboratory, Jaipur, India

Figure 26. The sapphire contains nested zones of minute particles, such as those shown here with a slightly tilted rhomboid profile. Finer zones of particles extend from the lower-left corner of this inclusion cluster. Photomicrograph by G. Choudhary; magnified 65×.

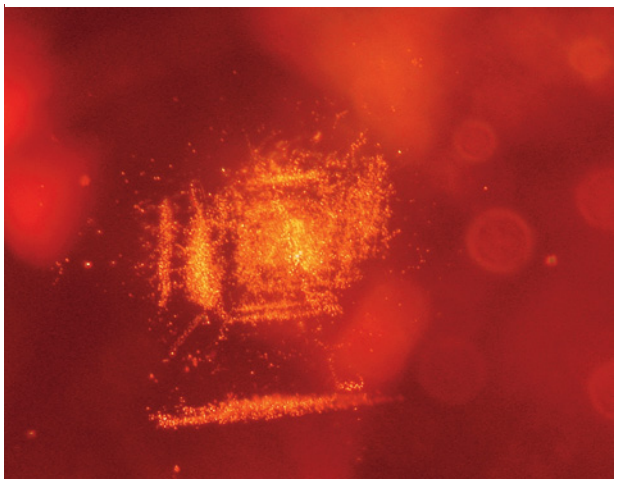

Figure 27. Immersed in methylene iodide, the Be-diffused sapphire displayed concentric oval to cushion-shaped color bands. Photomicrograph by G. Choudhary; magnified 45×.

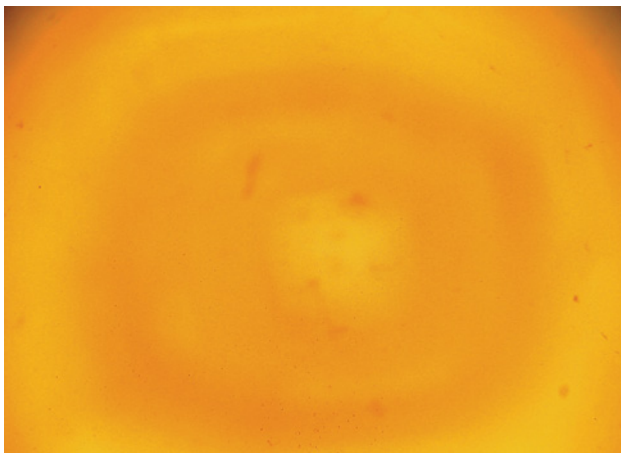

Figure 28. The "Golden Tridacna" beads on the left (7–8 mm in diameter), some with green patches, were fashioned from naturally colored conch shell. All the conch shell beads on the right were found to be dyed. Photo by Jun Su.

Dyed conch shell beads. In recent years, beads fashioned from contemporary conch shells that are represented as fossil conch from the Himalaya Mountains have been sold in the Chinese market as "Neptunian" or "Golden Tridacna" products (see, e.g., Winter 2008 GNI, pp. 376–377). They are usually orangy brown (sometimes orangy yellow or dark green) with off-white striae; the colored portions may have an attractive sheen. We are not aware of any genuine fossil conch shell beads; all the conch shell beads currently in the market appear to have been manufactured from contemporary material. Buddhists treasure these beads for their color patterns, which are similar to the Taiji (yin-yang) symbol, and there is good demand—especially for the more strongly colored pieces.

Recently, a bracelet of baroque-shaped orangy brown beads was submitted to the Beijing laboratory of the National Gemstone Testing Centre (NGTC) for identification. Visual observation suggested the beads were fashioned from conch shell, though careful examination revealed concentrations of color in the surface cracks, which raised suspicions that they might have been dyed.

To further investigate the color origin of such products in the Chinese market, we obtained more than 100 "Golden Tridacna" and "Neptunian" samples from various sources (figures 28–30). These consisted of pale yellow and pale brown beads, some with light green patches—that is, with coloration expected for natural shell material—that did not show any visual evidence of dyeing (figure 28, left), as well as some distinctly colored yellow to orange-brown beads (figure 28, right).

Figure 29. When some of the shell beads were broken open, the pale-colored ones (left, 7 mm in diameter) did not show any features indicative of dyeing. However, the orange beads on the right had color concentrations in fractures, along the drill holes, and in some areas near their rims. Photo by Jun Su.

Figure 30. Color concentrations were seen in the surface-reaching fractures of the dyed beads. Photomicrograph by Jun Su; magnified 15×.

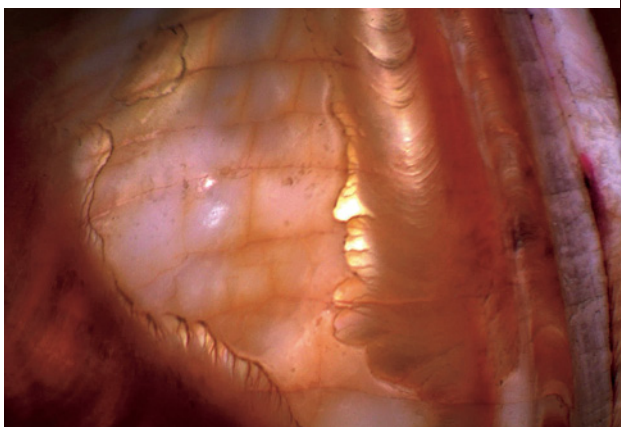

Figure 31. This gemstone tapestry (~106 × 60 cm) consists of diamonds, emeralds, and sapphires set in 18K gold. Photo by A. Malsy; © Gübelin Gem Lab.

The distinctly colored beads did not show any obvious evidence of dye when viewed from the exterior, but on breaking open three of them, we saw varying degrees of color concentrations near fractures, coating the drill hole, and along the outer edge of the broken surface, indicating that they had been dyed (figures 29 and 30). The dye only penetrated certain areas of the beads, leaving the white striae undyed (due to their more compact texture) except where penetrated by fractures.

Raman spectroscopy of five dyed beads revealed peaks at 1085 and 702 cm^{-1} that were attributed to aragonite. However, no features were seen at 1525 and 1134 cm^{-1}, which are related to carotenoids (organic pigments) and are usually associated with natural color in shells (Gang-sheng Zhang, "Study on mollusk shells by laser micro-Raman spectrometry," *Journal of Analytical Science*, Vol. 19, No. 1, 2003, pp. 27–29). Both of these carotenoid Raman peaks were recorded in a natural-colored yellow shell that was analyzed for comparison.

Our study found that all the distinctly colored "Neptunian" and "Golden Tridacna" beads we examined from the Chinese jewelry market, including the bracelet that was submitted for identification, consisted of dyed contemporary conch shell.

Jun Su (kaximaya@hotmail.com), Taijin Lu, and Zhonghua Song
National Gemstone Testing Centre (NGTC), Beijing

MISCELLANEOUS

Unusual gemstone tapestry. Recently, the Gübelin Gem Lab (GGL) encountered a unique object: a decorative prayer rug (~106 cm × 60 cm) with 27,104 gemstones (figure 31). According to documentation that accompanied the tapestry, it also contains 15.90 kg of 18K yellow gold, which is used in the stone settings and in fringes consisting of delicate gold chains. According to the owner, Kathryn Bonanno, the tapestry was made in France during the 1980s–1990s. It reportedly took five years to gather and cut all the gemstones, and another five years to assemble the final piece. The workmanship is exceptional, with

Figure 32. The fine workmanship of the tapestry is seen in the uniform size, shape, and color of the gems (left), as well as the precise nature of their prong settings (right). Photos by L. Kiefert (left) and A. Malsy (right); © Gübelin Gem Lab.

the gems in perfect alignment, yielding attractive patterns and a smooth and even surface (figure 32).

In the tapestry we counted 1,242 diamonds, 4,580 emeralds, 1,888 rubies, 8,428 blue sapphires, 1,298 pink sapphires, and 9,668 yellow sapphires, with a total reported weight of >14,000 carats. All the stones were oval and measured ~6.0 × 4.0 mm. The diamonds were brilliant cut, while all the other stones had a brilliant-cut crown and step-cut pavilion. The gems were set with prongs in a fashion that is also used for fine bracelets (again, see figure 32), in patterns typical of those seen in prayer rugs.

GGL randomly examined ~1% of the stones in the tapestry by attaching a gemological microscope head to a metal plate with a rod, which was slid under the tapestry and moved along one side. The diamonds were observed with a loupe and a long-wave UV lamp. We did not see any evidence of treatment in the diamonds, while clarity enhancement in the emeralds ranged from none to moderate. The rubies showed indications of heating with minor-to-moderate residue in fissures, the blue and yellow sapphires were heated, and the pink sapphires were a mix of unheated and heated stones.

The beauty of this remarkable piece lies in the number of gemstones it contains and their uniformity, as well as in the patterns they form and the craftsmanship of the tapestry.

Lore Kiefert (l.kiefert@gubelingemlab.ch),
Anna Malsy, and Pierre Hardy
Gübelin Gem Lab
Lucerne, Switzerland

DIFFRACTION GRATINGS ON DIAMOND SURFACES

In the article by A. Gilbertson et al. describing a combination of microlithography and plasma etching to improve dispersion in diamonds (Winter 2009 *G&G*, pp. 260–270), the authors describe some technological developments at the California Institute of Technology. Your readers may be interested to know that two of the coauthors were part of a team that recently published a patent application relating to the process described (G. Maltezos, A. Scherer, and J. Witzens, *Enhancing the Optical Characteristics of a Gemstone*, U.S. Patent Application 2007/0157667A1, July 12, 2007, and International Patent Application WO2007/067696A1, June 14, 2007). The patent documents provide schematic drawings of the various steps used to create the diffraction grating patterns. Further improvements on the techniques are discussed in a later application by Maltezos and Scherer (*Gemstones and Methods for Controlling the Appearance Thereof*, U.S. Patent Application 2009/0126402A1, May 21, 2009; International Patent Application WO2009/073576A2, June 11, 2009).

The 2007 Maltezos et al. application was mentioned in a review summarizing patent documents about various surface treatments of gemstones (K. Schmetzer, "Surface treatment of gemstones, especially topaz—An update of recent patent literature," *Journal of Gemmology*, Vol. 31, No. 1/2, 2008, pp. 7–13), which also provides additional information for the interested reader. A recently published patent application by G. L. W. Cross, W. McKenzie, and J. B. Pethica (*Process and System for Fabrication of Patterns on a Surface*, International Patent Application WO2010/003600A1, January 14, 2010, and European Patent Application EP 2 144 117 A1, January 13, 2010) describes further developments in the surface treatment of diamonds. Well-defined periodical patterns were prepared by treatment of the diamond's surface with a focused ion beam and subsequent plasma etching. These publications also present a general review of the technical literature dealing with surface patterning and nanostructuring.

Karl Schmetzer
Petershausen, Germany

'10

TAKE THE GEMS & GEMOLOGY CHALLENGE

The following 25 questions *are based on information from the Spring, Summer, Fall, and Winter 2009 issues of* GEMS & GEMOLOGY. *Refer to the feature articles, Notes and New Techniques, and Rapid Communications in those issues to find the* **single best answer** *for each question.*

Mark your choice on the response card provided in this issue or visit gia.edu/gandg to take the Challenge online. Entries must be **received no later than Monday, August 2, 2010.**
All entries will be acknowledged with an email, so please remember to include your name and email address (and write clearly!).

Score 75% or better, and you will receive a GIA CONTINUING EDUCATION CERTIFICATE *(PDF format). If you are a member of the GIA Alumni Association, you will earn 10 Carat Points. (Be sure to include your GIA Alumni membership number on your answer card and submit your Carat card for credit.) Earn a perfect score, and your name also will be listed in the Fall 2010 issue of* GEMS & GEMOLOGY. *Good luck!*

1. Beginning in the 1970s, supplies of sapphire on the market greatly increased due to
   A. improvements in marketing and distribution.
   B. the use of beryllium diffusion.
   C. the end of the Vietnam war.
   D. the introduction of effective heat-treatment techniques.

2. In treated "green amber," the _____ can prove that the starting material was amber, not copal.
   A. FTIR spectral features
   B. hardness
   C. resistance to solvents
   D. specific gravity

3. The French Blue diamond represented one of the earliest examples of the
   A. brilliant cut.
   B. mirror cut.
   C. Mazarin cut.
   D. octahedral cut.

4. Copper is the critical chromophore in Paraíba-type tourmalines. At what approximate wavelengths in the visible–near infrared spectrum do the primary absorptions produced by copper in tourmaline occur?
   A. 415 and 700 nm
   B. 700 and 900 nm
   C. 520 and 700 nm
   D. 440 and 610 nm

5. Yellow coloration and blue fluorescence are associated with the presence of _____ impurities in type I diamonds.
   A. boron
   B. hydrogen
   C. nitrogen
   D. vanadium

6. Sheet Ammolite tends to have stronger iridescence and more of the popular _____ coloration than the fractured material has.
   A. blue
   B. yellow
   C. orange
   D. red

7. _____ is the chromophore of aquamarine from Italy's Masino-Bregaglia Massif.
   A. Chromium
   B. Cobalt
   C. Iron
   D. Nickel

8. During the 1950s, several *G&G* articles dealt with the newly refined process of altering diamond color through
   A. heat treatment.
   B. glass filling.
   C. high pressure and high temperature.
   D. irradiation.

9. The presence of _____ impurities in gray-to-blue-to-violet diamonds from the Argyle nine in Australia is believed to be responsible for some of their unusual characteristics.
   A. hydrogen, nitrogen, and boron
   B. hydrogen (alone)
   C. hydrogen, nitrogen, and nickel
   D. nickel and platinum

10. In cases where gem coral from the endangered *Stylaster* genus

CHALLENGE

cannot be distinguished by its surface features, Raman spectroscopy can identify it by the presence of _____ pigments.
A. betalain
B. carotenoid
C. copper carbonate
D. unmethylated polyenic

11. Computer modeling of the Tavernier Blue diamond revealed that the top-view table facet was nearly parallel to a(n)
A. cubic {100} crystal face.
B. octahedral {111} crystal face.
C. dodecahedral {110} crystal face.
D. None of the above

12. Hackmanite is usually distinguished from sodalite by its ability to change color in response to the application or absence of certain wavelengths of light, a property known as
A. adularescence.
B. aventurescence.
C. phosphorescence.
D. tenebrescence.

13. The "fluorescence cage" exhibited by HPHT-treated type I diamonds can be observed with a fluorescence microscope and possibly a _____ instrument.
A. Diamolite
B. DiamondProbe
C. DiamondView
D. Gem*e*wizard

14. In the past two decades, _____ has developed into the most important new source of blue and fancy-color sapphires.
A. Australia
B. Madagascar
C. the United States
D. Vietnam

15. _____ is a brown variety of andalusite that displays a black cross pattern.
A. Chiastolite
B. Verdelite
C. Viridine
D. Indicolite

16. A recent theory that Henry Philip Hope may have owned the French Blue diamond prior to its recutting is based on the discovery of
A. documents belonging to the Achard family of Parisian jewelers.
B. drawings made by its original cutter in the Muséum National d'Histoire Naturelle.
C. museum catalogue entries associated with a cast of the diamond.
D. an 1812 sketch and description by John Francillon in the Harry Winston archives.

17. The simplest way to identify Nanocut plasma-etched diamonds is to look for
A. double refraction.
B. the flash effect.
C. magnetism.
D. unpolished-looking pavilion facets.

18. Demantoid from Val Malenco, Italy, contains fibrous inclusions, identified as _____, in the typical "horsetail" arrangement.
A. chrysotile
B. hematite
C. pyrite
D. rutile

19. Studies suggest that rare instances of pink color surrounding growth tubes and cracks in blue to blue-green Cu-bearing tourmaline from Mozambique is caused by exposure to _____ solutions.
A. acidic
B. aqueous
C. hydrothermal
D. radioactive

20. Microscopic evidence of polymer filling in aquamarine recently encountered on the Chinese market includes all of the following *except*:
A. cloudy areas of reduced transparency that appear white.
B. flash effects.
C. high-relief areas.
D. round gas bubbles.

21. Because of their color and opaque-to-translucent appearance, chrysoprase and prase opal have been used as substitutes for
A. chalcedony.
B. jade.
C. turquoise.
D. variscite.

22. The most common internal features in peridot from the Italian island of Sardinia are _____ and liquid inclusions.
A. dark spinel crystals
B. decrepitation halo cleavages
C. nail-head spicules
D. partially healed fractures

23. Besides Tanzania, chrysoprase is also found in
A. Australia.
B. Poland.
C. Brazil.
D. All of the above

24. The yellow-green color of haüyne from northern Tanzania is quite different from that of the well-known gem-quality blue haüyne from
A. Germany and Myanmar.
B. Italy and Germany.
C. Madagascar and Mozambique.
D. Madagascar and Tanzania.

25. One of *G&G*'s most important articles from the 1970s was Campbell Bridges's firsthand description of a new gem that became known as
A. jeremejevite.
B. moissanite.
C. tanzanite.
D. tsavorite.

GUIDELINES FOR AUTHORS

Authors should use the following guidelines when submitting a manuscript to *Gems & Gemology*, or the paper may be returned unreviewed. If you have any questions about these guidelines, please contact Editor Brendan Laurs by e-mail (blaurs@gia.edu), fax (760-603-4595), or phone (760-603-4503). More detailed suggestions for preparing articles on gem localities, synthetic gem materials, instruments and techniques, and pearls can be found online at www.gia.edu/gandg.

Remember that these are general guidelines only. Your best source for appropriate topics is *G&G* itself.

APPROPRIATE TOPICS

G&G publishes original articles on gem materials and research in gemology and related fields. Appropriate topics include (but are not limited to) colored stones, diamonds, gemological instruments and identification techniques, gem localities, gem treatments, gem substitutes (simulants and synthetics), gemstones for the collector, jewelry manufacturing arts, jewelry history, legal issues related to gemology, and contemporary trends in the trade.

Manuscripts may be submitted as:

Feature Articles—full-length articles describing previously unpublished studies and laboratory or field research. Such articles should be no longer than 6,000 words plus tables, illustrations, and references.

Review Articles—comprehensive reviews of important topics in the field. Length of text should not exceed 8,000 words.

Notes & New Techniques—brief reports of recent discoveries or developments in gemology and related fields (e.g., new instruments or identification techniques, gem minerals for the collector, and lapidary techniques). Articles for this section should be approximately 1,500–4,000 words.

Rapid Communications (RC)—brief descriptions of notable gem materials, localities, and identification or treatment techniques, as well as related topics such as museum exhibits and historical jewelry. Articles for this section should be approximately 750–1,500 words.

Gem News International (GNI) entries—very brief reports (less than 600 words and up to a maximum of three figures/tables) on new localities, unusual gem materials, or current events in the field.

Letters to the Editor—Replies to and comments on material published in *G&G*.

To be considered for publication, all contributions to *G&G* must be original work not previously published in English. We will consider articles already published in languages other than English only on a case-by-case basis and only if the authors inform us at the time of submittal when and where the article was first published.

G&G also includes these regular sections: *Lab Notes*—reports from the GIA Gem Laboratory; *Book Reviews*—reviews of books and other publications; and *Gemological Abstracts*—summaries of important articles related to gemology (please contact the Editor if you are interested in abstracting articles).

MANUSCRIPT PREPARATION

All text material (including tables, figure legends, and references) must be submitted as electronic files, with an accompanying hard copy (or a PDF version, if e-mailed). Microsoft Word (for Windows or Macintosh) is preferred for text.

Identify the authors on the title page only, not in the body of the manuscript or figures, so that author anonymity can be maintained during review (the title page is removed before the manuscript is sent to reviewers). The components of the manuscript should be arranged as follows:

Title Page. Page 1 should include: (a) the article title, (b) the full name of each author, (c) each author's affiliation, and (d) acknowledgments of persons who provided assistance to the author(s).

Abstract. The abstract (no more than 150 words for a feature or review article, 75 words for a Note or RC) should state the purpose of the article, what was done, and the main conclusions.

Text. Papers should follow a clear outline with appropriate headings. For example, for a research paper, the headings could be: Introduction, Background (e.g., a review of previous studies), Materials and Methods, Results, Discussion, and Conclusion. Use other heads and subheads as the subject matter warrants. Please avoid jargon, spell out the first mention of all nonstandard acronyms, and present your material as clearly and concisely as possible.

Important: Papers that describe original research must include a Materials and Methods section that contains, at a minimum, the numbers and descriptions of all samples examined and the techniques and instrumentation used to obtain the data.

References. References should be used for information taken directly from another publication, to document ideas and facts attributed to another writer, and to refer the reader to other sources on a particular subject. References must be cited in the body of the text (in parentheses), with the last name of the author(s) and the year of publication. Add the appropriate page number when citing a direct quote or a specific illustration or set of numbers or data; an example would be: (Koivula et al., 2000, p. 362). List references at the end of the paper in alphabetical order by the last name of the senior author. If there is more than one publication by that author or same group of authors, list those items in chronological order, starting with the oldest publication. List only references actually cited in the text (or tables or figures).

Include the following information, in the order given here, for each reference: (a) all author names (surnames followed by initials); (b) the year of publication, in parentheses; (c) for a journal, the full title of the article or, for a book, the full title of the book cited; and (d) for a journal, the full title of the journal plus volume number, issue number, and inclusive page numbers of the article cited; or (e) for a book, the publisher of the book and the city/state or country of publication. For Web pages, include the date accessed.

Sample references are:

Balfour I. (2000) *Famous Diamonds*. Christie, Manson & Woods Ltd., London.

Koivula J.I., Tannous M., Schmetzer K. (2000) Synthetic gem materials and simulants in the 1990s. *G&G*, Vol. 36, No. 4, pp. 360–379.

Levinson A.A. (1998) Diamond sources and their discovery. In G. Harlow, Ed.,

The Nature of Diamonds. Cambridge University Press, Cambridge, UK, pp. 72–104.

Welcome to GIA's online series of articles on diamond cut (2003) *GIA on Diamond Cut*, www.gia.edu/research/156/gia_on_diamond_cut.cfm [date accessed: Oct. 7, 2003].

Because of the Internet's transitory nature, Internet-only references are discouraged unless the document or information is not easily available elsewhere; access dates must be included. *G&G* does not currently publish DOIs.

Personal communications (for unpublished information obtained from someone with particular expertise) should be cited in the body of the text only, as follows: (G. Rossman, pers. comm., 2010). Permission must be obtained from the people cited to use their names for this purpose. Such persons must also be listed, with their affiliations, in the Acknowledgments section.

Tables. Number tables in the order in which they are cited in the text. Every table should have a title; every column (including the left-hand column) should have a heading. Terms and figures used in the table must be consistent with those used in the text.

Line Illustrations. We prefer that all line art (graphs, charts, etc.) be sent to us as electronic files (EPS and JPG formats preferred), accompanied by hard copy. If this is not possible, line art should be clearly drafted and the original sent to us (originals will be returned after publication).

Art that is not your original work must be submitted with the appropriate written permission from the copyright holder(s).

Color Photographs. All photos should be previously unpublished and sent in their original form, whether taken on film or with a digital camera. High-resolution digital files (JPG or TIF) are preferred.

Digital files should have a minimum resolution of 300 dpi (pixels per inch) at 4 × 5 inches (10 × 12 cm). Generally, an image that is at least 1200 pixels wide in its original form will be of sufficient resolution when printed. Remember, however, that this needs to be achieved with the proper settings on the camera; it is not possible to increase the actual resolution by digitally enlarging a low-resolution image.

Digital figures must be sent as separate files; please do not send them solely as embedded figures within the text of the manuscript. You may upload large digital files (anything over 10MB) to our FTP site; please contact the Managing Editor for instructions on access.

We reserve the right to reject photos that are not in keeping with our production standards. Any photograph that is not the original work of the author(s) or otherwise owned by them must be submitted with the appropriate written permission from the copyright holder(s). Please contact the Editor if you need help finding appropriate photographers or specimens.

All physical originals will be returned to the authors after publication of the manuscript. Production copies of figures published in *G&G* are retained by the GIA Visual Resources Library and may be displayed for educational purposes in GIA resident education classes; however, they are not reused or otherwise redistributed without permission from the copyright owner.

"Call Outs." All figures and tables must be called out at the appropriate place in the text. Figures and tables must be numbered consecutively, starting with the first mention in the text.

Figure Captions. Include figure captions separately from the figures. Each caption should clearly explain, in complete sentences, the significance of the figure and any symbols, arrows, numbers, or abbreviations used therein. Information in captions must be consistent with the text. For photomicrographs, please indicate the field of view (or size of the object being photographed) in the figure caption. It is also acceptable to give the magnification of the image (e.g., magnified 20x).

MANUSCRIPT SUBMISSION

Manuscripts can be submitted by either postal or electronic mail to the address below. Your manuscript package should contain: all electronic files (on CD-ROM if sent postal mail); one copy, printed on standard-size white paper (postal mail) or in PDF format (e-mail); any slides, transparencies, or line drawings of figures (slides and transparencies must be sent via postal mail; digital scans are not acceptable); and the signed copyright statement (in PDF format if e-mailed). Manuscripts will not be sent for review until all of these elements have been received. Send all submissions to:

Thomas W. Overton
toverton@gia.edu
Managing Editor
Gems & Gemology
5345 Armada Drive
Carlsbad, CA 92008 USA

Reprints. No payment is made to authors for articles or photos published in *G&G*. However, for each article, note, or RC, the author(s) will receive five copies of that issue. Contributors to the GNI section will receive one free copy. Offprints may be purchased in increments of 100 for an additional fee. Authors will also receive a free PDF version of their article (GNI contributors can request a PDF of the pages their entry appears on if desired). This PDF file may be shared with colleagues but should not be made available on the Internet or placed in a public database for general viewing without prior written permission from the Managing Editor.

REVIEW PROCESS

Manuscripts are examined by the editorial staff and at least three reviewers. Authors will remain anonymous to the reviewers, and (unless specific permission is given) reviewers will remain anonymous to the authors. Decisions of the editors are final and are revealed to the reviewers after the process is complete. All material accepted for publication is subject to copy editing. Authors will receive page proofs for review and are held fully responsible for the content of their articles.

EDITORS
Susan B. Johnson
Jana E. Miyahira-Smith
Thomas W. Overton

Modern Jewellery Design: Past and Present

By Reinhold Ludwig, 399 pp., hardcover, illus., publ. by Arnoldsche Art Publishers [www.arnoldsche.com], Stuttgart, Germany, 2008. US$85.00

To answer the question of what constitutes modern jewelry design, this dual-language German-English book first traces the roots of modernism through 20th century movements in art and architecture as expressed in jewelry.

True to the subtitle *Past and Present*, the first two of 11 chapters review cycles of innovation, reaction, and counteraction that gave pace to pre-modern art movements. The author cites England's Arts and Crafts movement—itself a reaction to what he calls the soulless mass production of the Industrial Revolution—that in turn gave rise to Art Nouveau, which was upended by the ensuing Art Deco period.

In 1919, the functionalism and geometry of Germany's Bauhaus school first appeared. While the school lasted only 14 years, its design paradigms influenced architecture, home goods, and furniture. Bauhaus largely bypassed jewelry design, but the movement still held sway over the middle-European metalsmiths who would later mentor and develop the generation of jewelry artists who defined post-1945 modernism.

Perhaps because German jewelry manufacture is concentrated in a few centers—Pforzheim, Hanau, Schwäbisch Gmünd, and Burg Giebichenstein—the goldsmithing renaissance of the post-war period gave rise to styles with continuity and connectivity not generally seen in American jewelry arts. At the time, modern jewelry design was driven by fashion and the new consumerism, both of which furthered acceptance of mass-production jewelry. But by the 1970s, a cadre of modernists had formed that would depart from the rote commonality of manufactured jewelry to embrace what the book translates as "one off jewellery," or one-of-a-kind works of art.

The book generously portrays the contributions of this last group, which recast modernist minimalism. To this day, their work shows a transition from the post-bling era marked by 2001's catastrophic terrorist events to the luxury of restraint seen in contemporary jewelry design. These artists follow muses into new terrain and use materials that show not only geometric form and linearity but also rich surface texturing and fluidity of design that are simultaneously austere yet tactile and romantic.

With its wealth of illustrations, the book shows how sculptural and kinetic designs took modernism to new heights. The author gives intriguing examples of jewelry designed for movement or changeability, as in 1990s' swivel rings and Jörg Heinz's innovative modular clasps. Modernist restraint is typified by tension designs, in which movement is controlled, defied, and nearly threatened.

The book also underscores the importance of platinum in modern design, with a recap of the metal's 1920s heyday to its ascendancy following the 1976 formation of the Platin Gilde International in Germany. Yet the photos of platinum jewelry lack the excitement of the modernist pieces rendered in gold, silver, exotic metals, and synthetic materials from plastics to porcelain.

No discussion of German modernism would be complete without recognizing the gem-cutting artistry of Bernd Munsteiner and his son Tom. Images of their lapidary *Wunder* hint at the inner lives of gems, which according to the younger Munsteiner appear to bridge the inanimate world with that of nature's living, breathing brethren.

Just as linearity and angularity prevail in these 12½-in. tall pages, the artist bios suffer from a somewhat metronomic chronology. Despite fits and starts of narrative flow, readers get to know each of the more than 80 profiled artists and design houses through snapshots of their geographic and familial origins, training, influences and inspirations, mentors, business strategies, and innovations. Readers also gain insight into how the artists address or incorporate emotion in their designs and how they view their artistic bodies of work. Notwithstanding occasional losses in translation, the devotion to craft, skill, and passion of this talented group is expressed by generous representation of their works.

Photographs of historic pieces are provided courtesy of Schmuckmuseum Pforzheim, whose catalogue of pre-modern jewelry was reviewed in the Spring 2006 *G&G*. Nearly all images are captured in exquisite detail, with approximately 200 full-page glossy photographs (including dates in captions) that well illustrate modernism's diverse facets.

This book, by the former editor of

Germany's *Schmuck Magazin*, should find its readership among students of art history and adornment, museum curators, collectors, jewelry historians, trendspotters, and anyone interested in the spirit and evolution of design.

MATILDE PARENTE
Indian Wells, California

Genuine Diamonds Found in Arkansas, 3rd Ed.

By Glenn W. Worthington, 182 pp. with DVD supplement, illus., publ. by Mid-America Prospecting [www.diamondsinar.com], Murfreesboro, AR, 2009. US$35.00

I wasn't sure what to expect when I opened this book. My initial assumptions were that it would cover geology, mineralogy, and mining—after all, this is my bias as a geologist who specializes in diamond and colored gemstone deposits. And the book does provide a cursory overview of these subjects. But the welcome surprise of this volume is its focus on the human history of the Murfreesboro deposit: the people who found Arkansas diamonds. Glenn Worthington does an excellent job documenting their stories. The extraordinary finds of gem-quality "canary," "cognac," and "champagne" diamonds at the Crater of Diamonds State Park near Murfreesboro, combined with a liberal sprinkling of good historical and modern photos, make this a must-have book for anyone interested in diamonds.

One of my favorite stories is of an illiterate pig farmer, John Huddleston, who found the first of the diamonds on his farm in 1906 and later sold his property for $36,000 (an extremely large sum at the time). Instead of placing his newfound fortune in a bank, he bought a safe—but not knowing how to *operate* a safe, he never bothered to learn the combination or rotate the locking mechanism. Thus it remained unsecured for a few years until one of his children rotated the dial. How did he later open it? You'll have to read the book to find out.

The book touches on unsuccessful efforts to mine the group of olivine lamproites in this area of Murfreesboro, as well as the involvement of De Beers and Henry Ford. It also describes the work done there by famed mineralogist George Kunz and the interest former Arkansas governor Bill Clinton showed in the diamonds. These accounts and more are accompanied by dozens of stories of everyday people who found diamonds and the few who had a brush with TV stardom after their finds.

As an added bonus, the package includes an 84-minute DVD, *How to Find Genuine Diamonds in Arkansas*. If you plan to prospect for diamonds or visit the Crater of Diamonds State Park, you need a copy of this DVD. It is excellent! I was very impressed by its quality and informational content. I only wish I had owned a copy of Mr. Worthington's book and DVD when I first visited the park in 1986 and conducted diamond exploration in Arkansas a decade later.

W. DAN HAUSEL
Gilbert, Arizona

Cartier: Innovation Through the 20th Century

By François Chaille, 271 pp., illus., publ. by Flammarion [http://editions.flammarion.com], Hoboken, NJ, 2007. US$65.00

This book was published to coincide with the Moscow Kremlin Museums' summer 2007 exhibition of the same name. Beautiful in presentation, and large in size, this hardback is among the best I've seen created for museum exhibitions in terms of the sheer scope and depth of information presented.

The book consists of two main sections. The first chronicles the history and evolution of the famed jewelry house. Its seven chapters begin with "A Dynasty Devoted to a House of Jewelry," which relates the company's founding and growth. "The Development of an Inimitable Style" discusses Cartier's groundbreaking concept of diamonds in millegrain platinum settings, and the influence of flora and fauna on many of its designs. "Perfect Timing: Cartier Clocks and Watches" highlights wristwatches and the legendary Cartier mystery clocks. The other chapters in this section look at Louis Cartier (and the 'Ballets Russes'), Cartier accessories, the company's "cultural heritage," and its famous clients.

The second section is the catalogue, with 14 chapters that include "The *Belle Époque* and the Garland Style," "The Call of the East, a World of Inspiration," and "Art Deco and Color Combinations." This section consists mostly of beautifully photographed Cartier jewelry, watches, clocks, and accessories, with some explanatory text. It also features photos of original design drawings and plaster casts of finished jewelry.

The book concludes with a chronology of Cartier's history and a bibliography.

I was very impressed with the quality of photos, the completeness of the historical accounts, and the overall layout. Any lover of Cartier jewelry—or art history, for that matter—will appreciate this amazing book.

JANA MIYAHIRA-SMITH
Gemological Institute of America
Carlsbad, California

The Most Fabulous Jewels in the World: Graff

By Meredith Etherington-Smith, 196 pp., illus., publ. by Cultureshock Media [http://cultureshockmedia.co.uk], London, 2007. £75.00

Knowing the Graff name and the jewels he has bought and sold, any reader of this book would expect to be wowed by pictures and stories, but this book exceeds all expectations. Open to any part and you'll be face–to-face with full-page, high-quality color photos of the rarest diamonds. Whether the subject matter is

double- and triple-digit carat "white diamonds" or colored diamonds of important size and unusual color, you immediately recognize that the value of this book is in its pictures.

The book is divided into three sections: "The Fable," "The Fabulous," and "The Jewels." The first is a wonderfully intimate background of Laurence Graff and his foray into the world of jewelry. From apprentice to jeweler to designer, salesman, and even mine owner, Graff worked his way through many areas within the trade, each of which shaped him and gave him the knowledge to become one of the greatest jewelers today. Many know of his rags-to-riches saga, but they may not be aware of the intimate details offered in this book.

"The Fabulous" is a brief overview of his continued success through some key purchases and the acquisition of important clients. A great example is from the 1980s, when colored diamonds were just becoming fashionable. The Argyle mine offered its first tender of pink diamonds, all of them extremely small. Graff, contrary to everyone's advice, bought the entire lot for $3.5 million. Whereas other diamantaires were concerned about how to sell so many small pinks, Graff combined them all into a single piece of jewelry. As luck would have it, so often the case with Graff, the Sultan of Brunei called for an audience. Within two minutes of seeing the piece, the Sultan purchased it. Still, though the account of Graff's rise from apprentice to the pinnacle is lively and interesting, I would have liked even more stories and details.

The final third, "The Jewels," is the most engaging section. It is a series of vignettes and accompanying photos of important jewels Graff has owned. Again, I would have preferred more details, but as many of the pieces are in private hands, readers will have to wait until their full histories can be revealed. From beginning to end, the stories are as big as the diamonds, and you will be mesmerized by the sheer size and color of Graff's jewels.

All proceeds from the sale of this book go to the Nelson Mandela Children's Fund.

JOSHUA SHEBY
New York City

OTHER BOOKS RECEIVED

Ruby, Sapphire, and Emerald Buying Guide, 3rd Ed. *By Renee Newman, 187 pp., illus., publ. by International Jewelry Publications [www.reneenewman.com], Los Angeles, 2009, US$19.95.* This is a revised and updated version of Ms. Newman's consumer reference on corundum and emerald (see Spring 2000 *G&G*, p. 83, for a review of the second edition). New for this edition are two chapters on geographic sources and laboratory grading reports and appraisals.

TWO

Tables of Gemstone Identification. *By Birgit Günther, 256 pp., illus., publ. by Verlagsbuchhandlung Birgit Günther, Idar-Oberstein, Germany, 2009, €87.50.* This revised and updated version of the 1981 original provides a quick reference guide (in German and English) to the gemological properties (RI, SG, birefringence, optic character, diaphaneity, dispersion, pleochroism, hardness, chemical composition, and spectroscope spectrum) of known gem materials. This edition includes 50 new materials and expanded data on synthetics, as well as revised properties for some gems based on localities discovered since 1981. TWO

Archaeomineralogy, 2nd Ed. *By George (Rip) Rapp, 348 pp., illus., publ. by Springer-Verlag [www.springer.com], Berlin, 2009, €139.05.* This work reviews the minerals and rocks, including gem materials, that were used from prehistoric times through the 17th century. Though intended primarily for archeologists who deal with rock and mineral artifacts, it includes two chapters on gem minerals and metals and their use throughout history; coverage in these chapters is broad but not deep.

TWO

Imperishable Beauty: Art Nouveau Jewelry. *By Yvonne Markowitz and Elyse Z. Karlin, 168 pp., illus., publ. by MFA Publications [www.mfa-publications.org], Boston, MA, 2008, $45.00.* Created to accompany the exhibit of the same name at the Boston Museum of Fine Arts, this work reviews both European and American contributions to the art form. Photos of the 90 pieces in the exhibit (all from a private collection) are included. TWO

2010 GEMOLOGICAL ABSTRACTS

COLORED STONES AND ORGANIC MATERIALS

A description and history of one of the largest nacreous pearls in the world. J. C. Zwaan [zwaanj@naturalis.nl] and H. A. Dommisse, *Journal of Gemmology*, Vol. 31, No. 5–8, 2009, pp. 196–202.

A large and uniquely shaped baroque pearl was investigated to help establish its historical significance. The pearl was mounted in gold with ruby, sapphire, and emerald beads on a jeweled lapis base to create a stylized lotus flower *objet d'art*. Because the pearl was tightly mounted on a gold peg, it was impossible to weigh loose, so its weight was calculated at 2,385 grains (119.25 grams). It exhibited good luster and orient over much of its surface, and X-radiography confirmed a natural origin.

Unlike other historical pearls, this specimen was thought to be of freshwater origin. Its size, color, and physical properties suggested a *Hyriopsis cumingi*, *Cristaria plicata*, or *Hyriopsis schlegeli* mollusk from China or Japan; historical references also point to Asia as the source.

The first record of the pearl is a 1778 print, prepared the year of its first sale, which was discovered in the Amsterdam city archives in 2009. The pearl was offered several times to respected jewel houses (including Fabergé) for sale to European royal families during the 19th and 20th centuries, and was eventually sold in 1979 to an Amsterdam art collector. In 1992, Antwerp goldsmith Jean Lemmens mounted the pearl in its present form.

It had been suggested that this pearl was actually the Arco Valley Pearl, offered at auction in Abu Dhabi in 2007, but the recently discovered 1778 print refutes this notion.

JEC

This section is designed to provide as complete a record as practical of the recent literature on gems and gemology. Articles are selected for abstracting solely at the discretion of the section editors and their abstractors, and space limitations may require that we include only those articles that we feel will be of greatest interest to our readership.

Requests for reprints of articles abstracted must be addressed to the author or publisher of the original material.

The abstractor of each article is identified by his or her initials at the end of each abstract. Guest abstractors are identified by their full names. Opinions expressed in an abstract belong to the abstractor and in no way reflect the position of Gems & Gemology *or GIA.*

Jaspilite—The gemstone of Ukraine. P. Baranov [baranov_pn@bk.ru], S. Shevchenko, W. Heflik, L. Natkaniec-Nowak, and M. Dumanska-Slowik, *Journal of Gemmology*, Vol. 31, No. 5–8, 2009, pp. 163–169.

Jaspilite is an iron- and silica-rich metamorphic rock of sedimentary or volcanic origin; it is also a general term for material geologists call banded iron formation. Decorative pieces of jaspilite are used for architectural facing stones, as well as for vases, cameos, and the like, while some are fine enough for jewelry use. Jaspilite has a wide range of banded colors, mainly red with areas ranging from bright red to deep brown, yellow, orange, blue, and gray with a metallic luster. Yellow-banded tiger's-eye and blue-banded falcon's-eye specimens are known; these optical effects are produced by fibrous and lamellar aggregates of amphibole. The textures include parallel-striated, wavy-striated, intensely folded (plicated), breccia-like, and "landscape" varieties. The geologic setting and mineralogical complexities of the different varieties are discussed. Principles of shaping jaspilite gems are illustrated, along with guides on optimizing the textures and colors of the rough.

Jaspilite is sold in the monthly World of Gemstones exhibition in Dnepropetrovsk. With considerable reserves available, there is potential to expand into global markets.

ERB

Role of polyenes in the coloration of cultured freshwater pearls. S. Karampelas [stefanos.karampelas@cnrs-imn.fr], E. Fritsch, J.-Y. Mevellec, S. Sklavounos, and T. Soldatos, *European Journal of Mineralogy*, Vol. 21, No. 1, 2009, pp. 85–97.

The authors analyzed 21 untreated freshwater cultured pearls from the *Hyriopsis* genus by diffuse-reflectance UV-Vis-NIR and Raman spectroscopy, at high resolution. All showed the two major Raman resonance features of unmethylated (unsubstituted) polyenes, rather than carotenoids. Their general formulas are R-(-CH=CH-)$_N$-R′, with N = 6–14. Each color is due to a mixture of pigments rather than a single one, and each pigment can be related to a specific absorption with apparent maxima in the 405–568 nm range, thus absorbing in the violet to yellow-green region. Recognizing the spectroscopic signatures of pigments in untreated cultured pearls can help separate them from their treated counterparts.

RAH

A signature for nephrite jade using its strontium isotopic composition: Some Pacific Rim examples. C. J. Adams [argon@gns.cri.nz] and R. J. Beck, *Journal of Gemmology*, Vol. 31, No. 5–8, 2009, pp. 153–162.

Because nephrite jade historically has been mined and traded in so many localities worldwide, there is great interest in determining its geologic provenance. Current chemical and mineralogical identification characteristics, while useful, may not be definitive in determining origin. This article presents a technique using radiogenic isotopic ratio patterns. Nephrite's age of formation can be determined by identifying the ratio of the $^{87}Sr/^{86}Sr$ isotopes, a composition inherited during formation from either serpentinite or sedimentary protoliths. The authors tested nephrite from Pacific Rim sources such as New Zealand, New Caledonia, Taiwan, Canada, and Russia. Nephrite from New Zealand—the principal source analyzed—demonstrated a strong association of age and isotopic history with its host rock. Data from other regions, while also promising, were not as conclusive and require further investigation.

AB

The study of various beads used for cultured pearls. A. Abduriyim, H. Kitawaki, and S. Akamatsu [ahmadjan@gaaj-zenhokyo.co.jp], *Gemmology*, Vol. 40, No. 482, 2009, pp. 22–27 [in Japanese with English supplement].

Since the early 1900s, numerous materials have been employed as beads for culturing pearls. Because of CITES and other regulations designed to protect endangered species, disclosure mandates, and new market considerations, the gem trade needs a means of identifying cultured pearl bead materials. To that end, 70 bead samples were subjected to standard gemological tests (visual examination, magnification, UV fluorescence, and specific gravity), spectroscopy (UV-visible and IR), and chemical analysis (EDXRF and LA-ICP-MS). In particular, LA-ICP-MS was used to analyze a nacre-covered bead by continuous laser ablation. The bead samples comprised shell (from freshwater mussels, marine oysters, and a marine snail), treated beads (exposed to "fluorescent bleach" and "Rongalite," and a composite material), and other materials such as ceramics and Bironite. Although the authors noted several differences in the properties of the various beads, none of the tests would be useful for nondestructively identifying a bead inside a cultured pearl.

ERB

Zur die Flammenstruktur bei einigen porzellanartigen Perlen [Explaining the flame structure of some non-nacreous pearls]. H. A. Hänni [h.a.haenni@gmail.com], *Gemmologie: Zeitschrift der Deutschen Gemmologischen Gesellschaft*, Vol. 58, No. 1–2, 2009, pp. 47–52 [in German].

Non-nacreous pearls may show alternating areas of bright and dark lines, and some also display spotted patterns. This is due to a crosswise array of bundles of aragonite laths or fibers. Small areas of these bundles alternate in their orientations; light striking the length of the bundles is reflected, while light perpendicular to the bundles is absorbed. The result is observed as a flame structure.

GL

DIAMONDS

Diamonds from placers in western and central Africa: A problem of primary sources. T. V. Posukhova [tposukhova@mail.ru] and F. N. Kolume, *Moscow University Geology Bulletin*, Vol. 64, No. 3, 2009, pp. 177–186.

This study examined alluvial diamonds and associated heavy minerals from placer deposits along the Bafit-Ngoku River in Sierra Leone and along the Kasai and Lubembe Rivers in the southern portion of the Democratic Republic of Congo to determine their properties and geologic origin. Minerals recovered from these placers exhibited little or no evidence of abrasion, which suggests transport over short distances from their primary sources. Characterization of diamonds from these placers by visual, luminescence, and spectroscopic methods revealed features that are distinct from those of known primary deposits in Africa or Siberia. The chemical compositions of the accessory garnet, ilmenite, and zircon differed from those of known kimberlite origin. This suggests that the primary source rocks could be lamproites, though the overall crystal morphology of the diamonds corresponded more closely to kimberlitic material. The occurrence of coated diamond crystals, and those with brown or yellow coloration, is comparable to some Canadian kimberlites. The diamonds in these placers are of mantle origin, but they have no direct analogues with known kimberlite or lamproite pipes in Africa. *JES*

The genesis of low-N diamonds. A. I. Chepurov [chepurov@uiggm.nsc.ru], E. I. Zhimulev, A. P. Eliseev, V. M. Sonin, and I. I. Fedorov, *Geochemistry International*, Vol. 47, No. 5, 2009, pp. 522–525.

The rarity in nature of low-nitrogen type IIa diamonds suggests that they crystallized under unusual geologic conditions in the mantle. The authors of this article have extensive experience with diamond synthesis by the HPHT temperature-gradient method, where metallic elements such as titanium are used to bond with nitrogen in the growth system so it does not become incorporated into the growing crystal. In this study, synthetic diamonds grown in an Fe-Co-C system containing titanium oxide were yellow, whereas those grown in a similar system containing titanium metal were colorless. Based on their experiments, the authors conclude that type IIa diamonds grew in the mantle in the presence of "nitrogen getters" such as titanium. When these elements are present as oxides, nitrogen-containing type Ib diamonds form. However, under the unusual strongly reducing conditions where the titanium occurs as a metal, colorless type IIa diamonds crystallize.

JES

Large Brazilian diamonds. D. B. Hoover [dbhoover@aol.com] and J. Karfunkel, *Australian Gemmologist*, Vol. 23, No. 10, 2009, pp. 440–446.

A brief history is presented of diamond production in the relatively small region of Alto Paranaiba, Minas Gerais, Brazil. In addition to 65 documented stones weighing >50 ct (details are listed for 40 of them), many more large diamonds are suspected to have been found by itinerant miners (*garimpeiros*) and smuggled out of the country. The area is also known for producing fine pink and red diamonds.

RAH

Magnetic susceptibility of natural diamonds. A. P. Yelisseyev, V. P. Afanasiev, and V. N. Ikorsky, *Doklady Earth Sciences*, Vol. 425, No. 2, 2009, pp. 330–333.

Magnetic susceptibility is a measure of the intensity of magnetization of a body that has been placed in a uniform magnetic field of unit strength. Diamagnetic materials have a very weak magnetic susceptibility; they are repulsed by a magnet and do not retain their magnetic properties when the external field is removed. Ferromagnetic materials have a strong magnetic susceptibility, which means that they are strongly attracted to a magnet and can retain their magnetic properties when the field is removed.

Pure diamond is a diamagnetic material. HPHT-grown synthetic diamonds, and occasionally natural diamonds, may appear ferromagnetic due to the presence of iron-containing inclusions. The authors measured the magnetization of 20 high-quality—and seven low-quality—natural diamond crystals, all of Siberian origin, and found a small range of diamagnetic behavior over a temperature range of 5–300 K. They suggest that careful magnetic measurements are useful for separating natural and HPHT-grown synthetic diamonds, and perhaps for determining the nature of iron-containing mineral inclusions in natural diamonds.

JES

Structural defects in natural plastically deformed diamonds: Evidence from EPR spectroscopy. R. M. Mineeva, S. V. Titkov [titkov@igem.ru], and A. V. Speransky, *Geology of Ore Deposits*, Vol. 51, No. 3, 2009, pp. 233–242.

When geologic stresses are applied, diamond crystals may undergo plastic deformation (i.e., permanent changes in their shape or structure without fracturing). This process can occur in the mantle or during transport by kimberlite volcanism. Two deformation mechanisms have been proposed: dislocation gliding and mechanical microtwinning. Plastic deformation can create a variety of defect centers in the atomic lattice, and these can often be detected by electron paramagnetic resonance (EPR) spectroscopy. In this study, type Ia diamonds of various colors (brown, pink-brown, black-brown, pink-purple, and gray) from Yakutia and the Ural region of Russia were studied, and several different nitrogen-containing defect centers were identified using EPR. Certain

defect centers seem to be associated with particular deformation-induced diamond colors. The wide variety of defect centers suggests that a range of deformation conditions can affect diamonds in the earth. The authors note that defect creation and destruction during HPHT annealing has been extensively studied, while diamond defects caused by plastic deformation have been largely overlooked. *JES*

Type II diamonds: Flamboyant megacrysts? A. E. Moore [andy.moore@info.bw], *South African Journal of Geology*, Vol. 112, No. 1, 2009, pp. 23–38.

Despite their high value as gems, low-nitrogen type IIa diamonds have not been well documented in the scientific literature. Important sources are the Premier (Cullinan) and Jagersfontein mines in South Africa, Orapa and Jwaneng in Botswana, and Letšeng in Lesotho. These diamonds typically display irregular or distorted crystal morphology, planar cleavage, little or no UV fluorescence, and high clarity (they may contain graphite as opposed to other mineral inclusions). They are typically colorless or display various colors (i.e., brown, pink), and form a relatively large proportion of giant diamonds. Considering their light carbon isotope–enriched composition, the author suggests that type II diamonds have a websteritic mantle paragenesis that differs from either eclogitic or peridotitic origins. The formation of these large diamond megacrysts is thought to have occurred from chemically evolved and fractionated, relatively low-temperature, residual pegmatitic magmas that are genetically related to kimberlitic magmas. *JES*

GEM LOCALITIES

Age and genesis of the Myanmar jadeite: Constraints from U-Pb ages and Hf isotopes of zircon inclusions. Z. L. Qiu, F. Y. Wu [wufuyuan@mail.igcas.as.cn], S. F. Yang, M. Zhu, J. F. Sun, and P. Yang, *Chinese Science Bulletin*, Vol. 54, No. 4, 2009, pp. 658–668.

The Hpakan area of north-central Myanmar has long been an important source of jadeite. Here, the material occurs as veins in serpentinized peridotites associated with various high-pressure metamorphic rocks. Complex topography, adverse weather, and other factors have limited the geologic field study of these deposits, and different theories as to their mode of formation and age have been proposed.

In this study, a yellowish green jadeite sample understood to be from the Hpakan area, and unusual for its abundant euhedral zircon inclusions, was analyzed by LA-ICP-MS and cathodoluminescence. *In-situ* analyses of 16 zircon grains yielded U-Pb ages of 158 ± 2 million years. The luminescence patterns in these crystals revealed an internal structure that was less regular than typical for magmatic zircons. The zircon grains also had lower concentrations of the heavy rare-earth elements. The authors conclude that the jadeite deposits are not genetically associated with magmatism or other geologic events that took place during the Cenozoic collision between the Indian and Asian continental plates. Rather, the deposits are believed to be the result of fluid-induced metasomatism of preexisting rocks during the Late Jurassic, with the fluids originating from the dehydration of subducted oceanic crust. *JES*

Colored gemstones from Canada. B. S. Wilson [brad@alpinegems.ca], *Rocks & Minerals*, Vol. 85, No. 1, 2010, pp. 24–42.

This article reviews Canadian production of colored gemstones and their localities. All major gem species with the exception of tanzanite and alexandrite have been discovered in Canada, and they occur in a variety of geologic environments. One of the best-known gems is hessonite, found in the Jeffrey mine in Quebec (one of Canada's most important mineral localities). While some gem species such as corundum and beryl have been discovered during mining for base metals, exploration for colored stones is new to Canada. A few historic localities have been known for centuries, but the majority were discovered much more recently, within the past 10–20 years. However only a limited number of Canadian mines are currently producing gem rough.

The relatively recent discovery of vast diamond deposits in Canada suggests a viable future in colored gemstone mining, and has stimulated interest among smaller mining companies. *MK*

Demantoid from a new source. K. Schmetzer [schmetzerkarl@hotmail.com] and S. Karampelas, *Gems & Jewellery*, Vol. 18, No. 4, 2009, pp. 10–12.

An illustrated description is given of crystals of green to yellowish green demantoid (6–7 mm in diameter) from Antetezambato, near Ambanja in northern Madagascar. Growth zoning revealed a combination of dodecahedral {110} and trapezohedral {211} forms. Most samples showed anomalous double refraction. Chemical analyses yielded 0.05–0.07 wt.% Cr_2O_3. UV-Vis-NIR spectra over the 280–1000 nm range showed strong absorption bands at 440, 590, and 860 nm, indicating that these andradites are colored by chromium and iron. *RAH*

Echte Edelsteine? Vulkanische Gläser aus der Eifel [Are volcanic glasses from the Eifel Mountains true gemstones?]. H. Locker, *Lapis*, Vol. 34, No. 9, 2009, pp. 13–19 [in German].

Rare volcanic glass found in the Eifel Mountains of Germany is comparable to aquamarine and tourmaline in color and transparency. The glass is thought to form when sandstone or pieces of quartz become fluidized after being trapped in an initially silicate-poor volcanic melt. If

the magma becomes a thick fluid, poor in gases but with sufficient silicate content, then a fluid-glass mixture develops. The viscosity of the melted material increases as the temperature of the lava rapidly decreases, resulting in the formation of volcanic glass. If Fe^{2+} dominates at high temperatures and reducing conditions, a green color is created; if Fe^{3+} dominates (oxidizing conditions) the glass will be yellowish brown. Blue and turquoise-like colors are caused by the presence of Cu^{2+}, while Mn^{3+} produces a violet color, with the latter showing a higher saturation with increasing alkali content (Na and K). Mn^{2+} is responsible for a weak yellow-brown color. The glass has a Mohs hardness of 5½–6 and an RI value ranging from 1.498 to 1.516. *GL*

Oxygen isotopes [*sic*] composition of sapphires from the French Massif Central: Implications for the origin of gem corundum in basaltic fields. G. Giuliani [giuliani@crpg.crns-nancy.fr], A. Fallick, D. Ohnenstetter, and G. Pegere, *Mineralium Deposita*, Vol. 44, 2009, pp. 221–231.

Oxygen isotope values for sapphires (alluvial, colluvial, and within xenoliths) from alkali basaltic rocks of the French Massif Central are presented. Two major sapphire groups were interpreted to represent distinct genetic origins. The first group (71% of the samples) was restricted to an isotopic range of 4.4–6.8‰, within the established range of sapphires from magmatic sources (predominantly basalts and syenites). The second group ranged from 7.6 to 13.9‰, implying a metamorphic origin such as biotite schist in gneisses or skarns. Some areas within the French Massif Central (i.e., Le Mont Coupet) contained sapphires of both ranges, suggesting a complex geologic history; models are presented. After comparing these results with oxygen isotope values for corundum worldwide, the authors conclude that these basalt-transported sapphires formed in either granulite-facies metamorphic rocks or magmas from the crust-mantle transition.

KAM

Precious opal from Java: Gemmological properties, micro- and nano-structures. T. T. Sun [fegemlab@singnet.com.sg], P. C. Mok, S. L. Paul, M. Paramita, C. E. S. Arps, W. Atichat, E. Fritsch, W. W. Kang, and K. Wijaya, *Australian Gemmologist*, Vol. 23, No. 11, 2009, pp. 513–528.

The mining of play-of-color opal (locally called *kalimaya*) on the Indonesian island of Java started in 1970. This study documents opals from near the village of Cilayang (~6°55′ S, 106°25′ E). White, brown, dark brown, and "jelly" opals are produced; black opal is mined elsewhere in the area. The samples showed all the characteristics of volcanic opal-CT. Both SEM and atomic force microscopy (AFM) imaging showed that the silica lepispheres may be arranged in an orderly or a disorderly manner; a well-ordered stacking provides the best play-of-color. Raman spectroscopy identified some of these opals as hydrophane, with a band at 965 cm^{-1} attributable to OH and another at 3200 cm^{-1} due to molecular water.

RAH

A study on the characteristics of some C- and CT-opals from Brazil. F. Caucia [caucia@crystal.unipv.it], C. Ghisoli, and I. Adamo, *Neues Jahrbuch für Mineralogie, Abhandlungen*, Vol. 185, No. 3, 2009, pp. 289–296.

The physical properties of blue and "fire" opals from Piauí State, Brazil, were determined by optical analyses, specific gravity measurements, X-ray diffraction (XRD), and IR spectroscopy; chemical compositions were measured with LA-ICP-MS and SEM-EDS. The samples had SG values of 1.98–2.28 and RIs ranging from 1.430 to 1.461. The presence of cristobalite was confirmed with XRD and IR spectroscopy. A "coralloid islands" structure, built of microspherules of amorphous silica, was observed with the SEM, and could explain the iridescence shown by some blue specimens. LA-ICP-MS analyses confirmed the presence of Fe as the principal cause of color in the fire opals (perhaps present as an Fe-oxyhydroxide); Mn was significant in only the darkest specimens.

RAH

Utah Ammolite. G. Musick, *Rock & Gem*, Vol. 38, No. 8, 2008, pp. 34–38.

The author, an amateur lapidary, describes his discovery of fossilized shell material near Clawson, Utah, that resembles Ammolite from Alberta, Canada. A general description of the location and material are provided. Samples were collected at the surface from an area of <2 acres. Gemological tests were not conducted, and identification of the material as Ammolite was based on its visual appearance and association with marine (likely Cretaceous-aged) fossils. Some simple assembled gems were prepared (polished fossil shell attached to quartz caps using epoxy). Photos of the material suggest that its color range is similar to lower-quality Canadian Ammolite; the predominant colors noted are reds, greens, and red-browns.

The author attempted to stake a mineral claim on the site but was refused by the Bureau of Land Management, as current regulations recognize Ammolite as a fossil rather than a gemstone.

[*Abstractor's Note:* Until proper testing is conducted, this abstractor cautions against labeling the material as "Ammolite" and suggests calling it "fossil shell."]

KAM

Zirkone von Tansania: "Malaya-Zirkon" [Zircons from Tanzania: "Malaya zircon"]. U. Henn [ulihenn@dgemg.com], *Gemmologie: Zeitschrift der Deutschen Gemmologischen Gesellschaft*, Vol. 58, No. 1–2, 2009, pp. 67–72 [in German].

Attractive gem-quality zircon showing brown, yellow, and

red coloration is found in the Tanga Province of northern Tanzania. The color similarity of some of these stones to Malaya garnet has given rise to the trade name "Malaya zircon." The zircon has an SG range of 4.67–4.72 and RI values (measured with a reflectometer) from 1.957 to 1.962, both consistent with high-property zircon. It has a typical absorption spectrum; the strongest lines (due to U^{4+}) are at 510, 538, 562, 589, 615, 620, 653, 682, and 690 nm. Inclusions are uncommon. Growth zoning parallel to the tetragonal prism faces and cracks with disk-like patterns were occasionally observed.

GL

INSTRUMENTS AND TECHNIQUES

Identification of black opaque gemstones. M. Okano and H. Kitawaki [ahmadjan@gaaj-zenhokyo.co.jp], *Gemmology*, Vol. 40, No. 480, 2009, pp. 12–15 [in Japanese with English supplement].

Black simulants and treated black gemstones pose special identification challenges and are often found mixed with natural black gems in jewelry. Black diamond, CZ, and synthetic moissanite all have RIs over the limit of the standard gemological refractometer, and their dark color makes it difficult to discern inclusions and growth patterns. This illustrated article shows several techniques for separating black opaque stones using common gemological tests, as well as the limitations of these methods. Among laboratory techniques, Raman spectroscopy is the most practical and effective, particularly for melee-set jewelry.

ERB

Traitement Zachery des turquoises: méthode d'identification simple fondée sur la microchimie [Zachery-treated turquoise: A simple identification technique using chemicals]. B. Mocquet [blanca.mocquet@free.fr], Y. Lulzac, E. Fritsch, and B. Rondeau, *Revue de Gemmologie*, No. 168, 2009, pp. 8–11 [in French].

While Zachery-treated turquoise cannot be detected through classic gemological methods, the material can be identified by its relatively high potassium content. This article describes a microchemical technique for detecting differences in potassium content without using sophisticated analytical methods such as EDXRF spectroscopy. Most fashioned turquoise undergoes surface treatment (e.g., with waxes, oils, or plastics), which must be removed prior to the test; a droplet of dilute nitric acid (30% by volume in water) is sufficient. Then, a drop of picric acid solution is placed on the unprotected surface of the turquoise. If long yellow needles form as the drop dries, the stone is Zachery treated. Untreated turquoise shows no reaction.

GL

SYNTHETICS AND SIMULANTS

Aquamarine—Natural or synthetic? A. Hodgkinson, *Australian Gemmologist*, Vol. 23, No. 11, 2009, pp. 495–499.

Synthetic aquamarine has been available since the late 1980s, and a considerable amount of it appeared at the Tucson gem shows in the late 1990s. This product requires close scrutiny to distinguish it from natural aquamarine. Synthetic aquamarine is seen in a range of color tones and saturations but often is darker than natural material. Commercial production of synthetic aquamarine generally employs seed plates that are cut parallel to a pyramidal face, and the crystal overgrowth exaggerates this feature. A pattern of characteristic growth lines is also diagnostic of the synthetic.

DAZ

The genetic approach for identification of varieties of crystalline and amorphous silica. V. S. Balitsky [balvlad@iem.ac.ru] and O. V. Balitskaya, *Australian Gemmologist*, Vol. 23, No. 11, 2009, pp. 500–508.

Correlations between certain gemological characteristics and growth conditions of natural and synthetic varieties of quartz and of play-of-color opal led the authors to outline a testing and identification approach described as "genetic gemology." Recognizing characteristic features exclusive to either natural or synthetic growth allows a gem material's origin to be determined unambiguously. Illustrated examples are given of color distribution in natural and synthetic quartz.

RAH

Kinetics of diamond single crystal growth in Fe-Co solvents doped with titanium and zirconium. V. V. Lysakovskii and S. A. Ivakhnenko, *Journal of Superhard Materials*, Vol. 31, No. 1, 2009, pp. 7–11.

The authors grew synthetic diamonds by the HPHT temperature-gradient method using Fe-Co alloy solvents with Ti and Zr as nitrogen getters to control their N content. Growth temperatures of 1380–1680°C and pressures of 5.5–6.1 GPa were used for these experiments. Lower amounts (~1 at.%) of Ti and Zr resulted in type Ib diamonds, whereas higher amounts (~6 at.%) resulted in type IIa crystals with slower growth rates (~3 mg/h vs. ~6 mg/h). Raising the growth temperatures changed the crystal morphology from cuboctahedral to octahedral. The results of these experiments allowed the authors to define the pressure-temperature conditions under which synthetic diamonds could be produced with particular colors, crystal morphologies, and probable inclusion phases.

JES

Synthetic sapphires with "natural-like" sheen. G. Choudhary [gtl@gjepcindia.com], *Gems & Jewellery*, Vol. 18, No. 3, July 2009, pp. 6–9.

A new type of synthetic sapphire displays sheen effects similar to those seen in some natural sapphires. Sheen is a kind of surface luster caused by the scattering of light from evenly distributed minute inclusions. Traditionally, the presence of such inclusions has provided a reliable indication of a natural stone. However, synthetic corundum is now being produced with inclusions that can create sheen. The samples tested were yellow, green, and greenish blue, but other colors such as red and blue are available.

A number of gemological properties distinguished these samples as synthetic. Microscopic examination revealed curved zones or clouds consisting of fine whitish pinpoints (possibly gas bubbles or unmelted feed powder); this indicated flame-fusion or Verneuil synthesis. Scattered spherical gas bubbles were present in all samples. In addition to these features, which are typical of synthetic corundum, a number of uncommon inclusions were present, and one of the gems appeared transparent to short-wave UV radiation (indicating a synthetic). Although routine gem testing was sufficient to identify these samples as synthetics, the lighter-colored gems could pose identification problems if they are not carefully examined.

DAZ

TREATMENTS

Gemological modification of local natural gemstones by ion beams. S. Intarasiri, D. Bootkul, L. D. Yu [yuld@fnrf.science.cmu.ac.th], T. Kamwanna, S. Singkarat, and T. Vilaithong, *Surface & Coatings Technology*, Vol. 203, No. 17/18, 2009, pp. 2788–2792.

Rough and polished corundum from Thailand and Myanmar were treated by implanting either low- or medium-energy oxygen or nitrogen ions to change their color. Implantation conditions included energies of 20, 60, and 120 keV, beam currents of 0.1 to a few milliamps, and fluences of 10^{18} to 10^{19} ions/cm^2. The target gemstones reached temperatures of 200–600°C during the treatment. According to the authors, the samples' clarity, color distribution, luster, and brilliance improved following ion implantation. They suggest that the color alterations result from changes in the oxidation state of the transition metals (such as iron), or the creation of charge-transfer mechanisms or defect color centers within the samples. However, no data about the depth of ion implantation in the samples is provided. The process does not induce any residual radioactivity, and it is much faster than traditional heat treatment.

JES

MISCELLANEOUS

Building peace with conflict diamonds? Merging security and development in Sierra Leone. P. Le Billion and E. Levin, *Development and Change*, Vol. 40, No. 4, 2009, pp. 693–715.

In developing nations with diamond resources, there is significant debate over which delivers the most social benefit while keeping the diamonds within legitimate trading channels: corporate mining or artisanal digging. This paper describes the diamond areas around Kono, recounts the brutal history of the 1990s civil war, and explores the potential benefits and problems of both mining policies. The authors conclude that the positive effects of artisanal mining have been largely overlooked.

RS

Diamonds, governance and "local" development in post-conflict Sierra Leone: Lessons for artisanal and small-scale mining in sub-Saharan Africa? R. Maconachie [roy.maconachie@manchester.ac.uk], *Resources Policy*, Vol. 34, 2009, pp. 71–79.

The complex problems facing post–civil war Sierra Leone create significant challenges in forming diamond-mining policies that can truly benefit the different communities rather than encourage corruption. Several development initiatives have been launched to equitably distribute proceeds from local alluvial diamond diggings. While these initiatives achieved some success, in some communities the majority of the proceeds went to a handful of "local elites." In addition, alluvial diamonds are easily extracted and their deposits are scattered over wide areas, which makes them susceptible to illegal mining and theft. At the same time, the government has not been effective at monitoring diamond exports. Meanwhile, long-entrenched dealers who have profited from illegal mining activities have a strong interest in maintaining the status quo. The author argues that it will take considerable time to develop good governance practices and the necessary accountability to make such programs work effectively.

RS

Tanzanite as a conflict gem: Certifying a secure commodity chain in Tanzania. R. A. Schroeder [rschroed@rci.rutgers.edu], *Geoforum*, Vol. 41, No. 1, 2010, pp. 56–65.

Shortly after the September 11 terror attacks, reports in the American press claimed that some tanzanite dealers were actively funding terrorist activities. While a subsequent U.S. State Department investigation debunked the connection to terror, later articles focused on the hazardous working conditions of independent tanzanite miners and the allegedly harsh methods employed by TanzaniteOne, the one large mining operation, in protecting its concession from poachers. TanzaniteOne dealt with these public relations challenges by implementing an unbroken supply chain to the market that complies with the USA PATRIOT Act, though it has experienced ongoing difficulties maintaining this chain in an area with a large, informal economy. *RS*

Because Public Education Happens at the Counter.

GIA launches Retailer Support Kit and website

A $97.00 value, shipping and handling extra.

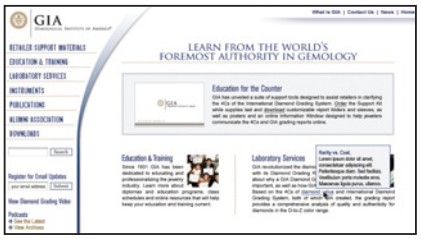

GIA's Retailer Support Kit has been developed to help sales associates educate the public about diamonds, the 4Cs, and thoroughly explain a GIA grading report. Take full advantage of all that GIA has to offer by visiting www.retailer.gia.edu

To order your FREE kit, log on to www.retailer.gia.edu

GIA
Gemological Institute of America®

RTGG08

GIA

Gemological Institute of America